Universität Stuttgart

Institut für Wasser- und Umweltsystemmodellierung

Mitteilungen

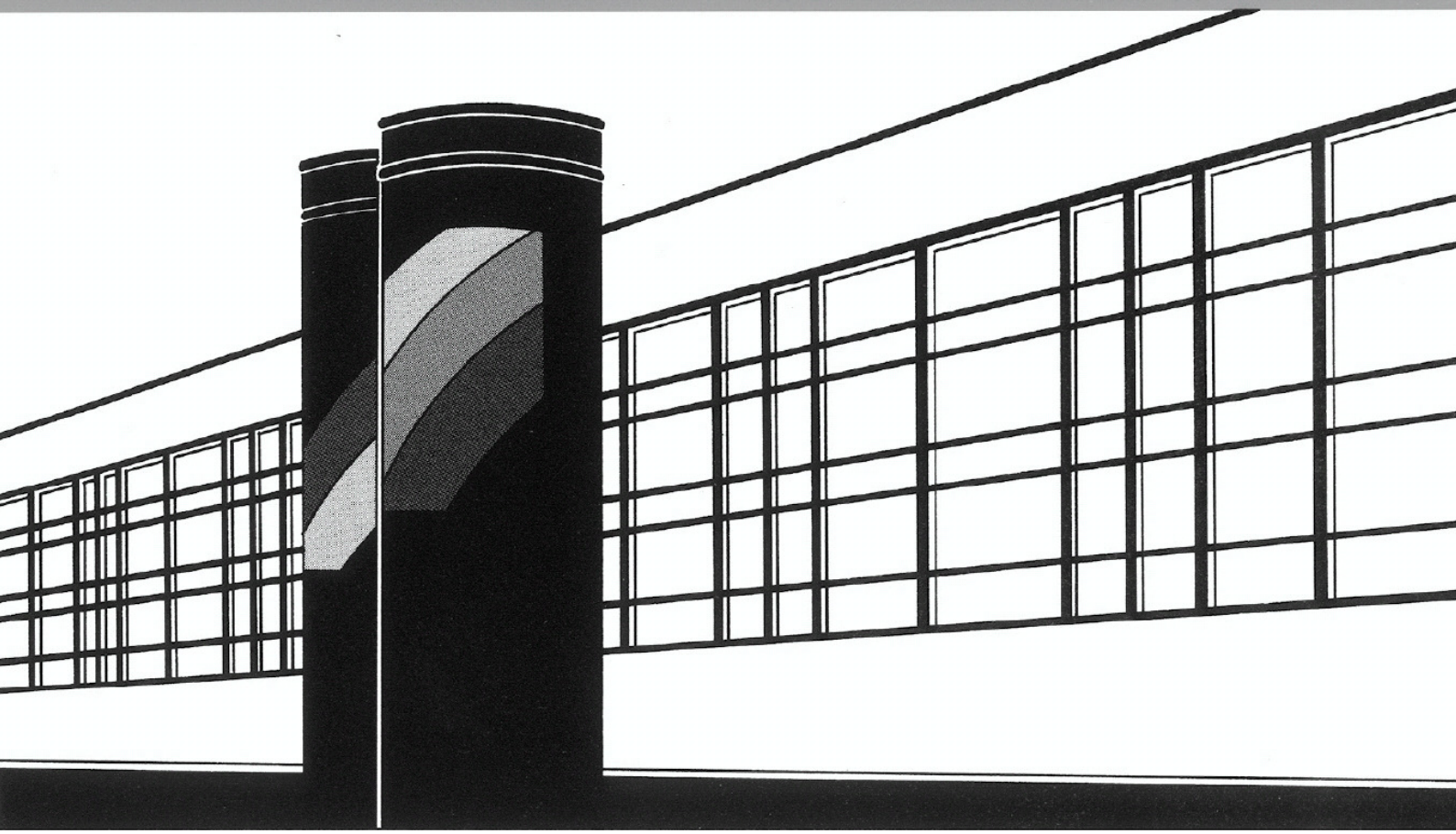

Heft 226 Maria Magdalena Eder

Climate Sensitivity of a Large Lake

Climate Sensitivity of a Large Lake

Von der Fakultät Bau- und Umweltingenieurwissenschaften
der Universität Stuttgart zur Erlangung der Würde eines
Doktor-Ingenieurs (Dr.-Ing.) genehmigte Abhandlung

Vorgelegt von

Maria Magdalena Eder

aus Karlstadt (Main)

Hauptberichter:	Prof. Dr. rer.nat. Dr.-Ing. András Bárdossy
Mitberichter:	Prof. Dr. h.c. Dr.-Ing. E.h. Helmut Kobus, PhD
	Prof. Dr. rer. nat. Karl-Otto Rothhaupt

Tag der mündlichen Prüfung: 15. Oktober 2013

Institut für Wasser- und Umweltsystemmodellierung
der Universität Stuttgart
2013

Heft 226

Climate Sensitivity of a Large Lake

von
Dr.-Ing.
Maria Magdalena Eder

Eigenverlag des Instituts für Wasser- und Umweltsystemmodellierung
der Universität Stuttgart

D93 Climate Sensitivity of a Large Lake

Bibliografische Information der Deutschen Nationalbibliothek
Die Deutsche Nationalbibliothek verzeichnet diese Publikation in der Deutschen Nationalbibliografie; detaillierte bibliografische Daten sind im Internet über http://www.d-nb.de abrufbar

Eder, Maria Magdalena:
Climate Sensitivity of a Large Lake von Maria Magdalena Eder. Institut für Wasser- und Umweltsystemmodellierung, Universität Stuttgart. - Stuttgart: Institut für Wasser- und Umweltsystemmodellierung, 2013

(Mitteilungen Institut für Wasser- und Umweltsystemmodellierung, Universität Stuttgart: H. 226)
Zugl.: Stuttgart, Univ., Diss., 2013
ISBN 978-3-942036-30-6

NE: Institut für Wasser- und Umweltsystemmodellierung <Stuttgart>: Mitteilungen

Herausgegeben 2013 vom Eigenverlag des Instituts für Wasser- und Umweltsystemmodellierung

Druck: Document Center S. Kästl, Ostfildern

Danksagung

Ich danke Prof. Bárdossy für die gute Betreuung meiner Arbeit, sowie den Mitberichtern Prof. Kobus und Prof. Rothhaupt für ihre Korrekturen und Anregungen. Besonderer Dank geht an Prof. Kobus, der mich ermutigt hat, die Arbeit zu schreiben, und mich für das Stipendium vorgeschlagen hat.

Die Arbeit wurde finanziert durch das IPSWAT-Stipendium (International Postgraduate Studies in Water Technologies) des Bundesministeriums für Bildung und Forschung. In diesem Zusammenhang möchte ich auch Gabi Hartmann herzlich danken, die mir als Leiterin des Doktorandenprogramms EnWat (Environment Water) an der Uni Stuttgart vor allem in administrativen Fragen immer eine große Hilfe war.

Meinen Kollegen am Lehrstuhl für Hydrologie und Geohydrologie danke ich für eine schöne Zeit, unterhaltsame Kaffeepausen und viele interessante Diskussionen. Ich habe von euch allen viel gelernt, besonders von Dirk und Thomas, die mir das Programmieren beigebracht haben.

Diese Arbeit ist entstanden aus der Zusammenarbeit mit meinen Kollegen und Freunden Marieke Frassl und Dirk Schlabing. Ohne euch wäre sie nicht das geworden, was sie ist. Vielen Dank für die Zusammenarbeit und für Eure Unterstützung.

Contents

List of Figures

List of Tables

Notation

The following table shows the significant symbols used in this work. Local notations are explained in the text.

Symbol	Definition	Dimension
Greek Letters:		
ρ	density	[kg/m3]
θ	air temperature	[°C]
Φ	relative humidity	[-]
Latin Letters:		
f	coriolis parameter	[1/s]
u	westerly wind component	[m/s]
v	northerly wind component	[m/s]
Q_{sw}	short wave radiation	[W/m^2]
$ILWR$	incident long wave radiation	[W/m^2]

List of Abbreviations

BWG	Bundesamt für Wasser und Geologie (Switzerland)
CAEDYM	Computational Aquatic Ecosystem Model
doy	day of year
ELCOM	Estuary, Lake and Coastal Ocean Model
ENSO	El Niño Southern Oscillation
GCM	General Circulation Model, sometimes also Global Climate Model
HDV	Hydrographischer Dienst Vorarlberg (Austria)
NAO	North Atlantic Oscillation
RCM	Regional Climate Model
VG	Vector-autoregressive weather generator
ELCD	ELCOM-CAEDYM coupled model
ECHAM5	GCM developed by the Max Planck Institute for Meteorology in Hamburg

Kurzfassung

Seen sind komplexe Ökosysteme, die einerseits durch die definierten Grenzen in sich einigermaßen abgeschlossen sind, andererseits auf mannigfaltige Weise mit der Umwelt, vor allem mit ihrem hydrologischen Einzugsgebiet und der Atmosphäre verknüpft sind.

Die Reaktionen von Seen auf klimatische Einflüsse sind von den physikalischen Eigenschaften des Wassers, insbesondere des Süßwassers, geprägt: Wasser hat eine hohe spezifische Wärmekapazität und eine geringe Wärmeleitfähigkeit. Zusammen mit der thermischen Schichtung, die in tiefen Seen der mittleren Breiten den größten Teil des Jahres herrscht, führt das zu langen Aufenthaltszeiten von Wärme und Wasserinhaltsstoffen im Hypolimnion. Seen können daher klimatische Einflüsse über eine Zeitspanne von mehreren Jahren integrieren.

Untersuchungsgebiet

Diese Arbeit behandelt die Klimasensitivität großer Seen am Beispiel des Bodensees. Der Bodensee bietet sich an, da die Seenforschung hier auf eine lange Geschichte zurückblicken kann und daher umfangreiche Daten vorhanden sind.

Der See liegt an der Grenze der Länder Österreich, Schweiz und Deutschland am Nordrand der Alpen auf einer Höhe von 395 m über dem Meeresspiegel. Der See besteht aus zwei Teilen, dem größeren und tieferen Obersee und dem flacheren und kleineren Untersee, die durch den 4 km langen Seerhein verbunden sind. Er ist maximal 253 m tief, hat eine Oberfläche von insgesamt 535 km^2 und ein Volumen von 48.45 km^3. Das Einzugsgebiet des Sees umfasst 11890 km^2 und liegt zu einem großen Teil in den Alpen. Der See ist mono- bis oligomiktisch. Eine vollständige Durchmischung tritt etwa alle 2-3 Jahre ein.
Nach einer Phase intensiver Eutrophierung in den siebziger und achtziger Jahren des 20. Jahrhunderts ist der See inzwischen wieder in seinem natürlichen oligotrophen Zustand.
Aus dem Bodensee wird Trinkwasser für etwa 5 Millionen Menschen in Deutschland und der Schweiz entnommen.

Modelle und Validierung

In dieser Arbeit wurden die numerischen Modelle ELCOM und CAEDYM verwendet. ELCOM (Estuary, Lake and Coastal Ocean Model) ist ein dreidimensionales Modell zu Berechnung von Strömung, Temperatur, Salinität und Dichteschichtung im See. Es kann mit dem ökologischen Modell CAEDYM (Computational Aquatic Ecosystem Model) gekoppelt

betrieben werden. CAEDYM berechnet den Nährstoffkreislauf von Stickstoff, Phosphor, Kohlenstoff und Silizium sowie Sauerstoffkonzentration sowie Primär- und Sekundärproduktion in Form von Phyto- und Zooplankton.
Beide Modelle sind bereits in der Vergangenheit auf den Bodensee angewendet worden.

Zur Validierung der Modelle wurden drei verschiedene Datensätze verwendet: Beobachtungen an einem trüben Dichtestrom im See nach einem Hochwasser im Alpenrhein, eine seeweite Messkampagne zur Verteilung von Phytoplankton und Temperatur, sowie Langzeitbeobachtungen zu Temperatur und Sauerstoff im Hypolimnion.

Im August 2005 führte der Alpenrhein nach einem Starkregen in den Alpen Hochwasser. Die große Schwebstofffracht erhöhte die Dichte des Flusswassers so stark, dass es im See als Trübestrom am Grund entlang bis zum tiefsten Punkt floss. Messungen von Temperatur und Trübung an verschiedenen Stellen im See dokumentieren den Fließweg und zeigen eine Asymmetrie des Trübestroms. Am tiefsten Punkt des Sees wurde eine Temperaturerhöhung um mehr als 3 °C von 4.5 °C auf 8 °C gemessen.
Mit Hilfe der Modelle ELCOM und CAEDYM konnte der Weg des Flusswassers im See, die Temperaturerhöhung und die Verteilung der sedimentierten Schwebstoffe am Grund nachgebildet werden. Ein Simulationsexperiment belegte den Einfluss der Corioliskraft auf den Dichtestrom und die Verteilung der Sedimente.

Im Frühjahr 2007 fand am Bodensee eine Messkampagne zur Erfassung der dreidimensionale Verteilung von Wassertemperatur und Plankton statt. Die horizontale Verteilung von Algen im See entsteht einerseits durch Gradienten in den physikalischen Bedingungen, wie Wassertemperatur, Strömung, Licht und Nährstoffkonzentrationen. Andererseits spielen auch biologische Faktoren wie der Wettkampf zwischen verschiedene Arten und Fraßdruck durch Zooplankton und Fische, und auch der Zufall eine Rolle. Während der Messkampagne gab es einen Sturm, der zu großräumigen Strömungen an der Seeoberfläche führte und damit zu deutlichen Gradienten in Wassertemperatur und Algenkonzentration. Der Vergleich der Messdaten mit den Ergebnissen einer Simulation dieses Zeitraums zeigt, dass das Modell die physikalisch bedingten Unterschiede in der Phytoplanktonverteilung gut erfasst, die aufgrund von internen und zufälligen Faktoren jedoch weniger.

Das Modell bildete die in den Jahren 1980-2000 gemessenen Zeitreihen von Temperatur und Sauerstoff im Hypolimnion korrekt nach. Dies deutet darauf hin, dass die vertikalen Mischungsprozesse im Modell richtig wiedergegeben werden. Im gewählten Zeitraum war der See sowohl von der Re-Oligotrophierung als auch von klimatischer Erwärmung beeinflusst. Der von der Klimaerwärmung verursachte Anstieg der Wassertemperatur wurde vom Modell richtig wiedergegeben. Die Effekte der Re-Oligotrophierung sind vielschichtiger, wurden aber bis zu einem gewissen Grad auch vom Modell wiedergegeben.

Klimaszenarien

Ausgehend von dem Modellaufbau für die Jahre 1980-2000 wurden Klimaszenariensimulationen durchgeführt. Das Augenmerk lag dabei in erster Linie auf der Entwicklung von Temperatur und Sauerstoffkonzentration im Tiefenwasser und damit auf den vertikalen

Schichtungs- und Durchmischungsprozessen, sowie auf dem Wärmehaushalt des Sees.
Die meteorologischen Randbedingungen für die Klimaszenarien wurden mit Hilfe eines Wettergenerators erzeugt. Eine andere Möglichkeit wäre gewesen, Ergebnisse von Szenarienrechnungen globaler Klimamodelle (Global Circulation Models GCM) zu verwenden. Die Verwendung eines Wettergenerators hat demgegenüber den Vorteil, dass verschiedene klimatische Kenngrößen unabhängig voneinander beliebig variiert werden können. Damit kann die Sensitivität des Sees in Bezug auf Veränderungen von mittlerer Temperatur, klimatischer Variabilität und jahreszeitlichen Schwankungen getrennt voneinander untersucht werden. Die Ergebnisse dieser Studie sind daher nicht als Prognosen zu interpretieren, sondern als "was-wäre-wenn"-Szenarien, die durchgeführt wurden, um die Vorgänge im See besser zu verstehen.
Für die Szenarien wurden nur die meteorologischen Randbedingungen verändert. Die Zuflussrandbedingungen wurden von der Simulation der Jahre 1980 – 2000 übernommen. Einflüsse von Klimaveränderungen auf Prozesse im Einzugsgebiet wurden also vernachlässigt.

Die Studie führte zu den folgenden Erkenntnissen:
Eine **Erhöhung der mittleren Lufttemperatur** führt zu einer Erwärmung des Sees. Da die Wärmezufuhr von oben erfolgt, erwärmen sich die oberen Wasserschichten stärker und schneller als das Tiefenwasser. Das verstärkt die vertikalen Temperaturunterschiede und damit auch die Stabilität der Dichteschichtung. Dadurch wird eine vollständige Durchmischung des Sees etwas seltener. Allerdings findet auch in einem um 5 °C wärmeren Klima noch etwa alle 4 Jahre eine vollständige Durchmischung statt. Die Wassertemperatur bei ungeschichteten Verhältnissen im Winter und damit auch die Wassertemperatur im Hypolimnion erhöht sich um etwa 2.5 °C.
Während der geschichteten Phasen ohne Tiefenwassererneuerung wird dem Hypolimnion kein Sauerstoff zugeführt. Gleichzeitig laufen wegen der höheren Wassertemperatur viele biochemische Vorgänge schneller ab, was die Sauerstoffzehrung beschleunigt.
Außerdem ist die Löslichkeit von Sauerstoff in wärmeren Wasser geringer als in kälterem. Deshalb gehen die Sauerstoffkonzentrationen auch in oberflächennahen Schichten leicht zurück.
Die Aufenthaltszeit des Wassers im Hypolimnion erhöht sich mit zunehmender Lufttemperatur.

Für die Auswirkungen auf das Tiefenwasser ist es entscheidend, zu welcher Jahreszeit die Erwärmung stattfindet. Wärmere Winter haben einen stärkeren Effekt als wärmere Sommer. Im Sommer sorgt die thermische Schichtung dafür, dass das Temperatursignal an der Oberfläche bleibt und damit auch für eine erhöhte Wärmeabstrahlung sorgt. Die stärksten Auswirkungen auf den Wärmeinhalt des Sees hat eine Erwärmung in den Monaten Dezember und Januar, die geringsten Auswirkung eine Erwärmung der Monate Mai bis Juli.

Klimatische Variabilität wurde im Rahmen dieser Studie definiert als Episoden, in denen die Lufttemperatur über beziehungsweise unter dem langjährigen Mittelwert für diesen Tag im Jahr liegt. Diese klimatische Variabilität kann mit zwei Zahlen beschrieben werden: der mittleren Länge der Episoden in Tagen und der Standardabweichung der Temperaturabweichung in °C.

In den Temperaturmessdaten aus Konstanz aus den Jahren 1980-2000 ist die Episodendauer exponentialverteilt mit einem Mittelwert von 5.3 Tagen und die Abweichung vom langjährigen Mittelwert ist annähernd normalverteilt mit einer Standardabweichung von 2.3 °C.
Die Auswirkungen einer erhöhten klimatischen Variabilität sind in wärmeren Seen stärker. Wenn der See auch im Winter wärmer ist als 4 °C, dann führt jede besonders kalte Episode, die das Wasser an der Oberfläche abkühlt, zu einer Destabilisierung der Schichtung. Das kältere Wasser sinkt ab und verursacht damit auch eine Abkühlung der tieferen Schichten. Gleichzeitig wird auch Sauerstoff von der Oberfläche ins Tiefenwasser transportiert.
Warme Episoden dagegen verstärken die thermische Schichtung des Sees. Eine Erwärmung findet vor allem an der Oberfläche statt. Durch die höhere Oberflächentemperatur des Sees erhöht sich die Abgabe von Wärme an die Atmosphäre. Dadurch ist in einem variableren Klima die mittlere Wassertemperatur des Sees geringer und die mittlere Sauerstoffkonzentration höher als in einem weniger variablen Klima bei gleicher mittlerer Lufttemperatur.
Wenn die winterlichen Wassertemperaturen jedoch im Bereich von 4 °C liegen, hat eine erhöhte Variabilität kaum Auswirkungen auf Wassertemperaturen und Sauerstoffkonzentrationen. Das liegt daran, dass das die Dichteanomalie eine gewisse Pufferwirkung hat: Hat das Wasser des Sees eine Temperatur von 4 °C, so führt sowohl eine Erwärmung als auch eine Abkühlung der Oberfläche zu einer thermischen Schichtung. Das Temperatursignal bleibt in beiden Fällen an der Oberfläche.

Im Hinblick auf die kommerzielle Fischerei im Bodensee sind sowohl die Nährstoff- als auch die Sauerstoffkonzentrationen im See von großem Interesse. Höhere Nährstoffkonzentrationen bedeuten eine höhere Produktivität des Sees und damit einen größeren Fischbestand und einen potentiell größeren Ertrag für die Fischer. Gleichzeitig können erhöhte Nährstoffkonzentrationen zu erhöhter Sauerstoffzehrung im Tiefenwasser führen. Unter wärmeren klimatischen Bedingungen mit längeren Phasen stabilerer Schichtung kann das am Seegrund zu Gebieten mit Sauerstoffmangel führen. Dies wiederum stellt eine Gefahr für die natürliche Fortpflanzung einer der wirtschaftlich wichtigsten Arten im See, dem Blaufelchen (*Coregonus lavaretus wartmanii*), dar. Die gelegentlich auftretende Forderung, die Nährstoffkonzentration im See zu erhöhen, um einen größeren Fischertrag zu erreichen, ist daher besonders im Hinblick auf den Einfluss einer klimatischen Erwärmung auf den See kritisch zu sehen.

Zum Schluss wird erörtert, inwieweit die Ergebnisse dieser Studie auch für andere Seen als den Bodensee gelten.
Die Reaktionen des Bodensees auf den Klimawandel werden von seinen physikalischen, geographischen und ökologischen Eigenschaften bestimmt. Die hydrodynamische Reaktion wird beeinflusst vom Mischungstyp, Wassertemperaturen und der Aufenthaltszeit des Wassers im See. Eine Rolle spielen auch die Tatsache, dass der See so gut wie immer eisfrei bleibt, und die geringen Salinitätsunterschiede im See.
Die Reaktionen des Ökosystems werden außerdem vom oligotrophen Zustands des Sees bestimmt. Die Ergebnisse der Klimasensitivitätsstudie können also auf andere tiefe, monomiktische, oligotrophe Süßwasserseen in gemäßigtem Klima übertragen werden.
Dem Bodensee in vieler Hinsicht am ähnlichsten sind die anderen Seen des Voralpenlands, vor allem der Genfer See.

Ausblick

Die Studie kann in verschiedener Hinsicht erweitert werden. Interessant ist sicherlich eine Berücksichtigung von Veränderungen im Einzugsgebiet und die Auswirkungen auf den Wasser- und Nährstoffhaushalt des Sees.
Der Wind hat einen großen Einfluss auf die Hydrodynamik des Sees. Daher könnten Szenarien mit einer gezielten Veränderung der Windverhältnisse untersucht werden.
Für eine detailliertere Betrachtung von Wasserqualität und Ökosystem kann das ökologische Modell erweitert werden.

Abstract

Lakes are complex ecosystems, that are on the one hand more or less enclosed by defined borders, but are on the other hand connected to their environment, especially to their catchment and the atmosphere.

The reactions of lakes to climatic influences are determined by the physical properties of water, especially of fresh water: Water has, compared to e.g. air, a high specific heat capacity and a low heat transport capacity. In combination with the thermal stratification, this leads to long residence times of both heat and substances in the hypolimnion. Large lakes are therefore able to integrate climatic influences over several years.

This study is examinig the climate sensitivity of large lakes using Lake Constance as an example. Lake Constance has been subject of intensive research at least for the last 100 years. Therefore it is a well-studied system.
The lake is situated in Central Europe at the northern edge of the Alps, at the boundary of Austria, Germany and Switzerland. It consists of two parts, the larger and deeper Upper Lake Constance and the smaller Lower Lake Constance. The maximum depth is 235 m, the total surface area is 535 km^3 and the total volume 48.45 km^2. The lake is mono- to oligomictic. Complete mixing occurs in late winter every two to three years. The lake suffered from eutrophication in the 1970ies and 1980ies. Nowadays, it has recovered its original oligotrophic state.

The numerical simulations in this study have been performed with the lake model system ELCOM-CAEDYM. The model system was validated using three different data sets: Observations of a turbid underflow after a flood flow in the main tributary, a lake-wide field campaign of temperature and phytoplankton, and long term monitoring data of temperature and oxygen in the hypolimion.

The model system proved to be able to reproduce the effects of a flood flow in the largest tributary, the Alpine Rhine. A huge turbid underflow was observed flowing into the main basin after an intense rain event in the Alps in August 2005. A numerical experiment showed the influence of the earth's rotation on the flow path of the riverine water within the lake.

The model also reproduced the temperature evolution and distribution and to some extent the phytoplankton patchiness measured in spring 2007 during an intensive field campaign. The patchiness in the biological variables that resulted from physical drivers, such as gradients in the water temperature and wind-induced surface currents emerged in the simulation as well. Beyond that, the measured plankton distribution showed additional patterns, that might be attributed to internal reasons in the ecosystem, or to randomness. This part of the patchiness could not exactly be reproduced by the model.

The model reproduced the measured time series of temperature and oxygen in the deep hypolimnion measured in the years 1980-2000. This indicates, that the vertical mixing and the lake's cycle of mixing and stratification was reproduced correctly. During this period the lake was influenced both by re-oligotrophication and climate warming. The increasing trend in the air temperature induced an increasing trend in the water temperatures in the lake, which was correctly simulated by the model. The effects of the oligotrophication on the lake's ecosystem was less linear, but was to some extend also reproduced by the simulations. The residence time of water in the lake was estimated with the help of a conservative tracer.

Based on the model set-up validated with long term monitoring data, climate scenario simualtions were run. The main focus was on temperature and oxygen concentrations in the hypolimnion, the cycle of stratification and mixing, and the heat budget of the lake.
The meteorological boundary conditions for the climate scenario simulations were generated using a weather generator instead of downscaling climate projections from Global Climate Models. This approach gives the possibility to change different characteristics of the climate independently. The resulting lake model simulations are "what-if"-scenarios rather than predictions, helping to obtain a deeper understanding of the processes in the lake.
For the scenarios, only the meteorological boundary conditions have been changed. The inflow boundary conditions are the same in all scenarios. This study thus only considers direct climatic influences on the lake surface. Indirect climate effects via changes in the catchment have been neglected.

The main results can be summarized as follows:
An **increase in air temperature** leads to an increase in water temperature, especially in the upper layers. The deep water temperature increases as well, but not to the same extent as the temperature of the epilimnion. This results in an increased vertical temperature difference. Due to the non-linear shape of the temperature-density curve (UNESCO, 1981), the difference in density grows even stronger than the temperature difference. This results in enhanced stratification stability, and consequently in less mixing. Complete mixing of the lake becomes more seldom in a warmer climate, but even in the scenario simulations with air temperature increased by 5 °C, full circulation took place every 3-4 years.
Less complete mixing events lead to less oxygen in the hypolimnion. Additionally, as many biogeochemical processes are temperature dependant, the oxygen consumption rate is larger in warmer water. Gases dissolve less in warmer water. Therefore, the oxygen concentration decreases with increasing temperature even in the surface layers.
The residence time of water in the lake tends to increase with warming climate. The half-life $T_{1/2}$ of water in the deep hypolimnion increased by more than one year with air temperature increased by 5 °C.

In the context of this study, **climate variability** is defined as episodes with daily average air temperatures deviating from the long-term average for this day of year. The episodes can be described by their duration in days and their amplitude in °C.
Changes in climate variability can have very different effects, depending on the average air and water temperatures. The effects are stronger in lakes with higher water temperatures: As long as the average isothermal temperatures during winter mixing are close to the temperature of maximum density, both water temperatures and oxygen concentrations are sim-

ilar in simulations with standard and with increased climate variability. This is due to the buffering effect of density maximum: When the water temperature equals the temperature of maximum density, and the surface layers are cooled down further, inverse stratification is established. The cooling takes places only at the surface. Surface heat fluxes from the lake to the atmosphere decrease.
But the higher the deep water temperature normally is, the more pronounced the effect of increased climate variability can be. For the same average air temperatures, simulated water temperatures are lower in those scenarios with increased climate variability. This indicates the larger importance of cold episodes: In a warm episode, water is heated at the surface. This stabilises the stratification, and the temperature change occurs mainly at the surface. The warmer surface leads to enhanced heat emission of the lake. A cold episode in contrast destabilises the stratification, letting the temperature change reach deeper regions. Remarkably cold winters cool down the whole water column, and produce an increased stability of the thermal stratification when the surface layer warm up again.

For the hypolimnetic conditions, the **seasonality** in warming is important: Increasing winter air temperatures have a much stronger effect on the water temperatures in the lake than increasing summer temperatures. The most efficient warming takes place in December and January. The least efficient warming takes place in the months May - July. The reasons for the seasonal differences lie in the stratification in summer and in the non-linear temperature dependence of surface thermodynamics.

The combined effects of a warmer climate and **higher nutrient concentrations** enhances oxygen depletion in the hypolimnion.

Finally, it is discussed, to what extent the results of this study are transferrable to other lakes. The reactions of Lake Constance to climate change are determined by the physical, geographical and ecological characteristics of the lake. Hydrodynamic reactions are defined by the mixing type, water temperatures and the residence time of the water in the lake. Furthermore it is important that the lake is almost never completely ice-covered, and that there are only minor salinity differences.
The reactions of the ecosystem are determined also by the oligotrophic state of the lake.
Results of this study thus can be transferred to other deep, monomictic, oligotrophic fresh water lakes, as for example the other large perialpine lakes of glacial origin.

1 Introduction

A lake is an aquatic ecosystem that is a perennial, enclosed or semi-enclosed waterbody with a measurable residence time. Lakes can be found all over the world in all climate zones. Being an enclosed system, the lake is an interesting model ecosystem to study.

> One finds in a single body of water a far more complete and independent equilibrium of organic life and activity than on any equal body of land. [...] Nowhere can one see more clearly illustrated what may be called the sensibility of such an organic complex,–expressed by the fact that whatever affects any species belonging to it, must speedily have its influence of some sort upon the whole assemblage. [*The creatures in the lake are*] remarkably isolated,–closely related among themselves in all their interests, but so far independent of the land about them.
>
> (Forbes (1887))

But the lake also has interactions with its catchment area and the global environment. The processes in the system are driven by the input of energy and mass via the surface and the tributaries. The lake thus will react on any terrestrial and atmospheric changes in its catchment.

Many lakes are of socio-economic interest as fresh water resources, for fishery, and due to their cultural and aesthetic value.

1.1 Lakes and Climate

The reactions of lakes to climatic influences are determined by the physical properties of water, especially of fresh water:
Water has, compared to e.g. air, a high specific heat capacity and a low heat transport capacity. As large lakes in the temperate climate are thermally stratified during most of the year, some water parcels are in contact with the atmosphere only for a short time. The lake's surface is directly connected to the environment by exchanging energy and mass with the atmosphere as well as with the in- and outflows. The hypolimnion of a deep stratified lake is almost not connected to the environment at all, the main input of energy and substances happens during winter mixing from the upper layers. This leads to long residence times of both substances and heat in the hypolimnion. In those zones of the lake that are separated from external influence by the stratification most of the time, the few signals that reach into these depths are memorized over a time span of several years.
Today, Lake Constance does not mix completely every year, but only once in 2-3 years. Whether complete mixing occurs is not only depending on the meteorological conditions

in the respective winter period, but also on the current thermal conditions in the lake and hence on the meteorological conditions in the preceding years. This means, that a large lake can integrate the meteorological conditions over a time span of several years. The lake's response to climate change thus depends on temperature increase itself as well as on its gradient and on inter-annual variability of meteorology. This lake-specific inertia in reaction to any external signals is more pronounced, the larger the lake is. It grows especially with mean depth (ratio: volume to surface area) and average residence time (ratio: volume to discharge).

The physical processes are influencing water quality and the lake ecosystem. The cycle of stratification and mixing determines the vertical distribution of substances in the lake. Of particular interest for the water quality of lakes is the hypolimnetic oxygen concentration: The redox potential controls biogeochemical processes in the water column and the sediments. Low oxygen concentration lead to nutrient release from the sediment and therefore self-fertilizing of the lake takes place. Anoxia affect organisms, as for example fish eggs of some species are laid in the deep water of lakes, for example the whitefish *Coregonus lavaretus wartmanii* in Lake Constance (Wahl and Löffler, 2009).

In the scientific literature, numerous papers on the effect of climate, respectively climate change on lakes can be found:
Adrian et al. (2009) identified key variables in lakes responding to current climate change, in terms of physical, chemical and biological variables. These variables differ in their significance and validity from lake to lake, depending on geographical, morphological and catchment characteristics. Although most of them are also influenced by non-climate anthropogenic changes, such as changes in nutrient content (eutrophication and oligotrophication), pH (acidification and de-acidification) or catchment characteristics (land use, population, ...), a climate signal can be extracted in many cases.

Schneider et al. (Schneider et al., 2009; Schneider and Hook, 2010) analysed summer night-time lake surface temperatures from satellite imagery between 1991 and 2009 and found significant trends of up to 0.08 °C/yr especially in the mid latitudes of the northern hemisphere. In the tropics and on the southern hemisphere, trends were less pronounced and less significant. In the south west of the United States, in the Great Lakes Region and in Northern Europe, the trends were even steeper than those of the regional air temperature.

Livingstone (2003) studied temperature data from Lake Zürich of the years 1947-1998. He observed a warming trend at all depths. The trend was stronger in the epilimnion (0.024, max 0.087 °C/yr) than in the hypolimnion (0.013, max 0.053 °C/yr). This leads to a more stable stratification and a longer stratification period. He especially found a strong relationship between daily minimum (night-time) air temperatures and the temperatures of the lake's surface mixed layer. He emphasizes that climate change in Switzerland is diurnally asymmetric: night-time temperatures are increasing significantly, while daily maximum values are not. This fact is assumed to be caused by increased cloud cover and atmospheric turbidity, decreasing incoming solar radiation during the day, and decreasing cooling at night.
Coats et al. (2006) came to similar results for Lake Tahoe (California/Nevada) in the years 1970 - 2002: warming of the lake (on average 0.015 °C/yr) was stronger in the epi- than in the hypolimnion. Besides that, they observed a decrease in thermocline depth in autumn.

Straile et al. (2003) stated a high correlation of the lake water temperatures to the North Atlantic Oscillation Index (NAO).
Blenckner et al. (2007) stated an influence of the NAO on lake water temperatures and ice conditions and, mainly because of that, effects on nutrients and organisms in the lake. In 18 lakes all over Europe they found coherent responses in spring nutrient concentrations and summer biomass of cyanobacteria and some zooplankton species (especially cyclopoid copepods).

Paleosciences are taking advantage of the climate's influence on lakes: Lake sediments are widely used for reconstructing past climate developments in paleoclimatological and paleohydrological analyses. Czymzik et al. (2010) reconstructed flood frequency from Lake Ammersee sediments, for the last 450 years, Arnaud et al. (2005) reconstructed hydrological activity in the Rhône for 7200 years. Niemann et al. (2012) used bacterial lipids in the sediments of an alpine lake as a proxy for temperature in the past.

On the other hand, lakes, at least lakes of a certain size, themselves influence the atmospheric processes and hence the (local) climate. They alter the processes of heat and mass transport and influence wind velocities due to their small roughness length.
In climate modelling and numerical weather prediction, including lake models is an actual concern. For this task, the lake models have to be computationally efficient and able to reproduce lake surface temperatures and potential ice cover dynamics reasonably. For this application, the two-layer bulk model FLake has been used widely (Mironov et al., 2010).
Samuelsson et al. (2010) compared simulations of a Regional Climate Model (RCM) with and without consideration of lakes using the FLake model. They found a significant warming in air temperature over land caused by neighbouring lakes, especially in Fennoscandia and north-eastern Russia around Lake Ladoga and Lake Onega, but also in the Alpine region. The warming mainly occurred in autumn and winter. The annual cycle of precipitation also changed: as long as the lakes' surface temperatures are lower than the surrounding land, in spring and early summer, precipitation heights are lower than in the simulation without lakes. In late summer and autumn, the presence of lakes rather increased precipitation.

1.2 Lake Constance

Lake Constance has been subject of intensive research at least since 1919, when the first institute for research on Lake Constance, the Max-Auerbach-Institut, was founded in Konstanz. Therefore it is a well-studied system. Long-term monitoring as well as intensive field campaigns on selected topics give a comprehensive picture of the physical and biological processes in the lake and their reactions to external forcings.
The reactions of the lake's ecosystem on the eutrophication in the 1960ies and 1970ies have been documented as well as those on the re-oligotrophication that took place after 1980. At the same time, and ongoing, the lake is influenced by the global climate warming.

1.2.1 Site Description

Lake Constance (Bodensee) is a lake of glacial origin. It is situated in Central Europe at the northern edge of the Alps, at the boundary of Austria, Germany and Switzerland. The geographic position of the centre of the lake is 47° 39′ North, 9° 18′ East and the average water level is at 395 m asl.

The lake's total surface area is approximately 535 km^2, the volume approximately 48.45 km^3. It is consisting of two parts: Upper and Lower Lake Constance, which are connected by a 4 km long river called Seerhein. Upper Lake Constance (Obersee) has a volume of 47.6 km^3, a maximum depth of 253 m and an average depth of 101 m. Lower Lake Constance (Untersee) is shallower, with a maximum depth of 40 m and an average depth of 13 m.
Lake Constance has a catchment area of 11,890 km^2. The main tributary is the Alpine Rhine with an average discharge of 230 m^3/s, followed by Bregenzerach (46.8 m^3/s). Both are alpine waterbodies, entering the lake at the eastern part from the South. The only outflow of the lake is the High Rhine (Hochrhein), which leaves Lower Lake Constance at the westernmost point of the lake close to Stein am Rhein (Wessels, 1998).
The lake's water level shows a yearly cycle, which is dominated by the runoff in the main alpine tributaries. Water level is minimum in March, and maximum in June, when snow melt in the Alps is at its maximum. The average water level difference between minimum and maximum is 1.5 m.
Total discharge of the Seerhein at the outflow of Upper Lake Constance is 347.8 m^3/s (10.976 km^3/a), giving an average residence time of the water in Upper Lake Constance of 4.34 years (4.2 years when considering evaporation and drinking water withdrawals, see Bäuerle (1998)).
For a more detailed description of the morphology and hydrodynamics of Lake Constance, see Bäuerle (1998) and Wessels (1998).
Lake Constance is monomictic to oligomictic, mixing completely in late winter every two to three years.

The limiting nutrient for phytoplankton growth is phosphorus. Having suffered from anthropogenic eutrophication, with a peak phosphorus concentration of 80 $\mu g/l$ around 1980, the lake is nowadays stated as oligotrophic with phosphorus concentrations of around 6 $\mu g/l$. (Güde et al., 1998; Internationale Gewässerschutzkommission für den Bodensee (IGKB), 2012)

The lake is used as a drinking water reservoir for 5 million people in Germany and Switzerland. Furthermore, it is used for tourism and commercial fishery.

Complete ice cover is very seldom at Lake Constance, the last so-called »Seegfrörne« took place in 1962/63. Numbers about the recorded Seegfrörne-events in the literature differ. Wagner (1964) mentions trafficability of the lake in twelve winters since the 13th century. Hollan (2001) counts 33 Seegfrörnen since 875 (27 since the 13th century).

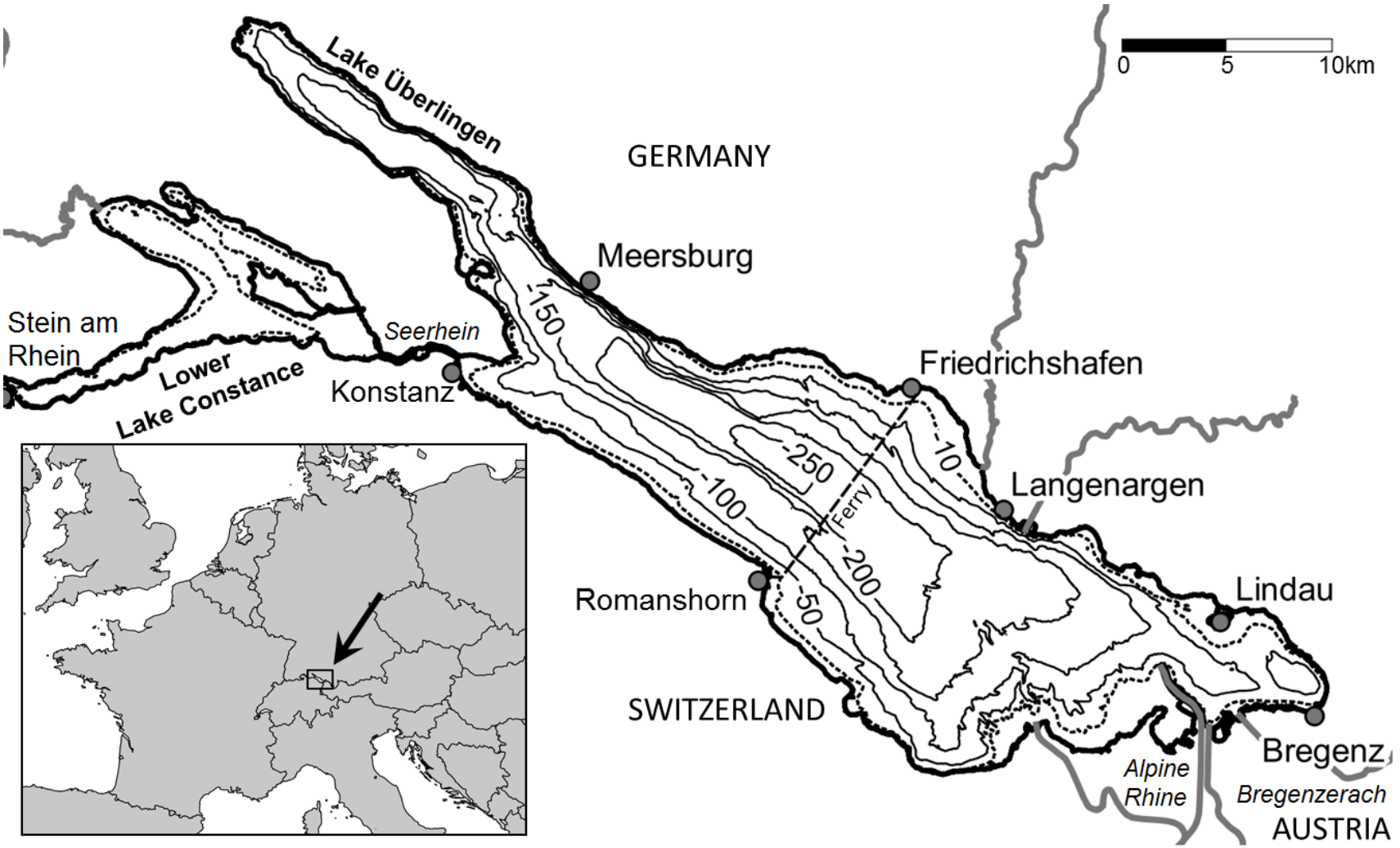

Figure 1.1: Map of Lake Constance and its position in Central Europe. Maps produced with QGIS, Data: small map: www.naturalearthdata.com, Depth contours: Bodenseetiefenvermessung (Braun and Schärpf, 1994), rest: OSM

1.2.2 Recent Climate Change at Lake Constance

Adrian et al. (2009) found a gradient of 0.021 °C/a in January and 0.037 °C/a in July in surface temperature data of Lake Constance between 1970 and 2007 . The trends' significance has been tested with the Mann-Kendall-Test on a significance level of p=0.01 and p=0.05, respectively.
Straile et al. (2003) recorded an increase of 0.06 °C/a in average winter air temperature (December - March) in the years 1962 - 1998, together with 0.017 °C/a increase in volume-averaged annual mean water temperatures. Both trends are highly significant ($P < 0.01$). It should be noted that their study period starts with the extraordinarily cold winter 1962/63. They stated a high correlation of the lake water temperatures to the North Atlantic Oscillation Index (NAO).
Hollan (2001) analysed historic ice-cover events. He found Seegfrörnen also in warm periods as the medieval warm period, because also under general warm climatic conditions winters with strongly negative NAO are possible.
Stich and Brinker (2010) analysed measurement data of several biotic and abiotic variables from the years 1980-2004, and found a strong negative impact of oligotrophication on total chlorophyll a, outweighing a much weaker positive impact of climate change.
Jöhnk et al. (2004) found a water level decrease of 22 cm since 1817. However, it was not continuously decreasing: in the years 1900-1925 they found an increase. Nowadays, the trend seems to be weakened. They noted that a change in run-off regime of the alpine tributaries might switch the highest floods towards an earlier time of the year. This would have significant effects on the lake's ecosystems, especially in the littoral zone.
Seasonal water level variability decreased since 1935, with a stronger trend since the 1960ies. This presumably results from the construction of hydro-power dams in the main tributaries.

1.3 Outline of the Thesis

In this study, the climate sensitivity of large lakes shall be examined, taking Lake Constance as an example. For this purpose, a three-dimensional coupled hydrodynamic and water quality model (ELCOM-CAEDYM) is applied. The models are explained briefly in chapter 2.
In chapter 3, the model system is validated using three different sets of measurement data: Measurements detecting an underflow in the lake after a flood flow in the main tributary, three-dimensional measurements of phytoplankton and temperature during a measurement campaign, and long-term monitoring data concerning temperature and oxygen in the hypolimnion.
In chapter 4, climate scenario simulations were run. Meteorological boundary condition data were not obtained by downscaling of output of global climate models. Climate scenarios were instead generated independently using a weather generator. This approach gives the possibility to change mean air temperature, and variability and seasonality of the

weather independently.
Lake model simulations were run to evaluate the effects of changes in mean air temperature and variability and seasonality of the weather on the deep hypolimnion of the lake.
At the end, the transferability of the results of this study to other lakes is adressed.

2 Models

A large variety of numerical models for lakes has been developed. Mooij et al. (2010) try to give an overview over the different approaches.
In terms of spatial dimensions, they range from simple, 0-dimensional box models (e.g. PCLoos/PCLake, Janse et al. (1992); Mooij et al. (2007)) over two- or three-layer-models and one-dimensional (e.g. DYRESM, Imberger and Patterson (1980)) to 3-dimensional models (e.g. ELCOM, Hipsey and Hamilton (2008)).

All models used for this study were developed by the Centre of Water Research at the University of Western Australia (CWR). The models used in this study were chosen because they had already been applied to Lake Constance several times for different problems, such as modelling of internal waves (Appt, 2003; Appt et al., 2004) and phytoplankton community dynamics (Rinke et al., 2009a).

2.1 Estuary, Lake and Coastal Ocean Model (ELCOM)

The three-dimensional hydrodynamic lake model ELCOM (Estuary, Lake and Coastal Ocean Model), code version 2.2.2, was developed by the Centre of Water Research (CWR) at the University of Western Australia. It simulates flow and transport processes on a Eulerian grid solving the three-dimensional Navier-Stokes and scalar transport equations separating mixing of scalars and momentum from advection and making use of the hydrostatic and Boussinesq assumptions (Hodges and Dallimore, 2006). The model was applied to Lake Constance without specific calibration of model parameters.

ELCOM has been shown to model successfully the baroclinic dynamics of stratified, large lakes: Hodges et al. (2000) and Gómez-Giraldo et al. (2006) applied ELCOM to model internal waves in Lake Kinneret, proving the ability of the model to reproduce the fundamental basin-scale motions such as the first mode of the wind-induced Kelvin-wave. Shimizu et al. (2007) applied ELCOM on Lake Biwa. Appt (Appt, 2003; Appt et al., 2004) applied the model ELCOM to Lake Constance, proving its ability to reproduce wind induced basin-scale internal waves.

Based on the findings by Appt, the joint research project BodenseeOnline developed a decision-support-system. (Lang et al., 2008; Lang and Paul, 2008)

Density ρ of lake water is calculated depending on temperature T (in $°C$) and salinity S (in PSS, if considered) using the UNESCO-formula for density of seawater at one standard

atmosphere (UNESCO, 1981):

$$\rho(T,S) = \sum_{i=0}^{5}(a_i \cdot T^i) + S \cdot \sum_{i=0}^{4}(b_i \cdot T^i) + S^{1.5} \cdot \sum_{i=0}^{2}(c_i \cdot T^i) + S^2 \cdot d_0 \tag{2.1}$$

with the parameters a_i, b_i, c_i and d_0 from table 2.1.
In all simulations mentioned in this thesis, salinity was not considered.

Table 2.1: Constants for the UNESCO-formula for density of seawater

	a	b	c	d
0	999.842594	0.824493	$-5.72466 \cdot 10^{-3}$	$4.8314 \cdot 10^{-4}$
1	$6.793952 \cdot 10^{-2}$	$-4.0899 \cdot 10^{-3}$	$1.0227 \cdot 10^{-4}$	
2	$-9.09529 \cdot 10^{-3}$	$7.6438 \cdot 10^{-5}$	$-1.6546 \cdot 10^{-6}$	
3	$1.001685 \cdot 10^{-4}$	$-8.2467 \cdot 10^{-7}$		
4	$-1.120083 \cdot 10^{-6}$	$5.3875 \cdot 10^{-9}$		
5	$6.536332 \cdot 10^{-9}$			

The time step length is constrained by the Courant-Friedrichs-Lewy (CFL) - condition. It defines that a water parcel should not traverse more than one grid cell (Δx) in one simulation time step. For the one-dimensional case, the CFL - condition is defined as follows:

$$\Delta t \cdot \frac{v}{\Delta x} \leq 1 \tag{2.2}$$

where Δt: length of simulation time step [s]
v: velocity [m/s]
Δx: size of grid cell [m]

The simulation time step thus depends on the chosen grid cell size. The constraining velocity in the lake is the phase speed of internal waves, which in Lake Constance is typically in the magnitude of 0.3 m/s (Appt, 2003).

2.2 Computational Aquatic Ecosystem Model (CAEDYM)

The water quality and ecosystem model CAEDYM (Computational Aquatic Ecosystem Model) was developed by the CWR. A description of the model structure of CAEDYM is given in Bruce et al. (2006) and Hipsey and Hamilton (2008). CAEDYM simulates nutrient cycling, oxygen dynamics as well as primary and secondary production. It can be coupled with different hydrodynamic drivers: either the 3D-model ELCOM (section 2.1) or with the 1D-model DYRESM.

CAEDYM had been successfully applied to Lake Constance by Rinke et al. (2009a) for simulating plankton dynamics over the course of the reoligotrophication of Lake Constance (1979-2000) in combination with the one dimensional hydrodynamic model DYRESM. The parametrisation of the ecological model given in Rinke et al. (2010) was, except for some

adaptation in the parametrisation of oxygen consumption, also used for the simulations performed in this work.

The water quality model CAEDYM is able to consider the effect of suspended material on water density. Suspended solids can be simulated in up to six different classes with different, user defined values for particle diameter, particle density, and critical shear stress for resuspension.
The increased water density is then calculated as follows:

$$\rho_{tot} = \rho_w + \sum_{i=1}^{n} (1 - \frac{\rho_w}{\rho_{SSOL,i}}) * c_{SSOL,i} \tag{2.3}$$

where ρ_{tot}: density of particle-loaded water [kg/m^3]
ρ_w: density of pure water (depending on temperature and salinity) [kg/m^3]
$\rho_{SSOL,i}$: density of suspended solids class i [kg/m^3]
n: number of suspended solids classes simulated
$c_{SSOL,i}$: concentration of suspended solids class i [kg/m^3]

Each suspended solids class has a constant settling velocity following Stokes' Law:

$$v_s = g * \frac{(\rho_{SSOL} - \rho_w) * d_{SSOL}^2}{18 * \mu} \tag{2.4}$$

where v_s: sinking velocity [v/s]
ρ_w: density of pure water (depending on temperature and salinity) [kg/m^3]
ρ_{SSOL}: density of suspended solids [kg/m^3]
d_{SSOL}: diameter of suspended solids [m]
μ: dynamic viscosity [kg/(s·m)]

The influence of turbulence on the settling of the particles is not considered.

Resuspension from the lake bottom is considered, too.

The CWR also developed a one-dimensional lake model, which can be coupled to the ecological model CAEDYM. It has not been used directly in this study, but in several other studies on Lake Constance this study is referring to.

The one-dimensional DYnamic REservoir Model DYRESM, simulates stratification and surface thermodynamics on a Langrangian grid (Bruce et al., 2006). It had been applied to Lake Constance by Hornung (2002), and, in combination with the ecological model CAEDYM, by Rinke et al. (2010).

3 Validation of the Models

A model that is used for scenario simulation has to be validated on measured data first. Appt (2003); Appt et al. (2004) has shown that ELCOM is able to reproduce basin-scale internal waves on a short to medium time scale. In this chapter, the suitability of ELCOM-CAEDYM shall be proven to reproduce different other phenomena in the lake: a turbid underflow, the distribution of biological parameters, and the long-term stratification and mixing behaviour.
For all phenomena, measurement data are available that can be compared to the simulation results.

3.1 Underflow caused by a Flood in the main Tributary

Flood events in tributaries can bring high amounts of suspended material from the catchment to the lake. The suspended material increases the density of the tributary water. If the sediment load and thus the density of the tribatry water is high enough, an underflow is formed: The tributary water sinks to the lake bottom and flows down the slope of the lake. Sedimentation of the suspended particles in the lake decreases the density of the fluvial water and dissolves the underflow.

If the lake or reservoir is used e.g. for drinking water abstraction or hydro-power generation, the distribution of suspended matter in the water column or the locations of sedimentation is of special interest.

Mulder and Syvitski (1995) describe underflows at river mouths into the oceans.
Chung et al. (2009) observed and modelled numerous underflows in a Korean reservoir using ELCOM-CAEDYM, but in the studied events, the main density difference was caused by temperature difference, not by suspended solids.

As already mentioned in chapter 1.1, the detection of layers of fluvial material in the lake sediments is used for the reconstruction of past flood events in the lake's tributaries (Czymzik et al., 2010; Arnaud et al., 2005).

Bringing tributary and epilimnetic water to the deep hypolimnion, underflows could play a role in the oxygen budget of the deep water zone. But depending on the amount of organic material in the underflow, this could be outweighed or over-compensated by additional oxygen consumption.

In this section, a simulation of the underflow observed in Lake Constance after a flood in the main tributary in August 2005 is described. Both observations and simulations will be published in Eder and Wessels (2013).

3.1.1 The Flood in the Alpine Rhine in August 2005

On August 22nd 2005, the north-western part of the Alps experienced extreme rainfall. The combination of an occlusion with relief rainfall at the edge of the Alps lead to daily precipitation sums of up to 250 mm, corresponding to a 150 to 250 year return period. As the air temperatures were relatively high, even in the higher regions only a small amount of the precipitation fell as snow. As the soil was already saturated with water due to rain in the preceding days, the rain event was followed by high peak flows in the alpine water bodies. A more detailed report (in German) on the rain event and the following flood in the alpine water bodies can be found in Gasser et al. (2005).
The discharge in the largest tributary of Lake Constance, the Alpine Rhine, reached 2252 m^3/s, which is slightly below the discharge with 100-year return period. In the Bregenzerach, the second largest tributary, the discharge reached with 1350 m^3/s the value for the 100-year return period (see figure 3.1).

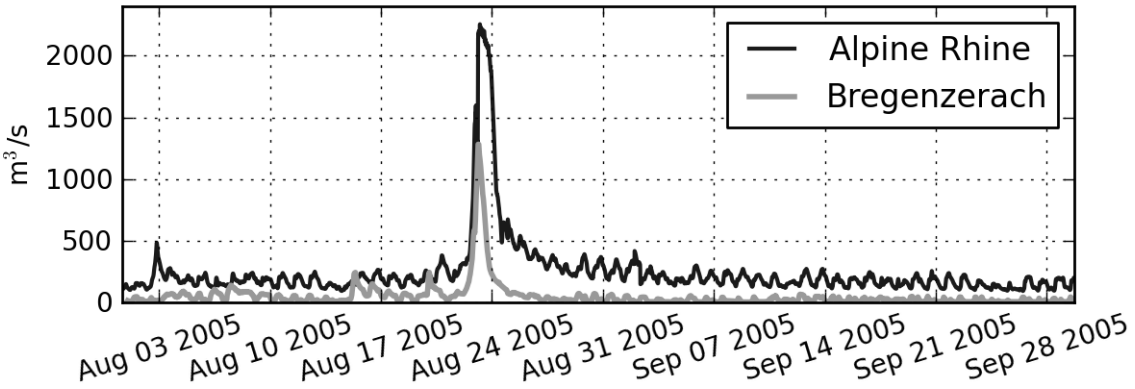

Figure 3.1: Discharge in Alpine Rhine and Bregenzerach, August 2005. (Data: BWG/HDV)

The high concentration of suspended solids in the fluvial water increased its density and created an underflow with considerable influence on the lake's hydrodynamics and water quality.
Consequences within the lake were directly registered by moorings (WH: blue + and FU: red x in figure 3.2). They measured temperature close to the lake bottom at water depth of 140 and 250 m. The measurement interval was 10 minutes (WH) respectively one hour (FU). At WH, flow velocity was also measured, but the measurement device was damaged by the underflow. In consequence, flow velocity measurements exist only for the beginning of the event. Velocity measurements stop three hours before the peak temperature was measured, that is seven hours after the underflow first arrived at the mooring. Spatial data of the path and form of suspended matter cloud within the lake were gathered using echo sounder and probe measurements (turbidity, temperature, salinity). An underflow with a temperature of 14 °C flowed with 1.4 km/h some 20 km into the lake. At the deepest point of the lake, a temperature increase of more than 3 °C from 4.5 °C to 8 °C was measured (figure 3.5).
The echo-sounder pictures showed the formation of plumes at the upper boundary of the underflow, where warm fluvial water with lower sediment concentration is rising.

Several days after the event, the fluvial sediments were detected as increased turbidity at the drinking water outtakes around the lake.

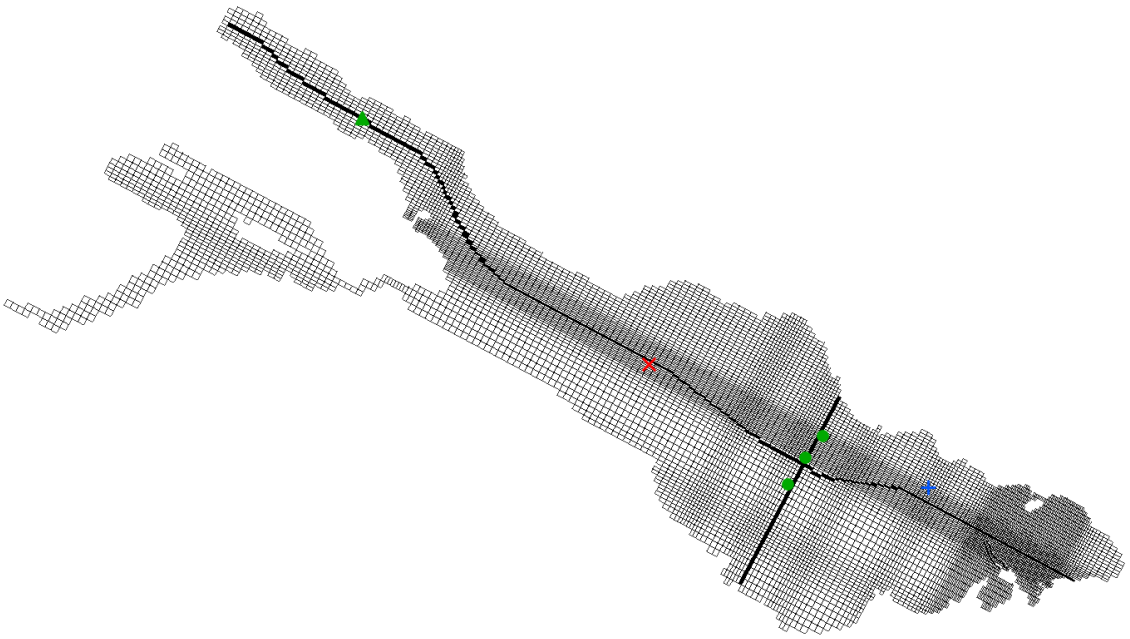

Figure 3.2: Simulation grid, measurement positions and transects

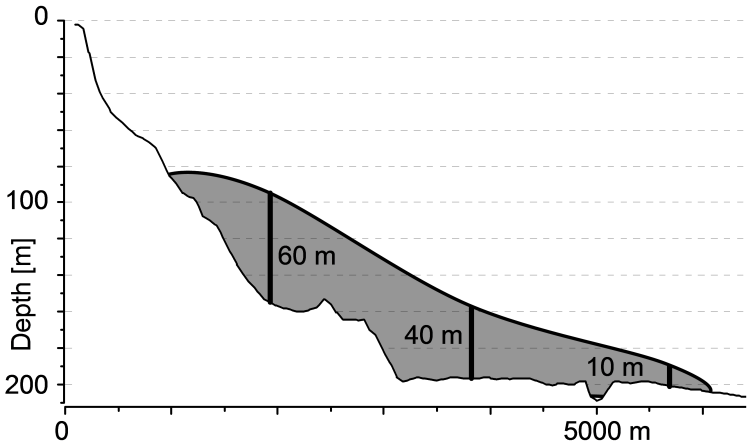

Figure 3.3: Lateral transect constructed from three temperature and transmissivity profiles, seen from downstream. Figure by Martin Wessels, ISF

The three profiles of transmissivity and temperature in the lateral transect near Langenargen (see figure 3.3) reveal an asymmetry of the underflow: the closer to the northern shore, the

bigger is the magnitude of the underflow. The profile at 150 m depth shows a magnitude of the warm turbid layer of 60 m, whereas at the southernmost profile at 200 m water depth the magnitude is only 10 m. Profile locations are indicated by green circles in figure 3.2. The three measurements used to draw this sketch were taken at 12:20, 12:35 and 15:17 (from left to right) on August 23rd, 2005.

Sediment cores sampled at the lake bottom in autumn 2006 and later reveal an asymmetric distribution of the sediments originating from this event: the highest magnitudes can be found north of the thalweg.

3.1.2 Simulation

For simulating the processes connected to the underflow in August 2005, a model grid with maximum horizontal grid cell size of 400 m*400 m and local refinements of up to 100 m*100 m close to the mouth of the main tributaries was used (figure 3.2).

As no continuous measurement data of sediment concentration in the tributaries is available, sediment concentrations were estimated depending on the discharge.
Müller and Förstner (1968) proposed a formula to describe the dependency of sediment concentration c from discharge Q:

$$c = a * Q^b \tag{3.1}$$

with a = 0.0004 and b = 2.2.
This formula was obtained using all achievable data, giving an overall average value. In fact, the sediment load can be quite different in different flood events, depending on the time in the year and preceding events. Rain induced flood-flows in later summer tend to bring higher sediment loads than snow-melt-dominated floods in spring and early summer. Furthermore, as flow velocities before the peak of the flood wave are higher than afterwards, the sediment transport capacity is also higher during rising discharge (Mulder and Syvitski, 1995). Based on sparse measurements of sediment load in Diepoldsau by the Bundesamt für Wasser und Geologie (Switzerland) for this flood event and another, smaller one in July 2008, different values for a and b were derived:

	a	b
Rising discharge: $Q > 480$ m^3/s	0.00002	2.8675
Declining discharge: $Q > 770$ m^3/s	0.047	1.6941
Else	0.0006	2.3428

The resulting sediment concentrations are shown in figure 3.4. The sediment concentration calculated from discharge was divided into two sediment classes:

Sediment class	**particle diameter** μm	**density** kg/m^3	**sinking velocity (10°C)** m/s
1	4	1450	$3.0 \cdot 10^{-6}$
2	37	2650	$9.5 \cdot 10^{-4}$

Using these values, the density of the fluvial water with temperature 11.9 °C was at the peak flow 1050.84 kg/m^3, compared to 999.74 kg/m^3 without the sediment's density effect and 1000.21 kg/m^3 in the deep hypolimnion of the lake (4.5 °). These density differences caused by the sediment load in the tributaries are the driving force for the underflow. However, the inflow concentrations are only a rough estimate.

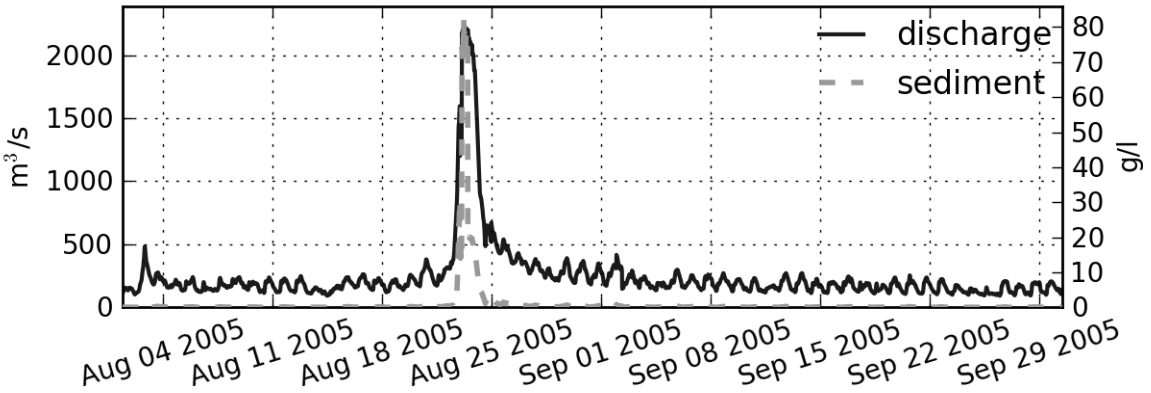

Figure 3.4: Discharge (measured) and sediment concentration (calculated) in the Alpine Rhine in August 2005

3.1.3 Results

The simulation recreates the following features of the observations of the underflow event:

- sinking of the sediment-loaden fluvial water
- underflow with flow velocities of more than 40 cm/s and temperatures several $°C$ higher than the surrounding lake water
- settling of the coarser fractions
- re-rising of the warm fluvial water in plumes
- drifting of fine parts in depth of the drinking water intakes

At the first mooring (WH, figure 3.5, for mooring position see blue + in figure 3.2), the simulated underflow arrives exactly in time, but the maximum temperature is about 1-2 °C too low. The underflow reaches the second mooring at the deepest point of the lake (FU, red 'x' in figure 3.2) with seven hours delay. The peak temperature increase of almost 4 °C is reached in the model.

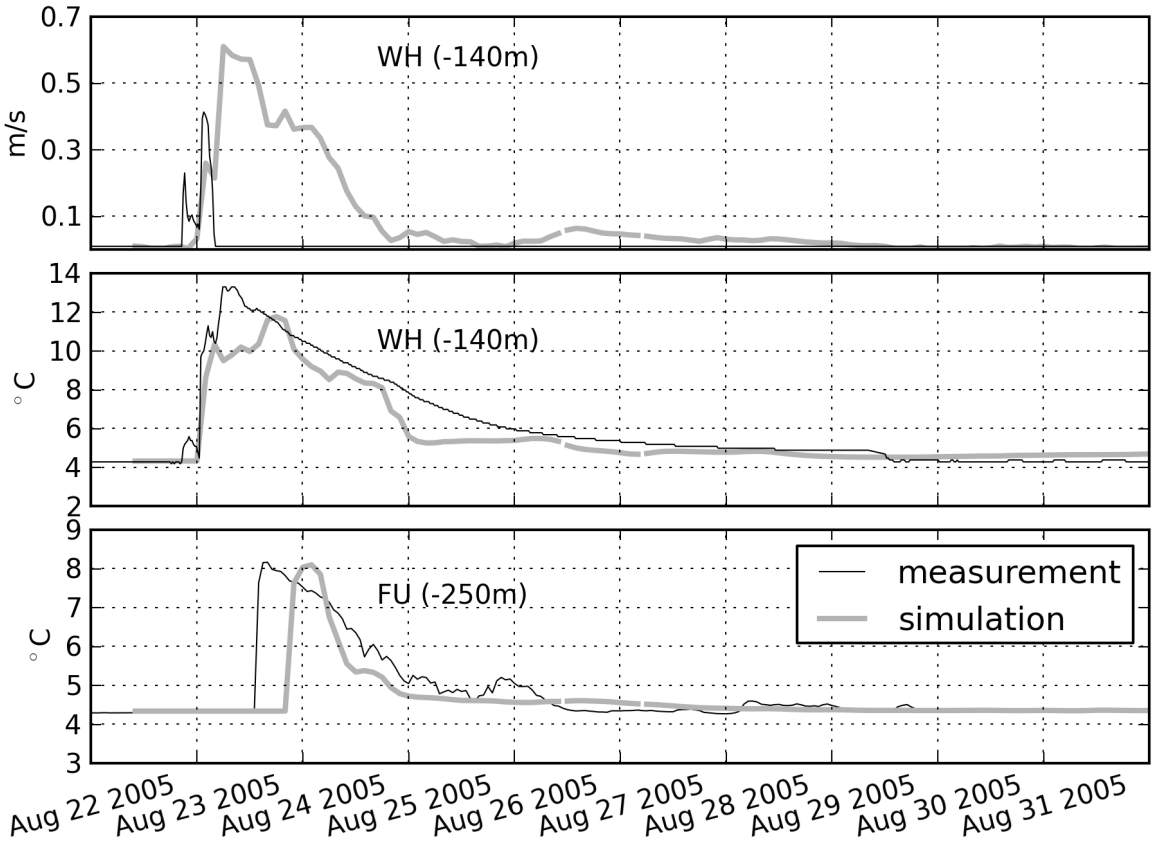

Figure 3.5: Speed (upper panel) and water temperature (middle panel) at mooring WH and water temperature at mooring FU (lower panel).

Figure 3.6 shows the simulated water temperature and suspended sediment concentrations in a longitudinal transect of the lake. The transect is shown in figure 3.2. It follows the thalweg through the whole lake. Four time steps are shown: at the beginning of the flood event, during the peak flow in the Alpine Rhine and shortly after the peak. The warm turbid underflow travels down to the deepest point with an average speed of 0.25 m/s. At the beginning of the event, close to the river mouth an interflow is formed: part of the river water with lower sediment concentration enters the thermocline, only visible in the sediment concentrations, not in the temperatures. Especially in the last plot, at the upper boundary of the underflow, plumes of rising water are visible in both temperature and suspended solids concentration. These plumes are 1-2 °C warmer than the surrounding water. Simulated vertical velocities in the plumes are ≤ 0.013 m/s.

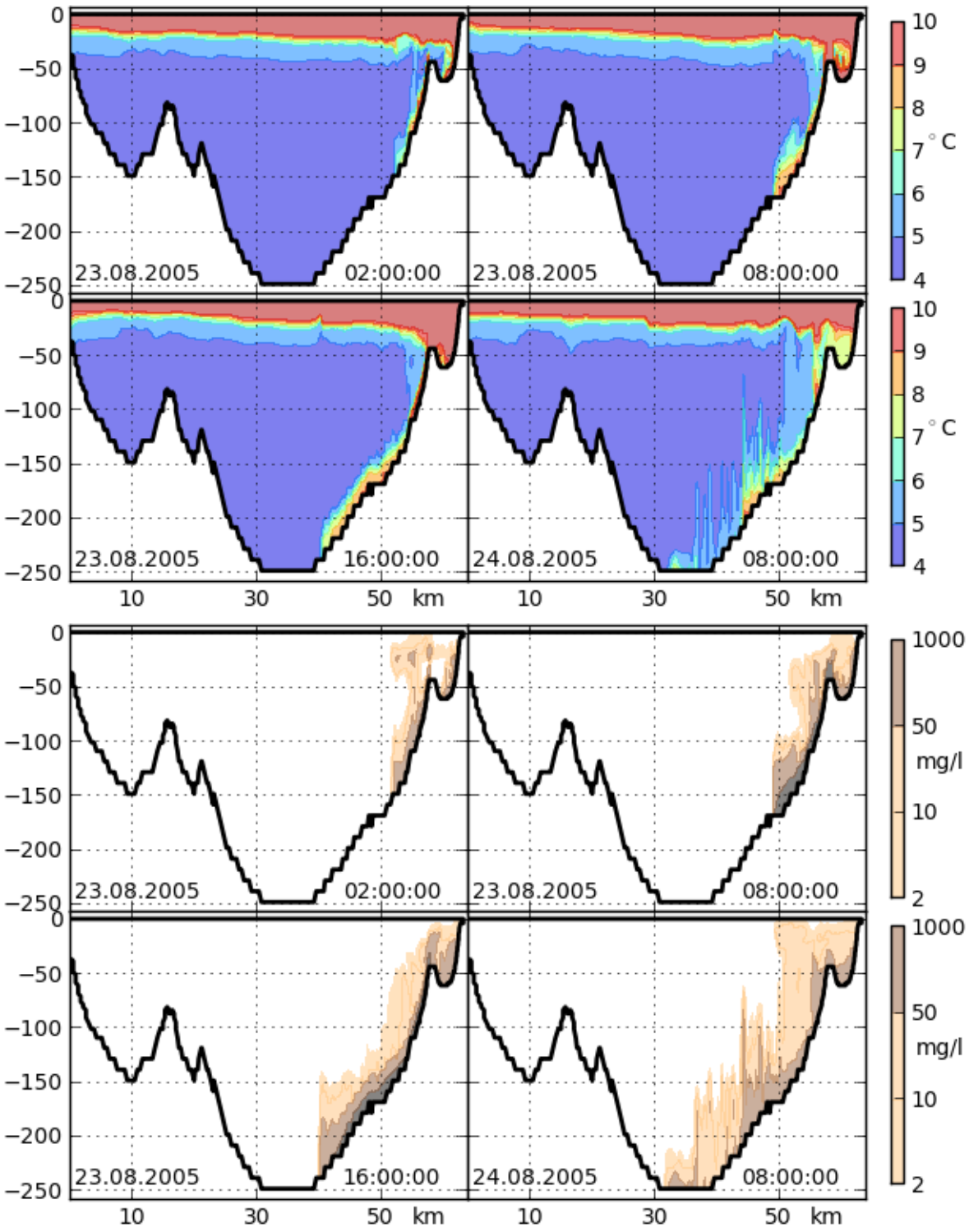

Figure 3.6: Longitudinal transect of Lake Constance: Simulated water temperature and sediment concentration.

Influence of earth rotation:
The underflow's tilt towards the northern shore observed in the measurements (see figure 3.3 in section 3.1.1) is also visible in the simulation (figure 3.7).

A possible reason for that is the Coriolis force deflecting the underflow to the right and thus pushing it up the slope.
Whether the Coriolis force has a significant influence on a current can be estimated with the dimensionless Rossby number Ro, comparing the inertial force to Coriolis force:

$$Ro = \frac{u}{L * f} \tag{3.2}$$

where u: current speed [m/s]
L: distance [m]
f: Coriolis parameter (depending on latitude) [1/s]

The Rossby number is a measure for the ratio of inertia to Coriolis force. For small Rossby numbers ($Ro << 1$), the influence of earth rotation can not be neglected. In this case, u is taken as 0.4 m/s, L (from the mouth of Alpine Rhine to the Bay of Friedrichshafen) is about 25 km and the Coriolis parameter f is at Lake Constance (47° North) 0.000106371 s^{-1}.
Ro is thus 0.15, saying that the rotation of the earth can not be neglected.

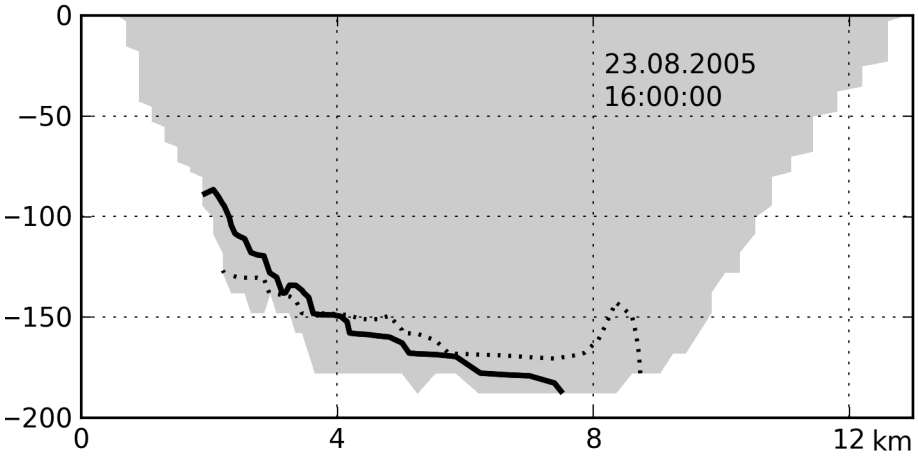

Figure 3.7: Asymmetry of the underflow: Simulated sediment concentration in transversal transect, isoline 40 mg/l, in simulation with (solid line) and without (dotted line) accounting for Coriolis force.

A reference simulation with the Coriolis effect turned off also shows that the flow path of the underflow is significantly influenced by the earth rotation. Figure 3.7 shows the transversal transect (see figure 3.2). The view is upstream, i.e., the northern shore is on the left. Isolines are 40 mg/l suspended solids concentration. The simulated underflow not affected by Coriolis force lies almost flat on the lake bottom, whereas the one with Coriolis is tilted almost in the same angle as the measurements are indicating.
Figure 3.8 shows the underflow in the two simulations in a three dimensional view: The lake is cut at the position of the curtain in figure 3.7. View is towards the mouth of the Alpine

Rhine, e.g., upstream the underflow. Time and concentrations are the same as in figure 3.7. In the simulation neglecting the Coriolis effect, the underflows spreads more to the right, i.e. towards the Swiss shore.

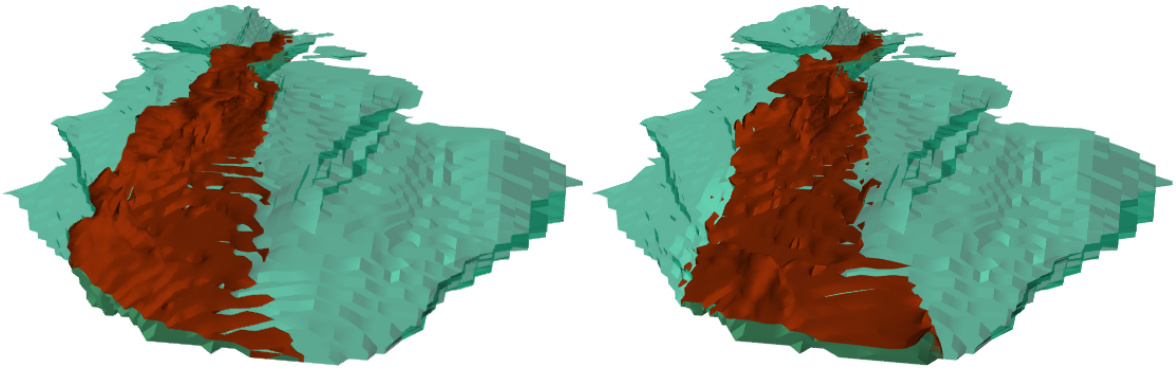

Figure 3.8: Asymmetry of the underflow: Simulation with Coriolis effect (left) and simulation without Coriolis effect (right). Isosurfaces are concentration of suspended solids >= 40 mg/l, 23.08.05 16:00.

The Coriolis force also influences the distribution of the fluvial sediments on the lake bottom after the event. Figure 3.9 shows the simulated sediment distribution at the lake bottom after the underflow has disappeared. In the simulation without Coriolis force (dashed lines), the underflow went more towards the southern shore, especially in the direction Bay of Arbon and Romanshorn. But it also reached more north-western points along the thalweg. The Coriolis-influenced underflow (solid lines) stayed closer to the northern shore and entered the Bay of Friedrichshafen. It did not go as far along the thalweg.

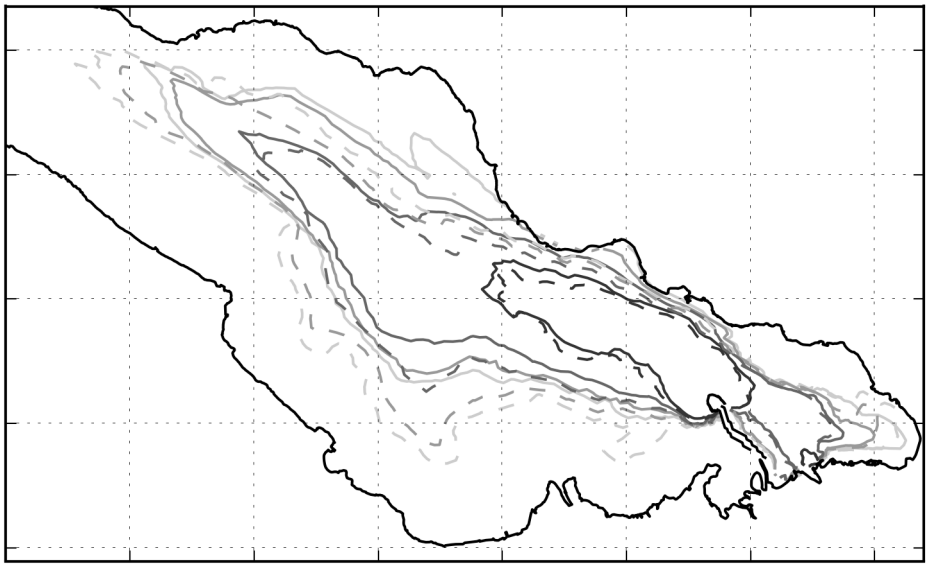

Figure 3.9: Deposited sediments at the lake bottom: Simulations with (solid lines) and without (dashed lines) Coriolis influence. Isolines of 10^2, 10^3, 10^4 and 10^5 g/m^2.

Güde et al. (2009) subdivided the area of the lake bottom of Upper Lake Constance into five sediment provinces. The province "allochthonous Alpine Rhine", that is dominantly characterized by sediments originating from the Alpine Rhine, covers the area on the right side of the thalweg. Close to the mouth of the Alpine Rhine, the area is quite narrow, but later on it expands to a width of approximately 10 km. The shape of the province indicates a common influence of the Coriolis force on the water of the Alpine Rhine. Compared to the area covered by deposited sediments from the August 2005 flood in the simulation (figure 3.9), the sediment province "allochthonous Alpine Rhine" is even more restricted to the northern shore, and it reaches farther along the thalweg. Most parts of that deposition area not covered by the sediment province "allochthonous Alpine Rhine" lie in the sediment province "allochthonous transition zone". Here sediments from the tributaries Bregenzerach and Alpine Rhine are still dominating, but autochthonous material is more important than in the sediment province "allochthonous Alpine Rhine".

Internal surge

As the rain event on August 22 was also accompanied by strong wind, the underflow is not the lake's only hydrodynamic response: in figure 3.6, a clear tilt of the thermocline to the right (to the south-east) is visible. In addition, almost exactly at the height of the tip of the underflow, an internal surge travels along the thermocline. At the measurement buoy of the

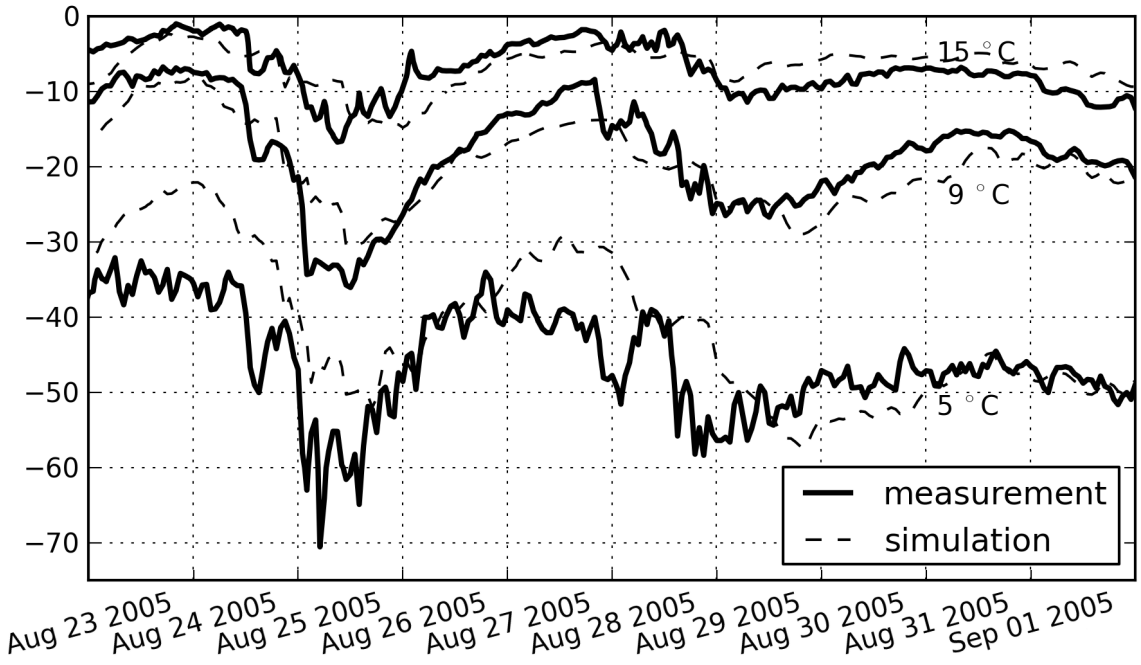

Figure 3.10: Internal waves at the measurement buoy in Lake Überlingen.

University of Constance in Lake Überlingen (green triangle in figure 3.2), this internal surge was detected in the thermistor chain measurements. Figure 3.10 shows the 15, 9 and 5 °C isolines in measurement and simulation. The internal surge first reaches the measurement buoy in the evening of August 24. The largest amplitude is reached on August 25, when the

surge is returning after being reflected at the north-western end of Lake Überlingen. Three days later, on August 28, the wave is arriving once again from south-east.

Even though it travels exactly parallel to the underflow, the surge seems to be independent of the flood event: In a simulation run without in- and outflows, the internal surge appears as well.

3.1.4 Conclusions

A huge turbid underflow caused by a flood in the major tributaries was observed in Lake Constance. Based on measurements originating from moorings at the lake bottom and ship measurements, flow path, shape and magnitude of the underflow can be described in detail. The dominating processes could be reproduced with a rather simple model set-up. The Coriolis force was identified to be an important influence on the underflow path and on the distribution of the particles sedimented on the lake bottom after the event.

3.2 Lake-Wide Distributions of Phytoplankton and Temperature

Several coupled hydrodynamic-ecological models have been applied to Lake Constance by Peeters et al. (2007a), Peeters et al. (2007b), Rinke et al. (2010, 2009a), Kerimoglu et al. (2013), and others, studying different questions. Most aquatic ecosystem models are one-dimensional, they concentrate on the vertical dimension, assuming horizontal gradients to be small compared to vertical.
But, especially in large lakes, horizontal patchiness in biological parameters can be considerable. Often this is due to external factors, i. e. gradients in physical conditions such as water temperature, light and nutrient availability. Internal factors and randomness can either enlarge the effects of the physical gradients, or even produce biological patchiness in a homogeneous physical environment (Hillmer et al., 2008; Vilar et al., 2003). Three-dimensional aquatic ecosystem models can at least account for the part of biological patchiness that is due to physical drivers. However, monitoring of lakes is often done in a one dimensional way, measurements are available only for one, or few, profiles. So the three-dimensional model is lacking a possibility for verification.

In this section, results of a three-dimensional simulation are compared to measurement data obtained in a lake-wide field campaign in Lake Constance in spring 2007.

3.2.1 Field Campaign 2007

In May 2007, a field campaign to measure the three-dimensional distribution of temperature, phyto- and zooplankton, and fish in Lake Constance was conducted by the Limnological Institute of the University of Constance, the Institute for Lake Research, Langenargen, and the AWBR (Rinke et al., 2009b).

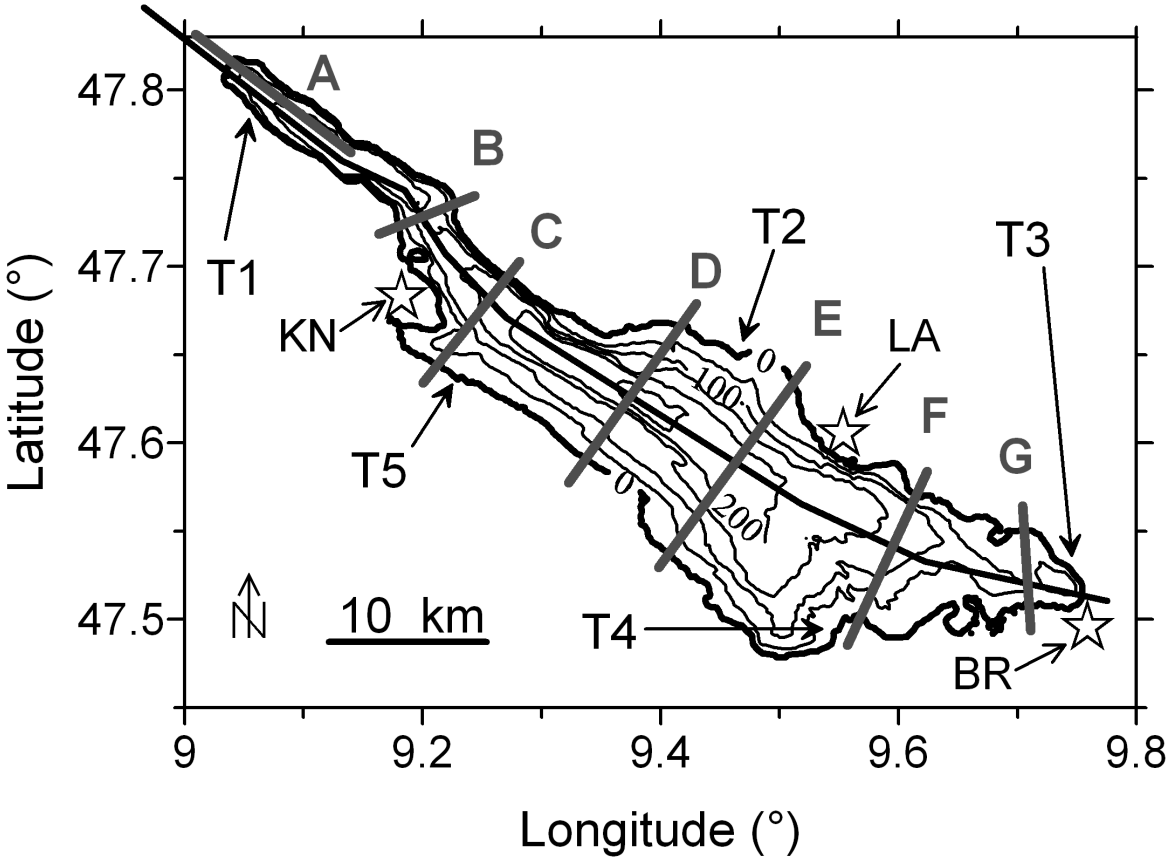

Figure 3.11: Location of the longitudinal cross section (black line) and the 7 transversal cross sections (A-G, grey lines). Positions of five thermistors (T1-T5) are indicated by arrows. Meteorology measurement locations are indicated by stars. Map from Rinke et al. (2009b), modified

Five thermistors were employed in the littoral zone of Lake Constance. These thermistors, distributed almost equally around the lakes shore, achieved a continuous temperature measurement over the whole sampling period from mid of March till end of May and by that provided information about the dynamics of temperature distributions and the spatial extent of upwelling events. All thermistors were fixed at a water depth of 1.5 m. Water temperatures measured by the thermistors are shown in figure 3.12. For thermistor locations see figure 3.11.

Ship measurements were taken along seven transects in Lake Constance covering the whole lake. In order to assess the lake-wide 3D-distribution of temperature and chlorophyll all transects were sampled during two campaigns on 10 May 2007 and on 16 May 2007 (Figure 3.16). In addition, two transversal transects in the middle of the lake (transects C and D) have also been sampled on 25 April 2007 and on 03 May 2007, i.e. one and two weeks before the whole-lake campaign. (Figure 3.14) The sampling of all transects resulted in 48 profiles taken quasi-synoptically by three research vessels, which sampled all transects within 6-7 hours depending on the wind conditions. A longitudinal section along the main axis of the

lake was sampled by two research vessels on 07 May 2007, i.e., three days before the first whole-lake assessment. This sampling took place within 8 hours and is comprised of 26 profiles. The horizontal distance between these sampling points varied between 250 m and approximately 3.5 km (figure 3.13). For locations of the transects see figure 3.11.

Meteorological conditions were measured at three locations: by the LUBW/ISF in Langenargen (LA, only wind speed and direction), by the DWD in Konstanz (KN, wind speed and direction, air temperature, short wave radiation, humidity, cloud cover), and by the municipality of Bregenz in Bregenz (BR, wind speed and direction, air temperature, short wave radiation, humidity). Wind speed and direction were measured at 10 m height. For locations of the measurement stations see figure 3.11.

During the measurement period, at May 8 and 9, strong wind from westerly directions with peak velocities of 13 m/s in Friedrichshafen were recorded.

3.2.2 Simulation

A uniform horizontal grid with a mesh size of 400 m was used. Vertical grid sizes varied gradually between 2.5 m in the epilimnion and 10 m in the hypolimnion of the lake. The minimum water depth of littoral grid compartments was set to 3 m, to make sure that there are always at least two vertical layers in each horizontal cell, as in cells with one single layer baroclinic flows are not possible leading to unrealistic temperatures (Appt, 2003).

The simulation time step was set to 240 s.

The parametrisation of the water quality model CAEDYM used in this study is described in Rinke et al. (2010).

Boundary conditions
The wind field for the surface stress boundary condition was constructed by linear spatial interpolation of measurements from the three stations Konstanz, Langenargen and Bregenz. To account for the smaller roughness over the lake, wind speeds were increased by 30 % (Zenger et al., 1990). Surface heat fluxes were modelled using the wind field and hourly measurements of air temperature, humidity, solar radiation and cloud cover of DWD measurement stations in Konstanz and Bregenz. Incident atmospheric long wave radiation was calculated from air temperature, humidity and cloud cover using the formula of Iziomon et al. (2003). Flow boundary conditions from 14 rivers and 13 waste water treatment plants were integrated in the simulation setting as lake inflows. Nutrient concentrations of the inflows were calculated using runoff-concentration-dependencies obtained from measurements in the tributaries in the years 1996 and 1997 (Bührer et al., 2000). To take into account the reduction of inflowing phosphorus over the years, the resulting phosphorus concentrations were reduced by 35 %. The model was initialized with a flat free surface, zero velocities all over the lake and a horizontally uniform single vertical profile for temperature and water quality parameters measured at the deepest point of the lake at 02 April 2007. The measured phytoplankton concentration was equally distributed on the four phytoplankton groups.
The simulated period covered days 92 - 136 (02 April - 16 May) of 2007. Starting day of

the simulation was determined by the dates of measurements of the physical and biological parameters and the need for a sufficient spin up time of the hydrodynamic model, which was identified by Appt et al. (2004) to be at least 9 days under low wind forcing. Since in our field campaign the first measurements were taken at April 25, we achieved more than three weeks for model spin up, which should be a sufficient time scale for the model states to settle down to local and seasonal conditions.

3.2.3 Results

Temperature in the littoral zone (thermistors)

In April the temperature at all thermistor locations showed a consistently increasing trend (Figure 3.12) reaching maximum temperatures at the end of April. Temperature recordings of the thermistors were at some times very similar but at other times, particularly when wind forcing was more intense, quite different resulting in temperature differences that were up to 5 °C. In both model and reality a diurnal temperature cycle is visible, but daily fluctuations in the model were of a lower magnitude. Overall, the intra- and interday variation of temperature appeared to be lower in the simulation than in the field measurements indicating a smoothing effect in the model. T5 has the best accordance between measurement and simulation (r^2=0.94), followed by T1 (r^2=0.89). Large systematic differences between simulated and measured temperature were apparent for locations T3 (absolute error = mean (simulated values − measured values) = -2.3) and T4 (absolute error = -1.6); simulated temperatures were too low throughout the heating period. From 04 May on, the agreement between simulation and measurement at T4 increased considerably. According to the spatial arrangement of the thermistors it is noteworthy to emphasize that temperatures measured by thermistors exposed in the western part of the basin were reproduced rather good while those in the eastern basin were characterised by poorer agreement between measurement and simulation. Although at T2 the model reproduced the temperature with a relatively high accuracy, it was unable to reproduce the wind-induced temperature fluctuations at the end of April and the first week in May. Temperature drop due to the wind event on May 08 and 09 was, however, simulated in good agreement with observations at T2. At T3, the model reproduces the temperature drop due to wind on April 30 and May 1, but not the returning of the warm water immediately afterwards. The upwelling due to the wind event on May 08 and 09 is most clearly visible in temperature data of thermistors T1, and T5, and less pronounced in T2, while T3 and T4 hardly show any response to the event. In general, the dynamics induced by the stronger and longer lasting wind event on May 08 and 09 were reproduced by the model with a higher accuracy than the corresponding dynamics are the wind event on April 30 and May 1.

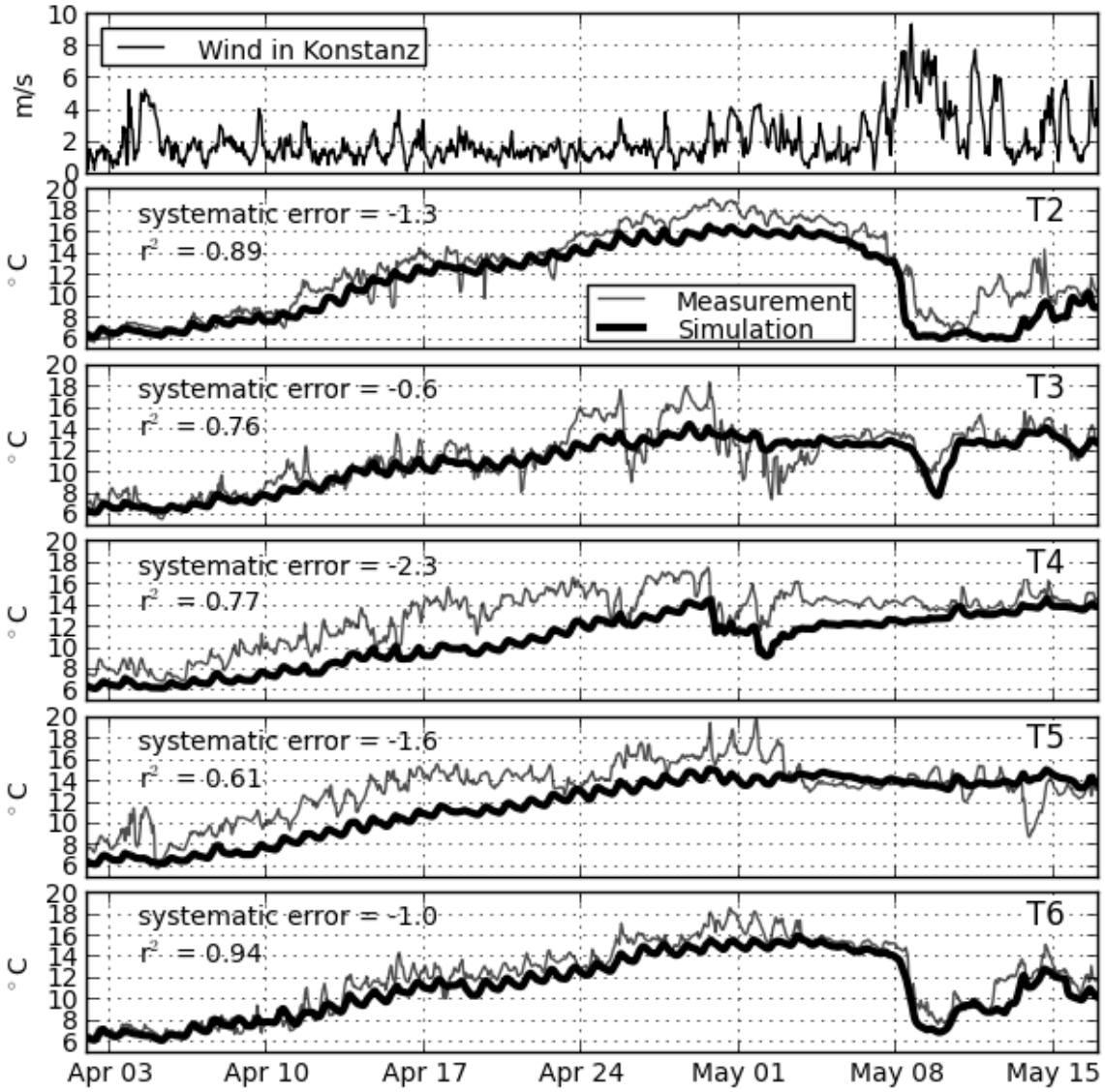

Figure 3.12: Wind speed measured in Konstanz and water temperatures at thermistors T2-T6 in measurement and simulation.

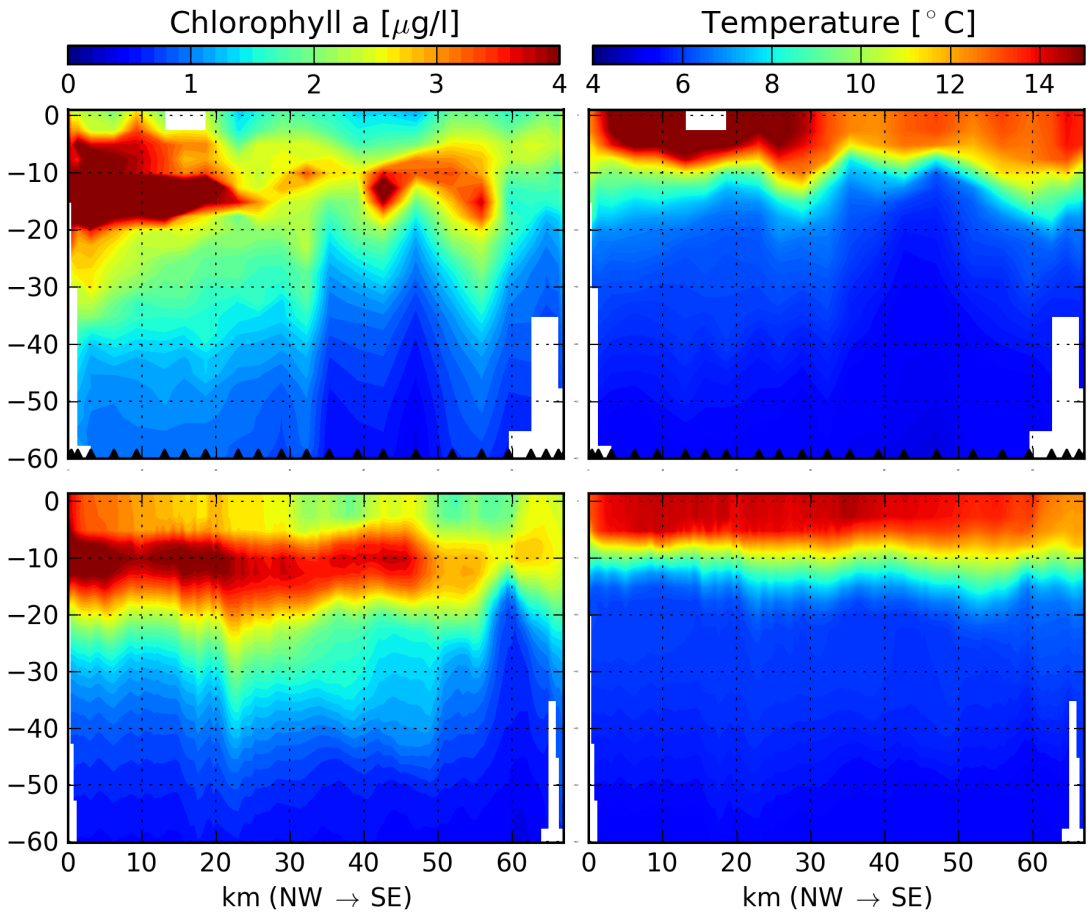

Figure 3.13: Longitudinal transect, chlorophyll a concentration and temperature in measurement (upper row, black triangles at the bottom indicate the measurement locations) and simulation (lower) on May 07.

Spatial distribution patterns of temperature and phytoplankton

The longitudinal transect on May 07 (figure 3.13) showed a slightly varying thickness of the epilimnion, indicating the presence of internal waves, with highest surface temperatures in the western part of the lake (Lake Überlingen, left end of the displayed transect). The model reproduced the observation of highest temperatures in Lake Überlingen and also the vertical thermal structure of the lake. However, horizontal temperature differences were less pronounced in the model output than in the observation and also internal wave activity along this transect was much weaker in the model. Phytoplankton concentrations were found to be higher in Lake Überlingen. Maximal phytoplankton abundance occurred between 10 m and 20 m depth. These patterns were also evident in the simulations.

The comparison of simulated and measured water temperatures along transect D is shown in figure 3.14. Transect D crosses the longitudinal transect perpendicularly close to the deepest point of the lake. The hydrodynamic model reproduces internal waves under low wind condition as well as the reaction to the wind event at May 08 and 09. At the first sampling date on April 25 when wind velocities had been very low (< 4 m/s the preceding 5 days) no thermocline tilt was visible. The thermal stratification was homogeneous along the transversal axis of the transect and this observation was reproduced by the model. The vertical distribution of phytoplankton was characterized by a subsurface chlorophyll maximum at depths between 10 and 15 m. Horizontal phytoplankton distribution was not uniform. Concentrations were higher (more than 4 μg/l) in the northern part, and the depth with maximum concentrations was shallower than near the southern shore. The model reproduced the pattern qualitatively, i.e. a subsurface maximum of phytoplankton that is slightly tilted towards the southern shore. From a quantitative perspective, however, the spatial distribution patterns in the model deviated from the observations and were less distinct. On May 03 the epilimnion became thicker and warmer on the southern shore than on the northern shore, resulting from wind from northern directions during the preceding days. This thermocline tilt is also visible in the chlorophyll distribution leading to maximum concentrations on the southern shore. Again, the model nicely reproduced temperature distribution along transect D but simulated patterns of phytoplankton distribution complied with observed distribution mainly in terms of qualitative patterns.

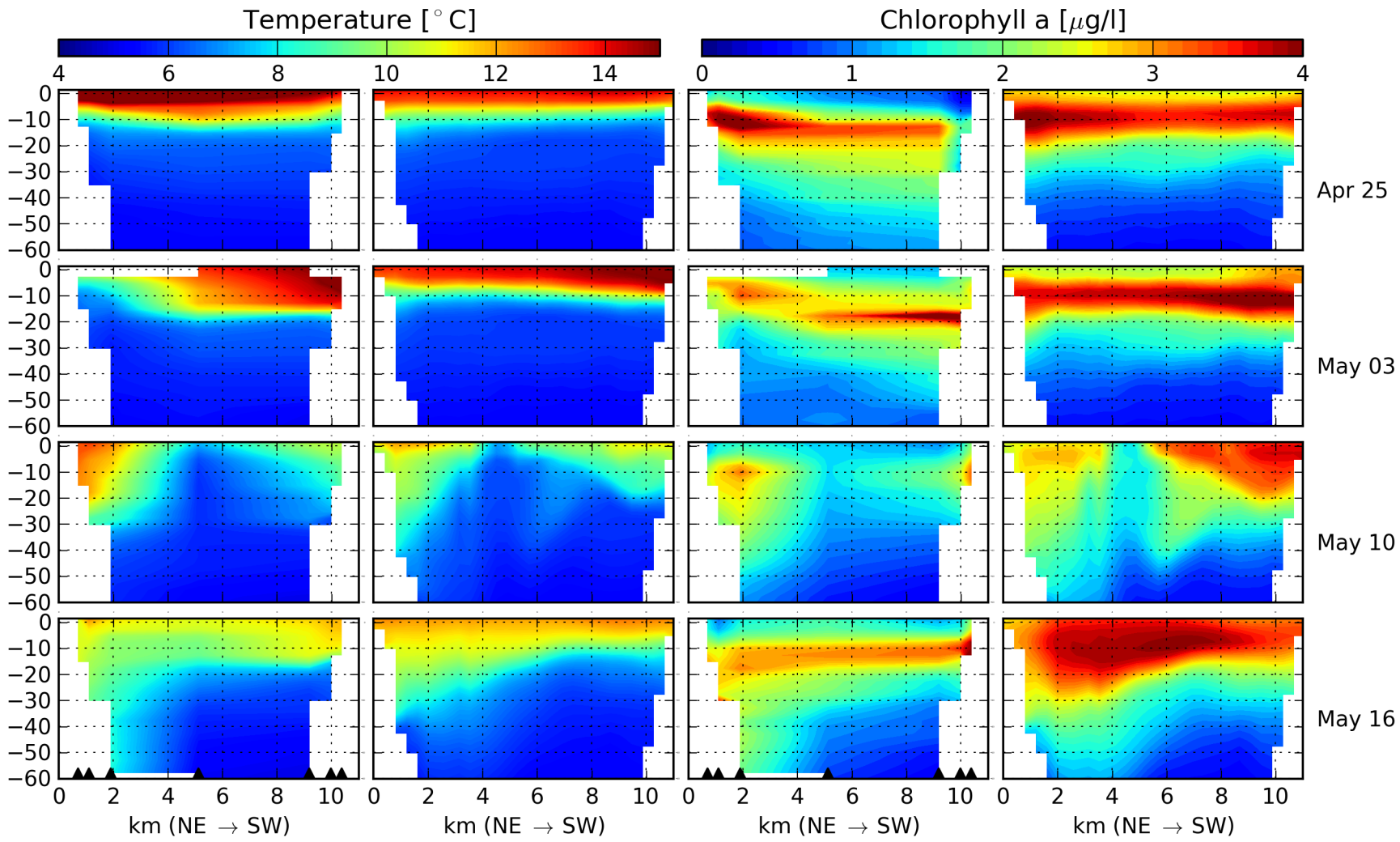

Figure 3.14: Transversal transect, temperature and chlorophyll a concentration in measurement (column 1 and 3) and simulation (column 2 and 4)

Figure 3.15: Conceptual sketch of surface currents during (left) and after the wind event.

The wind event from WSW on May 08 and 09 caused a considerable epilimnetic flow current into the eastern basin. In consequence, we observed a strong upwelling of hypolimetic water in Lake Überlingen and in the western part of the main basin on May 10 (see also figure 3.16 for horizontal distributions). In the central basin a tongue-shaped front of cold water is visible in the middle of the warm water zone in the western part of the lake. Model results showed the formation of this structure (figure 3.15): The surface current caused by the wind event is deflected southwards by the Coriolis force and thus pushes the epilimnion towards the south-east. On May 10 wind velocities decreased and the epilimnetic water started to float back, again deflected by the Coriolis force along the north-eastern shore, leaving in the central part of the main basin the tongue of cold water.

Transect D crisscrossed this structure showing warm water on both shores and cold water in the central part, which was precisely reproduced by the model. Since chlorophyll concentrations were lower in the cold water originating from deeper layers, a similar pattern was observed in the phytoplankton distribution along transect D on this day, with low concentrations in the centre and higher concentrations on the shores. As before, the simulation outputs complied with observations qualitatively.

One week after the wind event, on May 16, the thermal stratification was re-established in the whole basin, but surface temperatures were not as high as before the storm, indicating vertical mixing by the storm event. Although the horizontal distribution of temperature and chlorophyll in the surface layer was not disturbed by major wind events, it was characterized by a certain heterogeneity that emerged also in the simulations. In transect D, the epilimnion became thicker in the north, while the highest temperatures were found close to the southern shore, which complied to the simulation outputs. The phytoplankton showed higher concentrations in a shallower depth towards the southern shore. While the model showed maximal chlorophyll concentration in the centre of the transect, the tilting of the algal containing layer was visible in the simulation outputs.

The model also reproduces the horizontal temperature distribution in 5 m depth (figure 3.16): Highest water temperatures can be found in the eastern part of the lake (approximately 14 °C). At the northern shore of the main basin, a region with colder water (approximately 8 °C) indicate upwelling from deeper layers at the sill of Mainau. The chlorophyll distribution shows a different picture. In the measurements, two spots with high concentra-

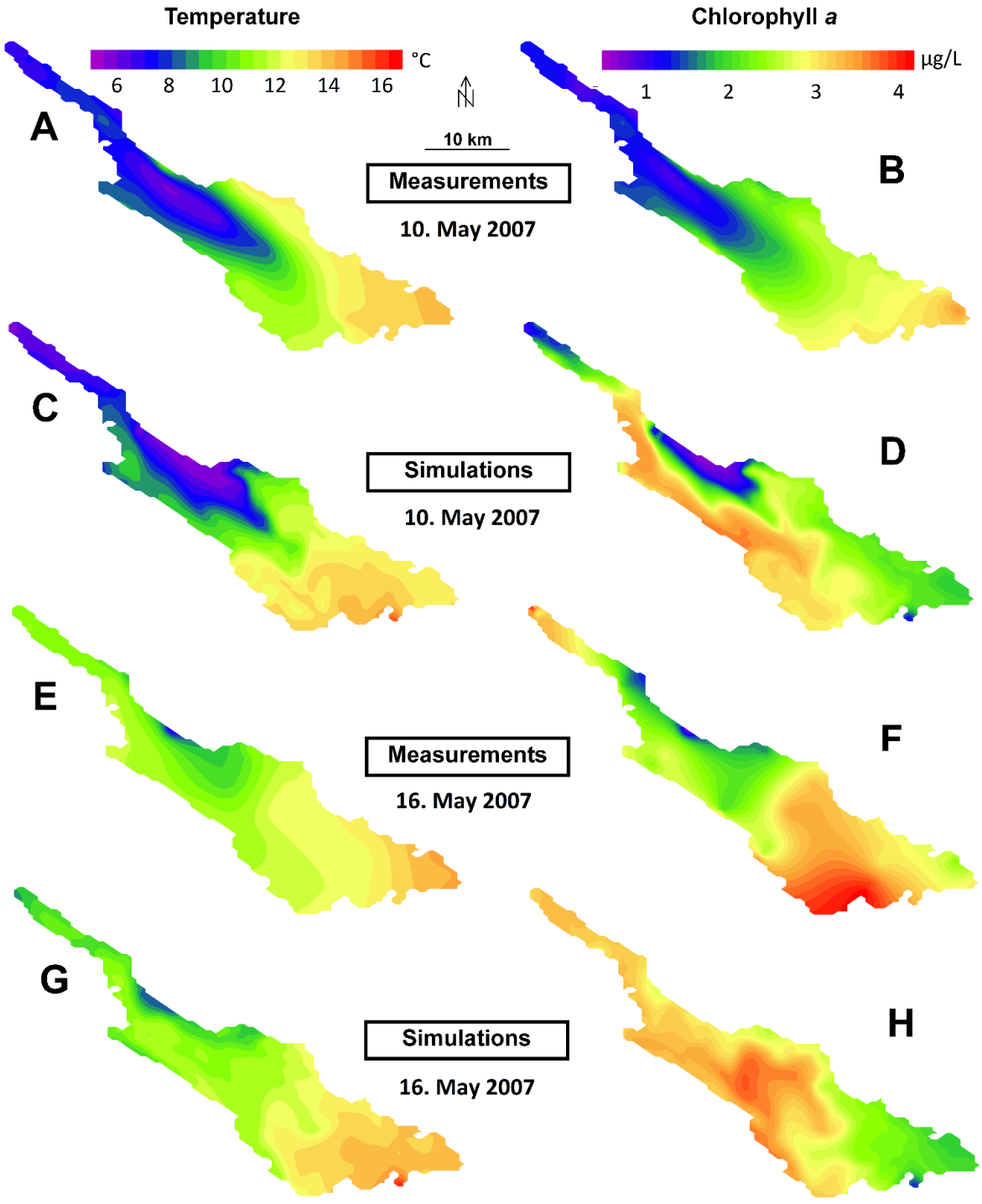

Figure 3.16: Horizontal distribution of water temperature and phytoplankton concentration in 5 m depth.

tions of phytoplankton are visible. Highest concentrations of up to 4 μg/l can be found in the southern main basin. Values of 3.5 μg/l are reached in the western end of Lake Überlin-

gen. Lowest concentrations can be found in the regions with lowest water temperatures.
In the simulation, the pattern of phytoplankton is stronger connected to the temperature: Highest chlorophyll concentrations can be found in the areas with moderate water temperatures around 11 °C. Both the cold upwelling region and the warmest areas show lower simulated chlorophyll concentrations.

The simulation produces a certain patchiness of chlorophyll in the horizontal distribution, and the range of chlorophyll concentrations is not much lower as in the measurements, but the pattern looks completely different.

3.2.4 Conclusions

During a field campaign in spring 2007, both the three-dimensional distribution and the temporal development of temperature and chlorophyll a was measured in Lake Constance. The horizontal distribution of phytoplankton proved to be dominated by the hydrodynamics under strong external forcings (i.e. during and immediately after strong wind conditions). In the absence of strong external forcings, phytoplankton patchiness was dominated by internal (biological) effects (Rinke et al., 2009b). ELCOM-CAEDYM reproduced the hydrodynamics, i.e. the water temperatures. The model proved to be able to account for patchiness in biological variables if they are caused by hydrodynamic drivers, such as internal waves, wind-induced surface currents and horizontal gradients in water temperatures. In situations without strong external drivers, the model produces some patchiness as well, but the pattern is different. One reason for this may lie in the simplified representation of the food web (only one zooplankton group, no fish). But there is certainly also random affecting the patchiness, which can not be reproduced by the deterministic model.

3.3 Long-Term Evolution of Temperature and Oxygen in the Hypolimnion

Climate change is not shifting from one state to the other within few days. Moreover it is a process permanently active and ranging over several decades. To analyse the effect of gradients in change, models have to be capable to run over a multitude of years.

In this section, the ability of ELCOM-CAEDYM to simulate long time periods is validated by running the model over several decades.
It is of special interest, whether the model is able to reproduce the observed cycle of stratification and mixing properly, and especially the deep water renewal and heat budget of the lake. Coupled to the question of deep water renewal, also hypolimnetic oxygen concentrations are studied.
The parametrisation of the water quality model considers nutrients (C, N, P, Si), phyto- and zooplankton.

The simulation period, also referred to as reference period, comprehends the years 1980 – 2000. This period was chosen, because measurement data was available both for boundary

conditions for the model (meteorology, tributaries) and verification (physical, chemical, and biological state of the lake).

3.3.1 Monitoring data 1980-2000

Meteorological data were provided as hourly measurements, except rain which is daily, at the DWD (German Meteorological Service) station in Konstanz.

The water temperature and water quality data were collected within the Lake Constance water information system BOWIS (Bodensee–Wasserinformationssystem), organised by the International Water Protection Commission for Lake Constance IGKB (Internationale Gewässerschutzkommission für den Bodensee). Measurements were taken every two to four weeks at the deepest point of the lake in 12 (partly 15) defined water depths of 0, (1, 2.5,) 5, (7.5,) 10, 15, 20, 30, 50, 100, 150, 200, 230, 250 meters. In 1995, temporal resolution increased from approximately monthly to approximately fortnightly, and in 1999 vertical spatial resolution decreased from 15 to 12 depths. In the simulation period, complete mix-

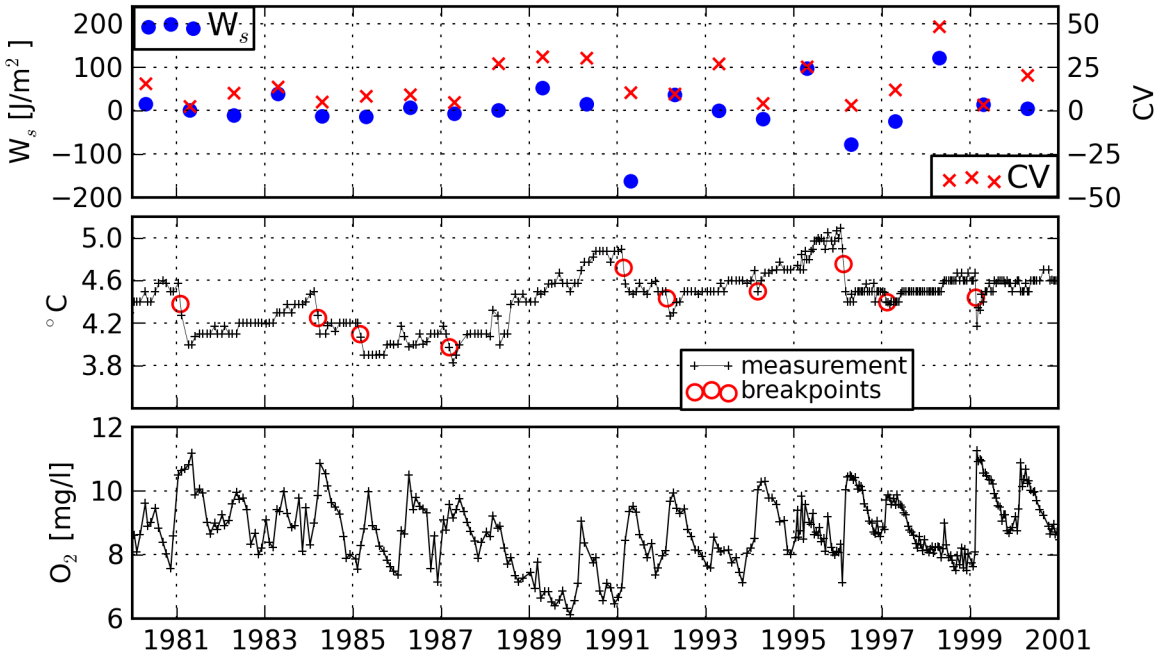

Figure 3.17: Upper panel: Yearly minimum values of W_S and CV, middle panel: deep water (below 200 m) temperature, lower panel: deep water oxygen concentration

ing took place in the beginning of year 1981, 1984, 1985, 1986, 1987, 1991, 1992, 1994 1996, 1997 and 1999, whereas the years 1982, 1983, 1988, 1989, 1990, 1993, 1995, 1998, the lake remained stratified throughout the winter season.

To quantify the mixing of a lake, several characteristics can be used. Roßknecht et al. (2007) used the yearly minimum coefficient of variation CV of measured PO_4 concentrations to

quantify mixing in Lake Constance.

$$CV = \frac{s_x}{\bar{x}} \tag{3.3}$$

where s_x: standard deviation of values in the profile
$\bar{x}$: average of values in the profile

They stated values below 0.1 for years with intense mixing, and much higher values in years with weak mixing. In figure 3.17, the yearly minimum CV values are shown as red crosses in the upper panel. When analysing longer time series of CV of measured PO_4, one has to keep in mind, that the reoligotrophication alters the vertical distribution of phosphorus in the lake and thus the values of the highly eutrophic period in the early 1980ies can not directly be compared to those of the years around 2000. The increasing trend in CV in the years without mixing, thus can not necessarily be interpreted as an increase in stability.

Another measure for the stability of lake stratification is the Schmidt stability (Schmidt, 1914, 1928), as cited in Idso (1973):

$$W_s = \frac{g}{A_0} \cdot \int_{z=0}^{z_{max}} (z - z_*) \cdot (\rho(z) - \bar{\rho}) \cdot A(z) dz \tag{3.4}$$

where W_s: work required to destroy the stratification [J/m^2]
A_0: surface area of the lake [m^2]
$A(z)$: area of the lake in depth z [m^2]
$\bar{\rho}$: average density of water [kg/m^3]
$\rho(z)$: density of water in depth z [kg/m^3]
z: depth (positive downwards) [m]
z_*: depth, where $\rho = \bar{\rho}$ [m]
The densities ρ were calculated from temperatures using equation 2.1.

The Schmidt stability is a very accurate measure for the stability of a lake's stratification (in case there are accurate measurements available), but it describes only a snap-shot, without any temporal development.
In figure 3.17, the yearly minimum W_s values are shown as blue circles in the upper panel. Years with complete mixing show generally small values of W_s. Negative values of W_s indicate an unstable stratification. The largest negative values arise in the years with the largest decrease in deep water temperature (1991, 1996). In the year 1992, yearly minimum W_s values were positive, even though mixing did occur, presumably because of the sparse temporal sampling resolution.
The other way round, small or even negative values of W_s do not necessarily mean, that the lake mixed completely.

Complete mixing events are visible as significant drops in hypolimnetic water temperatures. The detection of such break points in time series can be done by calculating a moving average and moving standard deviation over a time series and comparing the last value in the time window to it. If this value is lower than the mean minus n times the standard deviation, it is assumed that the temperature drop is significant, and it is likely that mixing had taken place. A time window of one year and n = 1.5 was found to be suitable to detect most of the mixing events in the measured deep water temperature time series of the reference

period.
In 1986, deep water temperatures were so low and close to the density maximum already before the mixing, that the moving standard deviation could not detect any step in the temperature data, but the increase in oxygen in the deep hypolimnion indicate mixing, as well as the low CV and low Schmidt stability.
In 1994 again almost no temperature drop is visible, even though oxygen, CV and Schmidt stability indicate mixing, and the deep water temperature is rather high (4.6 °C). In that winter, the main driving force for mixing seemed to be not the cooling, but wind: Roßknecht et al. (2007) counted 400 hours with average wind velocities above 6 m/s between November 1993 and March 1994, while for the other winters of the reference period this values lies between 30 and 230. Average air temperature in the months November - March was 3.8 °C in 1993/94. In the other winters with mixing, average air temperature was between 1 °C and 2.8 °C. In those years without mixing average air temperature ranged mainly between 3 °C and 4.3 °C, except 1982, where average air temperature was 1.8 °C.

For the years without complete mixing events, the mixing depth z_m was obtained from profile measurements of PO_4. The mixing depth is defined as the depth separating an upper layer with almost uniform values of a selected variable from a lower layer with rapidly changing values (Salmaso, 2005; Goldman and Jassby, 1990). In this study, measurement profiles of PO_4 concentrations were used to determine the maximum winterly mixing depth. The accuracy of the mixing depth strongly depends on the vertical and temporal sampling resolution. Table 3.1 gives the maximum winter mixing depths for the years without complete mixing.

Table 3.1: Maximum mixing depths

year	1982	1983	1986	1988	1989	1990	1993	1995	1998	2000
$\mathbf{z}_m$ **[m]**	100	100/150	230	150	100	150	100	100	100	200

Gradient in air temperature
The simulated period is a period of relatively strong temperature increase. A linear regression on the temperature data yields a gradient of 0.07453 °C/a, though an increase of 1.565 °C within the simulation period. An empirical mode decomposition (EMD, Huang et al. (1998)) results in a comparable gradient, here the overall increase is 1.588 °C (see figure 3.18).
In figure 3.19, a longer time period is shown: between 1971 (begin of hourly measurements of air temperature in Konstanz) and 2011, the temperature gradient gained by linear regression is only 0.047 °C/a, and that from EMD is even smaller (0.0334 °C/a)
To test the significance of the gradients in air temperature, a Mann-Kendall test (Kendall, 1970) was performed on the two time-series of daily average air temperatures. Both trends turned out to be highly significant ($\alpha < 0.01\%$).
The air temperature gradient is accompanied by changes in the other meteorological variables: the relative humidity tends to decrease slightly (linear regression: -0.11%/yr, Mann-Kendall-test: significant with $\alpha = 5\%$), solar radiation shows no trend, incident long wave radiation increases significantly (0.36 W/m^2/yr, $\alpha < 0.01\%$), and the wind speed shows also no significant trend.

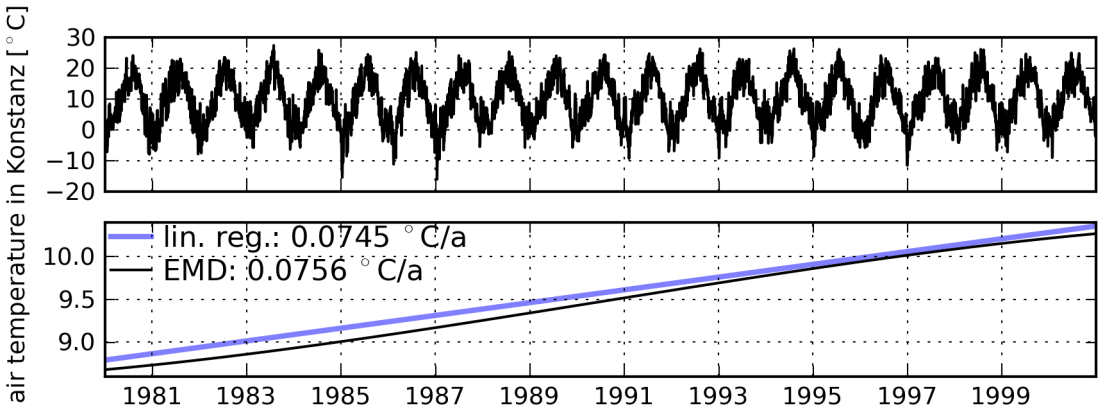

Figure 3.18: Upper panel: Daily average air temperatures, lower panel: gradients obtained by linear regression and EMD.

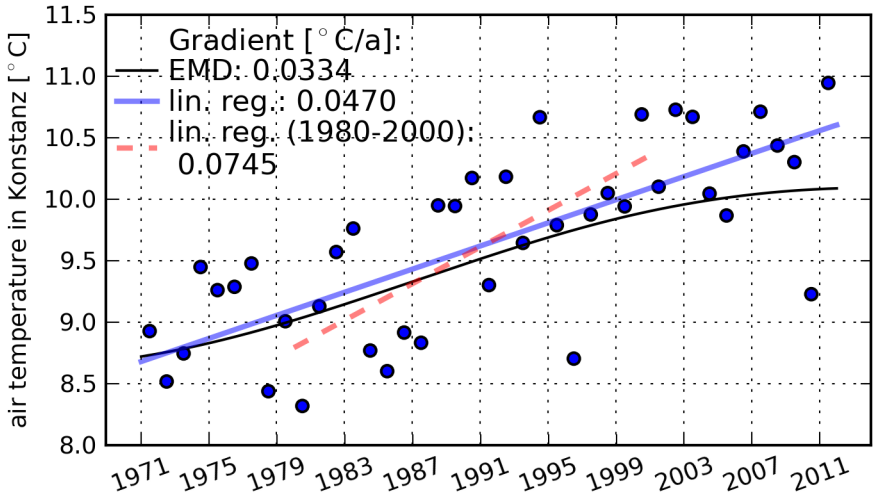

Figure 3.19: Yearly average air temperatures 1971-2011 and gradients obtained by EMD and linear regression for the periods 1971-2011 and 1980-2000.

Wind speed and relative humidity show a noticeable break point in August respectively April 1993, confirmed by a rank order change point test (Lanzante, 1996), which might stem from changes in the measurement devices or conditions. For these two variables, gradients are given for the period 1980-1993.

The change in air temperature gradient is not a local phenomenon, but was observed also in global temperature data. The reason for the changes in air temperature gradient had been subject to scientific discussion. Kaufmann et al. (2011) state a relationship between sulphur emissions and periods of reduced climate warming, whereas Foster and Rahmstorf (2011) succeed in explaining the changes in gradient with the influence of the three factors ENSO,

volcanic activity and solar radiation (sunspot activity). In the latter study, the anthropogenic influence thus creates a quite linear increase in air temperature, and all non-linearities derive from non-anthropogenic effects.

Gradients in water temperatures
Former studies observed a trend in Lake Constance water temperatures (cf. chapter 1.2.2), also it has already been mentioned that the reference period seems to be a period with a more-than-average increase in air temperature (cf. section 3.3.2).
Gradients in water temperature in the measured data during the reference period were obtained by linear regression (cf. table 3.4). Data is all-year-data that was deseasonalized by subtracting an average annual cycle before calculating the trend. The annual cycle was obtained by inverting the first four frequencies obtained by Fourier transformation.
All the gradients in water temperature are smaller than that in the air temperature. Gradients decrease with increasing depth. The gradient in the uppermost 20 m (0.0377 °C/a) is more than 1.5 times as high as the gradient in the lowermost 50 m (0.0239 °C/a).
The all-depths mean gradient (0.0279 °C/a) is more than 1.5 times higher than the gradient observed by Straile et al. (2003) for 1962 - 1998. To test the significance of the gradients in water temperature, a Mann-Kendall test (Kendall, 1970) was performed with α = 1%, 0.1% and 0.01%. All gradients in table 3.4 are significant on 0.01 % significance level, except the gradient in the upper 20 m, which is significant only on 0.1 % significance level.

3.3.2 Simulation: Discretisation, Parametrisation and Boundary Conditions

Discretisation
For ELCOM-CAEDYM-simulations of several decades, the model grid has to be coarse enough to reach reasonable computation times.
The grid mostly used in this study has a horizontal discretisation of 2000 m * 5000 m with the grid cells oriented along the longitudinal axis of the lake, e.g. rotated by an angle of 28^o (see figure 3.20). The model grid contains just Upper Lake Constance, which is divided horizontally into 47 grid cells. Lower Lake Constance is not considered in these simulations. Despite the coarse resolution, the model grid covers the overall shape of Upper Lake Constance and should therefore be able to reproduce in principle basin-scale internal waves.

Due to averaging of the water depth over the grid cell size of 10 km^2, the deepest cell has a depth of just 230 m, in contrast to the 254 m maximum depth of the real lake. Vertical discretisation contains 51 layers, with 2.5 m - 10 m magnitude. The total volume of Upper Lake Constance (47.637 km^3) is more or less preserved in this coarse grid representation (45 km^3). Minimum water depth of the cells is 10 m, to avoid the risk of grid cells running dry in long term simulations.

Simulation time step Δt is 600 seconds.

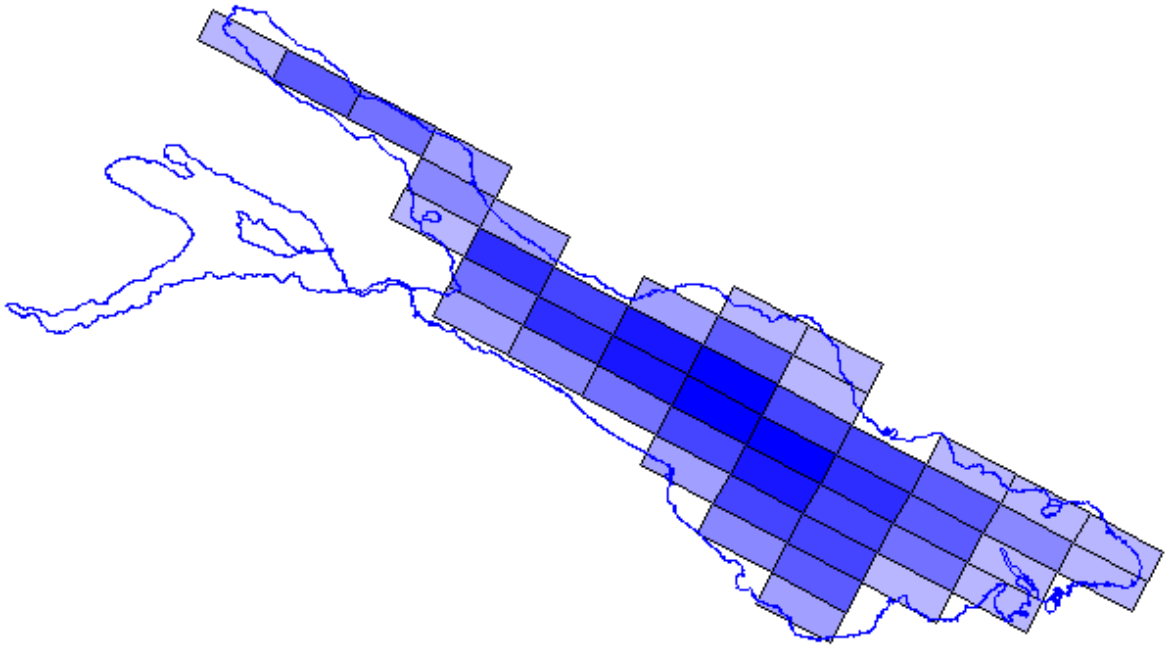

Figure 3.20: Model grid used for long-term simulations

Meteorological Boundary Conditions
Driving forces of the model are meteorology (air temperature θ, incident long wave radiation $ILWR$, short wave radiation Q_{sw}, relative humidity Φ, wind speed and direction, rain) and in- and outflow volumes, water temperatures, and water quality parameter.
Meteorological data were provided as hourly measurements, except rain which is daily, at the DWD (German Meteorological Service) station in Konstanz.
Gaps that had existed in the data measured by the DWD, have been filled by linear interpolation (if single values were missing), longer periods of missing values by values from neighbouring stations or by long year averages. In total, there had been 5027 values (of in total 184104 hours * 5 variables) missing (0.546%):

- cloud cover: 959 values (0.521%)
- wind: 948 values (0.515%)
- θ: 898 values (0.488%)
- dew point temperature: 927 values (0.504%)
- Q_{sw}: 1295 values (0.703%)

As long wave radiation is not measured directly at the meteorological station Konstanz, it was calculated from air temperature, humidity, and cloud cover, using an empirical formula found by Iziomon et al. (2003) for a nearby measurement station (in the Upper Rhine plain

212 m a.s.l., distance to Konstanz: approx. 120 km):

$$ILWR = \sigma \cdot T_a^4 (1 - X_s \cdot exp\left(\frac{-Y_s \cdot e}{T_a}\right)) \cdot (1 + Z_s \cdot N) \tag{3.5}$$

where T_a: air temperature [K]
e: vapour pressure [hPa]
N: cloud cover [Okta]
X_s: empirical parameter (0.35)
Y_s: empirical parameter (10.0)
Z_s: empirical parameter (0.0035)

Wind velocities were multiplied by 1.3, to account for the smaller roughness length over the lake (Rinke et al., 2010; Zenger et al., 1990).

Hydrological boundary conditions

13 tributaries are considered using daily measured values for runoff and water temperature where available. Measurements were performed by the Federal Agency for Water and Geology (Bundesamt für Wasser und Geologie BWG, Switzerland), State Agency for Environment Protection Baden-Württemberg (Landesanstalt für Umweltschutz Baden-Württemberg LUBW, Germany), and Hydrographic Service Vorarlberg (Hydrographischer Dienst Vorarlberg HDV, Austria). The tributary information was prepared by Hornung (2002) for modelling of mixing and stratification in Lake Constance using the one-dimensional lake model DYRESM.
Water temperature measurements were not available for all tributaries for the whole period. For most tributaries, at least some measurements were available. Hornung obtained daily values by linear regression either on the air temperature (T_{air}) of the 2-4 preceeding days or on water temperature of another tributary. In tributaries where no water temperature measurements were available at all, values of tributaries with similar properties (size

Table 3.2: Discharge and water temperature boundary conditions

tributary	runoff data	temperature data
Aach (Salmsach)	BWG	data from Leiblach
Argen	LUBW	linear regression on T_{air} of the last 2 days
Bregenzerach	HDV	HDV
Dornbirnerach	until 1984 linear regression on Bregenzerach, after 1984: HDV	
Goldach	BWG	data from Leiblach
Leiblach	HDV	linear regression on T_{air} of the last 4 days
Rhein	HDV	HDV
Rheintal-Binnenkanal	BWG	data from Leiblach
Rotach	LUBW	linear regression on T_{air} of the last 3 days
Schussen	LUBW	linear regression on T_{air} of the last 3 days
Seefelderach	LUBW	linear regression on T_{air} of the last 2 days
Steinach	BWG	data from Leiblach
Stockacherach	until 1987 linear regression on Seefelderach, after 1987: LUBW	

and runoff regime) were taken. See table 3.2 for detailed information on the tributaries' discharges and water temperatures sources.

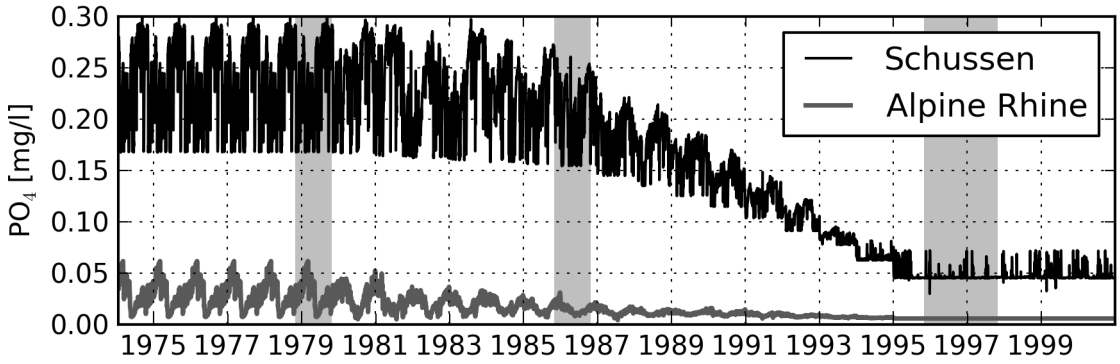

Figure 3.21: PO_4 concentrations in the tributaries Alpine Rhine and Schussen. Periods of measurement campaigns are highlighted in grey.

CAEDYM requires water quality information for all tributaries. In the parameterisation used in this study, this means concentrations of O_2, PO_4, NH_4, NO_3, SiO_2, and dissolved and particulate organic P, N and C.
The International Water Protection Commission for Lake Constance (Internationale Gewässerschutzkommission für den Bodensee IGKB) conducted three measurement campaigns to measure water quality parameters in the tributaries in 1978/79, 1985/86 and 1996/97. They developed runoff - concentration - relationships for the measured parameters (Bührer and Wagner, 1982; Wagner and Bührer, 1989; Bührer et al., 2000).
Rinke et al. (2009a) produced continuous time series for the water quality parameters by interpolating between the measurements periods. During the reference period, a considerable reduction of nutrient concentrations, especially phosphate concentrations, in the tributaries took place. This was the result of efforts to reduce the eutrophication in the lake, mainly by construction and enhancement of waste water treatment plants, and by the ban of phosphate in washing powder in the riparian states (Güde et al., 1998). In figure 3.21, PO_4 concentrations in two different tributaries are shown. The Schussen, a small lowland river (MQ = 10.9 m^3/s) draining a densely populated area, brings much higher concentrations than the larger Alpine Rhine (MQ = 240 m^3/s), which originates from a mountainous area and is partly fed by glaciers. For both rivers, the PO_4 concentrations decrease approximately by 1/5 during the simulation period. Due to the difference in runoff volume, the P-load coming from the Alpine Rhine to the lake is always about twice as high as that from the Schussen.

ELCOM does not calculate a water balance, but requires boundary condition information also for the outflow(s) of the lake. In the long simulation period of 21 years, small errors (minor tributaries and drinking water outtakes neglected, precipitation assumed homogeneous as measured in Konstanz, errors in evaporation) would sum up to unrealistic water table changes. To get a corrected outflow volume, daily ELCOM simulations were run and the outflow volume for the next day was calculated using the rating curve at gauge Kon-

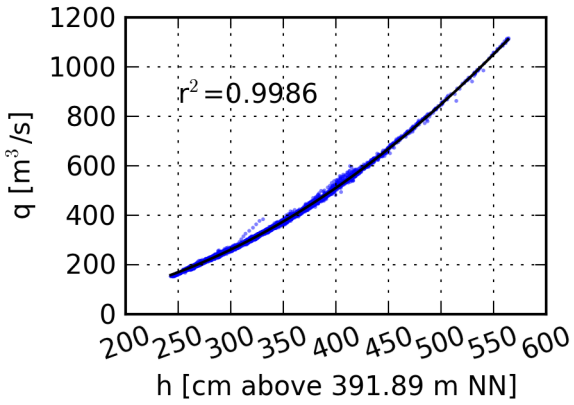

Figure 3.22: Measured water level and discharge at gauge Konstanz and fitted curve.

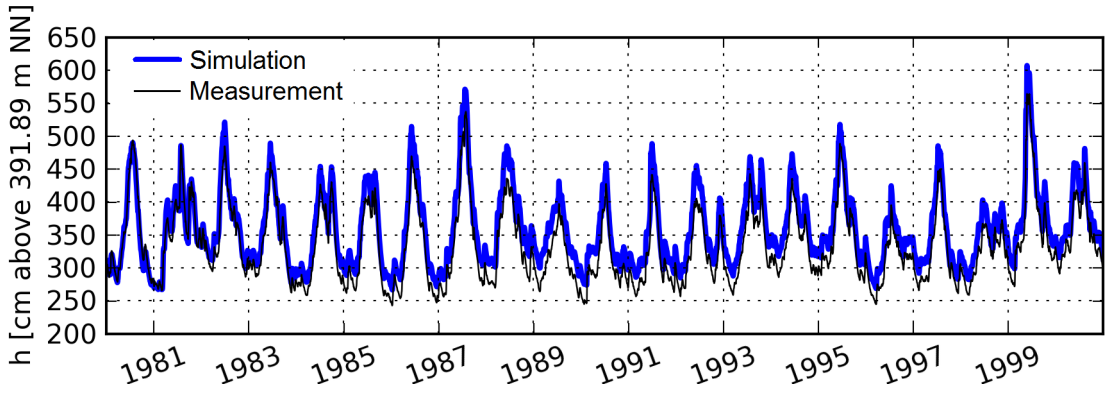

Figure 3.23: Simulated and measured water level in Konstanz.

stanz. The rating curve was found fitting a function to the available measurement data of discharge Q and water level H at gauge Konstanz in the years 1984-2000.

$$Q = 0.0044 \cdot H^2 - 0.6062 \cdot H + 44.1354 \tag{3.6}$$

where Q: discharge [m^3/s]
H: water level [cm above 391 m a.s.l.]

Figure 3.22 shows measured values and fitted curve. The r^2-value is 0.9986. The x-axis is in cm above 391.89 m asl, which is gauge zero at gauge Konstanz.
With these outflow volumes, a realistic development of the water level can be simulated (see figure 3.23). The temporal development of the water level is reproduced. The absolute values are on average 0.25 m higher than the measured values. The maximum difference is 0.53 m.

Parametrisation of the water quality model
The parametrisation of the water quality model CAEDYM was mainly taken from Rinke

et al. (2010): Zooplankton is represented by one group, phytoplankton is simulated using four functional groups (small and large diatoms and non-diatoms).
Sediment processes are represented by a "static" model, which is based on empirical relationships for water-sediment exchange rates.

Rinke et al. (2010) did not focus on deep water oxygen concentrations in their study. So the parametrisation of the hypolimnetic oxygen needed some adaptation. Oxygen consumption in the hypolimnion in the water quality model CAEDYM is mainly described by two equations representing sediment oxygen consumption (SOC, g/(m^2·d)) and oxygen consumption through microbial decomposition of organic material (MOC, g/(m^3·d)):

$$SOC = 0.9 \cdot 1.05^{T-20} \cdot \frac{DO}{DO + K_{DO,sed}} \tag{3.7}$$

where T: water temperature [°C]
DO: dissolved oxygen concentration [g/m^3]
$K_{DO,sed}$: half saturation constant for the control of SOC via DO: 12.5 g/m^3

$$MOC = MOC_{ref} \cdot 1.08^{T-20} \cdot \frac{DO + 0.8 \cdot K_{DO}}{DO + K_{DO}} \cdot Y_{O_2:C} \cdot DOC \tag{3.8}$$

where MOC_{ref}: reference MOC at 20 °C and optimal oxygen supply: 0.001 day^{-1}
K_{DO}: half saturation constant for the control of MOC via DO: 12.5 g/m^3
$Y_{O_2:C}$ stochiometric factor O_2:C: 2.67
DOC: dissolved organic carbon concentration [g/m^3]

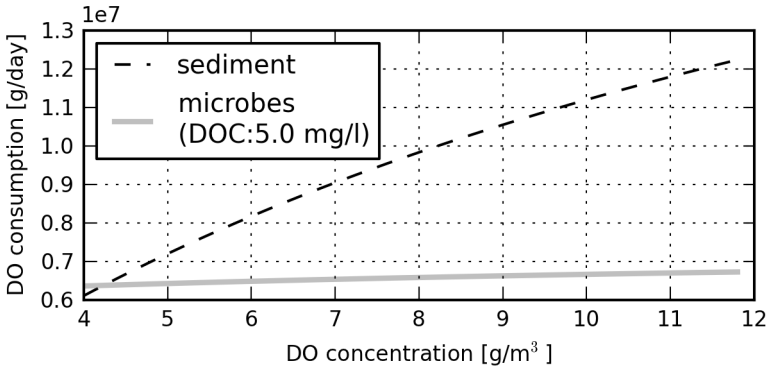

Figure 3.24: Relative importance of the oxygen consumption processes in Lake Constance below 200 m for a water temperature of 5 °C.

In the deep hypolimnion of Lake Constance, for oxygen concentrations above 5 mg/l, the sediment oxygen consumption (equation 3.7) is the dominating process. But at low oxygen conditions, equation 3.8 gets more important, because unlike equation 3.7, it also includes anoxic processes, e.g. the consumption rate decreases less with decreasing oxygen concentration (see figure 3.24).

Using the value 12.5 g/m^3 for $K_{DO,sed}$, equation 3.7 results in SOC = 0.13 - 0.23 g/(m^2· day) for temperatures between 4 and 7 °C and oxygen concentrations between 6 and 12 g/m^3.

Likewise, using the values 12.5 g/m^3 for K_{DO} and 0.001 day^{-1} for MOC_{ref}, equation 3.8 results in MOC = 0.0027 - 0.0053 g/(m^3· day) for temperatures between 4 and 7 °C, oxygen concentrations between 6 and 12 g/m^3, and DOC concentrations of 4 - 6 mg/l.
These values are in the same range as those found in the literature for the lakes Erie and Superior. Smith and Matisoff (2008) reported for Lake Erie values of sediment oxygen demand rates between 0.06 and 0.89 g/(m^2· day) from works published between 1972 and 2008. McManus et al. (2003) calculated rates between 0.003 and 0.012 g/(m^3· day) for Lake Superior. Lake Superior is oligotrophic, and Lake Erie is mesotrophic.

3.3.3 Results

Mixing: deep water temperature and oxygen
In figure 3.25, water temperature and oxygen concentration in the deep hypolimnion (below

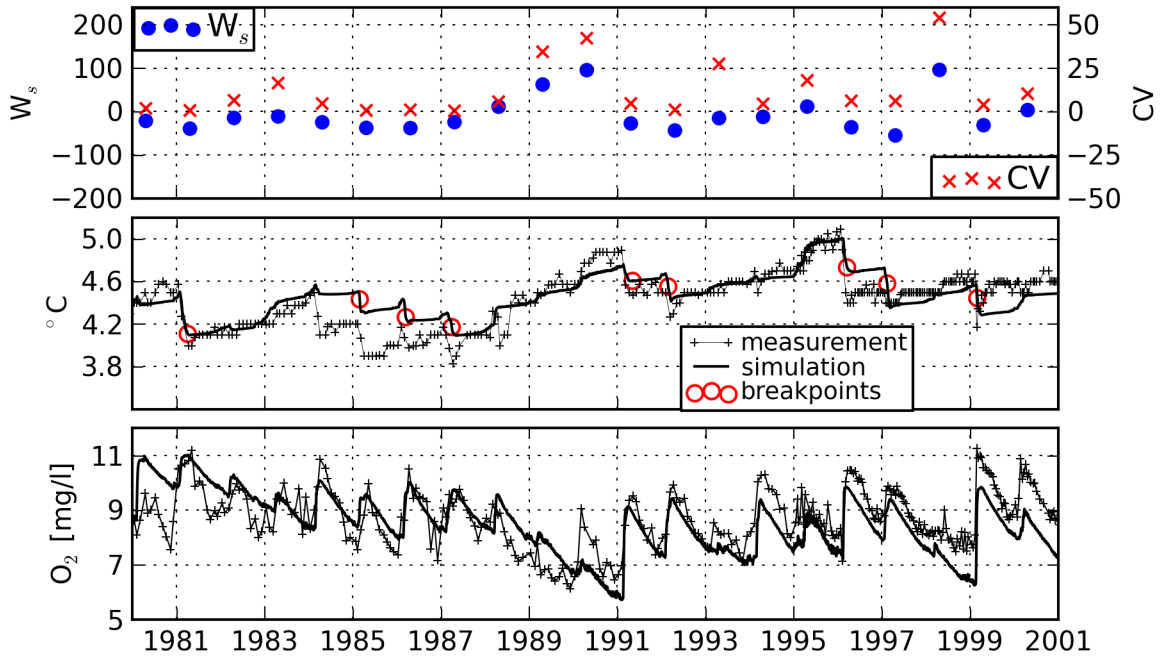

Figure 3.25: Upper panel: Yearly minimum values of W_S and CV, middle panel: deep water (below 200 m) temperature, lower panel: deep water oxygen concentration

Table 3.3: Maximum mixing depths in the simulation

year	1982	1983	1988	1989	1990	1993	1995	1998	2000
z_m **[m]**	205	165	205	165	120	150	165	150	155

200 m) in measurement and simulation is shown. Simulated values of both water temperature and oxygen concentration follow the measured curves quite closely, but the model fails to simulate the mixing in winter 1984/1985. Therefore, simulated deep water temperatures

in 1984 and 1985 are 0.3 - 0.4 °C higher than in the measurements. All other mixing events detected in the measured data (see section 3.3.1) are also visible in the simulations. Even the wind-induced mixing in the warm winter 1993/1994 is captured, where temperature does not show a clear signal, but the considerable increase in oxygen concentrations indicate the input of surface water.
The winterly minimum values of Schmidt stability (blue circles) show smaller values, as unlike the measurements, simulation results are available continuously. The same holds true for the CV. Here, an additional difference derives from the simplified sediment module in the water quality model: In the simulations, no phosphorus is released from the lakes sediments under anoxic conditions. This decreases the gradients in the PO_4 profiles and thus decreases the simulated CV values.
For the maximum winterly mixing depths in the winters without complete mixing (table 3.3), the availability of continuous data leads to higher values.

Gradients in simulated water temperatures
Table 3.4 compares gradients in measured and simulated water temperatures.

Table 3.4: Gradients in measured and simulated water temperatures in different depths

Depth	measured gradient	simulated gradient	
[m]	[°C/a]	[°C/a]	
air	0.075	-	
0-20 m	0.0377	0.0498	+
20-50 m	0.0279	0.0179	-
0-50 m	0.0314	0.0324	(+)
50-100 m	0.0264	0.0251	(-)
0-100 m	0.0287	0.0295	
100-200 m	0.0247	0.0254	
200-250 m	0.0239	0.0235	
0-250 m	0.0279	0.0282	

(+) and (-) indicate differences between the gradients in the simulated and measured values equal to or larger than 0.001 °C/a. The + and - indicate differences between the gradients in the simulated and measured values equal to or larger than 0.01 °C/a.
The model almost perfectly reproduces the all-depths temperature increase. The gradient in the deep hypolimnion (200 - 250 m) is also reproduced well, as well as in 100 - 200 m. Stratification, and the increase in stratification stability due to climate change is overestimated by the model: In the uppermost 20 m, simulated water temperature gradient is 0.012 °C/a larger than measured, whereas in 20 - 50 m depth, simulated gradient is 0.01 °C/a smaller than measured. Consequently, in the uppermost 50 m, the simulated gradient is slightly larger than measured (0.001 °C/a). In 50 - 100 m depth, the simulated gradient is again slightly smaller than measured (0.0013 °C/a), leading to a correct representation in the uppermost 100 m. To test the significance of the gradients in water temperature, a Mann-Kendall-test (Kendall, 1970) was performed with α = 1%, 0.1% and 0.01%. All gradients in table 3.4 are significant on 0.01 % significance level.

Reoligotrophication

During the simulation period, Lake Constance underwent a significant reoligotrophication (Güde et al., 1998). In 1980, the average PO_4 concentration during spring mixing was 74 μg/l, in 2000 it had dropped down to 10.6 μg/l.

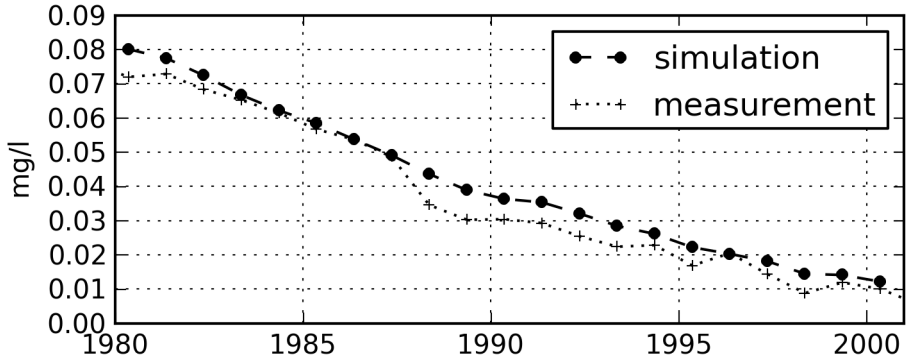

Figure 3.26: Maximum (winter circulation) PO_4-P concentration in the upper 20 m in measurement and simulation

Even though the model setup of the water quality model CAEDYM used for this study does not include phosphorus release from the sediment, the development of the yearly maximum (winter) epilimnetic PO_4 concentration was reproduced in the simulation (Figure 3.26). The years without complete mixing 1988 – 1990 stand out in the measurements due to lower maximum PO_4 concentrations in the epilimnion, as less PO_4 was brought to the upper layers from the deep water. In the simulation, this effect is less pronounced. Simulated summer

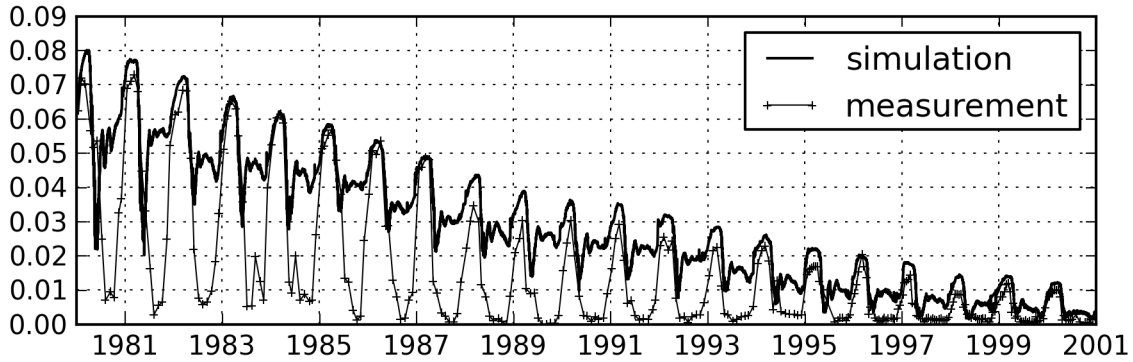

Figure 3.27: PO_4-P concentration in the upper 20 m in measurement and simulation

values in the upper 20 m are too high (see figure 3.27). Frassl et al. (2013) stated, that the phytoplankton in Lake Constance can enhance phosphorus depletion of the epilimnion via internal phosphorus storage. The algae take up more phosphate than they actually need, and when they settle down, phosphate is transported to the sediments. The algae in this model parametrisation have no possibility of storing phosphorus.

Phytoplankton productivity does not respond in a linear way to reoligotrophication. First,

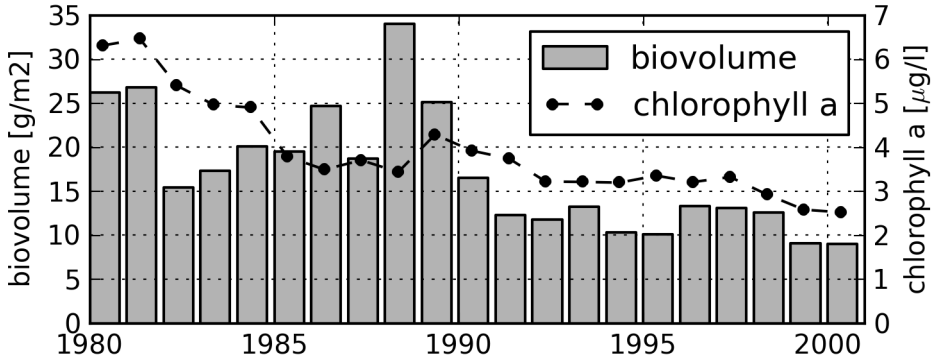

Figure 3.28: Yearly averages of measured biovolume and simulated chlorophyll a concentration in the upper 20 m.

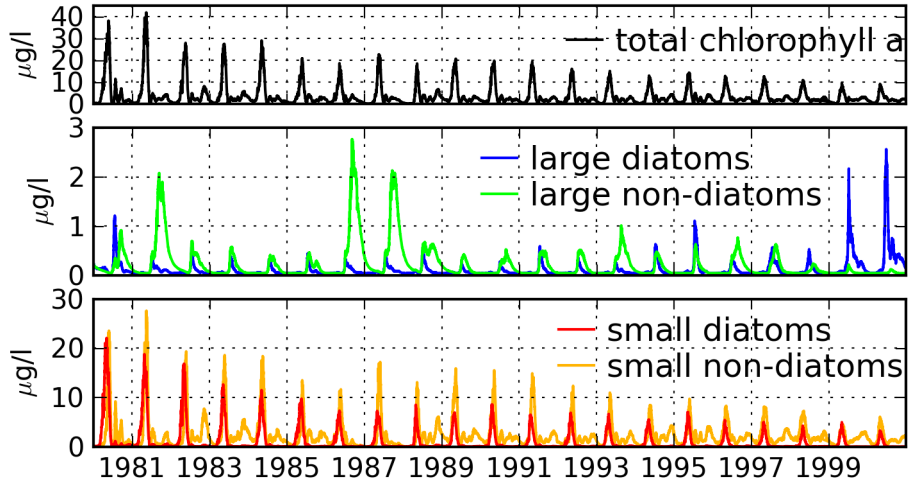

Figure 3.29: Simulated chlorophyll a concentration in the upper 20 m.

changes occur in community composition rather than in total chlorophyll a concentration (Güde et al., 1998). The annual average simulated phytoplankton concentrations as well as measured yearly average biovolume thus show a less monotonic decrease than observed in PO_4-P concentration (figure 3.28). This picture is very similar to that obtained by Rinke et al. (2009a) with the one-dimensional model DYRESM-CAEDYM, but the absolute simulated chlorophyll a concentrations are approximately 30 % lower in the three-dimensional simulation.

Figure 3.29 shows simulated chlorophyll a concentration in total and the succession of the four functional groups. The spring bloom is dominated by the two groups of small algae, small diatoms and small non-diatoms. During summer, the small diatoms disappear almost completely. Then the two groups of larger algae become more dominant. Over the whole simulation period, the concentrations of the large non-diatoms rather decrease, while those of the large diatoms increase.

Simulated residence time of the lake water

The time scales in which the lake is responding to external signals, as e.g. the reoligotrophication, is depending on the time the water stays in the lake.
To evaluate the residence time of the water in the lake, a conservative tracer was simulated. Initial tracer concentration was 1000 all over the basin. Inflow concentrations were set to zero. The tracer concentration during the simulation thus represents the fraction of water that has been in the lake at the beginning of the simulation. The basin-wide average tracer concentration shows approximately an exponential decay:

$$c(t) = c_0 \cdot e^{-t \cdot \lambda} \tag{3.9}$$

where c: tracer concentration
c_0: initial tracer concentration (1000)
t: time [years]
λ: decay constant ($(6.1a)^{-1}$)

$\lambda = (6.1a)^{-1}$ corresponds to a half-life of water in the lake of $\ln(2) \cdot 6.1 = 4.23$ years. After 4.23 years half of the lake water is replaced. Note that the basin average concentrations fit quite closely to the exponential function (see figure 3.30).
Tracer concentration decrease in the simulation is not strictly exponential, but shows a yearly cycle due to stratification and mixing. During summer stratification, in- and outflow volumes are highest, and thus the decrease in tracer concentration is fastest, but the exchange of water mainly takes place in the epilimnion, while in the hypolimnion tracer concentration stays almost constant.

The theoretical decay constant λ_{th} of a constantly fully-mixed Lake Constance can be calculated from total flow-through Q and lake volume V:

$$\lambda_{th} = Q/V = 10.73\frac{km^3}{a}/48.4km^3 = (4.5a)^{-1} \tag{3.10}$$

The corresponding theoretical half-life of a fully-mixed lake is 3.12 years (figure 3.30). Thus, the stratification increases the half-life of the water in the lake by more than one year.

For some parts of the lake, e.g. the deep hypolimnion or deep water behind the Mainauschwelle in Lake Überlingen, the residence time is much longer (see figure 3.31). $T_{1/2}$ in the deep hypolimnion (below 200 m depth) is 4.69 years. Even though the maximum depth of Lake Überlingen in the coarse grid, due to interpolation of water depth in the grid cell, does not exceed 103 m (148 m in reality), which is more than 100 m less than in the main basin, water exchange is much slower and the basin maximum residence times of 6.18 years can be found here. Especially in the case of the deep hypolimnion of Lake Überlingen, the decay function does not follow the tracer concentration curve very closely. The simulated tracer concentration decreases step-wise during winter mixing event, and stays almost constant in summer, as well as in winters without deep mixing.

It must be stated that these are purely theoretical considerations without any measurement evidence for the simulated period.

Measurements of radioactive substances, such as Cs-137 (half-life $T_{1/2}$=30.17 a), that came into the lake after the catastrophe of Chernobyl (Putyrskaya et al., 2009), can also give some

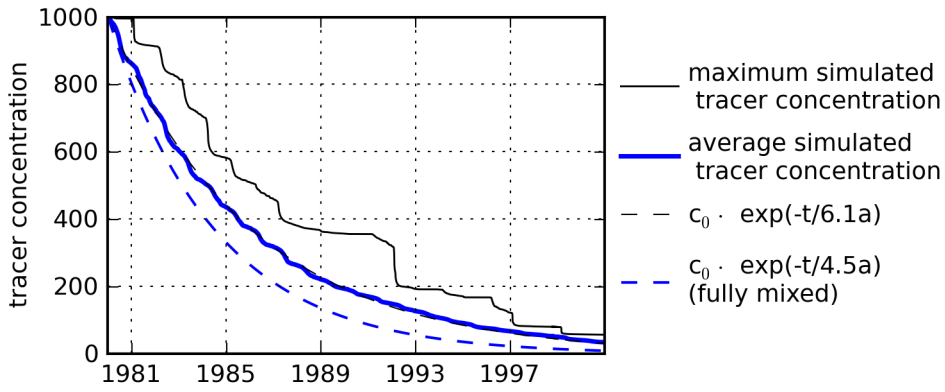

Figure 3.30: Tracer residence time curves: simulated basin maximum and average tracer concentration, decay function fitted to simulated average tracer concentration and theoretical tracer decay for fully-mixed lake.

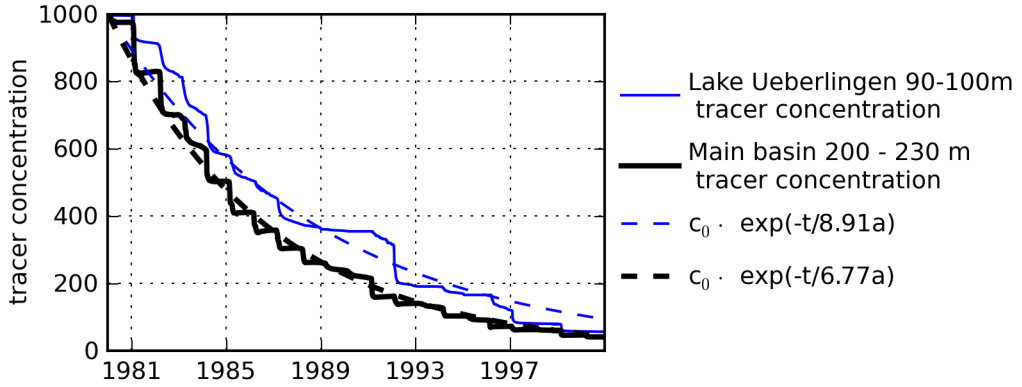

Figure 3.31: Tracer residence time curves: simulated tracer concentrations in the hypolimnion of Lake Überlingen and the main basin, and the corresponding decay functions.

information. In the initial phase after the fallout, Cs-137 was entering the lake via precipitation on the lake's surface, and brought from the catchment by the tributaries. As a result, the initial concentration was much higher in the epilimnion. Cs-137 is bound to particles and settles to the sediments, from where it can be re-suspended. It is also incorporated by aquatic organisms. After some years, the system is reaching an equilibrium, and the concentration of Cs-137 is mainly controlled by its decay and the residence time of water in the lake (Smith et al., 2005):

$$c(t) = c_0 \cdot e^{-t\cdot(\lambda_{Cs-137}+\lambda_{lake})} \tag{3.11}$$

where c: tracer concentration
c_0: initial tracer concentration (1000)
t: time [years]
λ_{Cs-137}: radioactive Cs-137 decay constant ($(43.53a)^{-1}$)
λ_{lake}: decay constant of water in the lake ($(6.25a)^{-1}$)

Using the data of Putyrskaya et al. (2009) measured between October 1990 and July 1999 (in March 2000, the detection limit was reached), equation 3.11 yields λ_{lake} = (6.25 a)$^{-1}$ and thus $T_{1/2}$ of the water in the lake is 4.33 a.
It has to be stated that the dataset used contains only six measurements, and that the exact values strongly depend on the choice of measurements used, i.e., on the question, when the equilibrium phase starts. If three more measurements of the years 1989 and 1990 are included, λ_{lake} decreases to (4.76 a)$^{-1}$ ($T_{1/2}$ = 3.3 a).

3.3.4 Conclusions

The model is able to reproduce the measured deep water temperatures, and also the oxygen concentrations. This gives confidence in the correctness of the simulated vertical mixing.
The oxygen concentrations in the hypolimnion could be reproduced with the model using the simple static sediment parametrisation.

The measured gradient in basin average water temperature was reproduced by the model, indicating a correct representation of the energy budget.

The effects of oligotrophication on the lake's ecosystem has already been simulated with the one-dimensional model DYRESM-CAEDYM by Rinke et al. (2009a). The three-dimensional simulation in this study showed comparable results.

By using conservative numeric tracer, the residence time of the water in the lake could be analysed theoretically.

4 Climate Scenario Study

In chapter 3, the ability of the model system ELCOM-CAEDYM to reproduce different processes and phenomena in the lake was proven. Especially the evidence for the correct representation of long-term mixing behaviour and heat balance in section 3.3 gives confidence in using the same model set-up for climate scenario simulations.

In this chapter, the influence of a changing climate on Lake Constance shall be examined with the help of scenario simulations. Special attention is paid on the mixing behaviour of the lake, the heat balance and the deep water oxygen budget. As the main goal was to get a deeper understanding of the relevant processes, artificial scenarios produced by a weather generator were used instead of climate projections produced by Global Circulation Models (GCM). This approach gives the opportunity to change different characteristics of the climate, such as mean and variability, both separately and combined.
Climate scenarios were generated with changes in mean air temperature, climate variability and seasonality. Additionally, simulations were run with changed nutrient concentrations and a warmer climate.

Apart from the simulations with higher nutrient concentrations, this study is ignoring changes in the catchment of the lake. This is ignoring the fact that a changing climate is expected to have influence on the lake's catchment and thus on runoff volumes and nutrients concentrations in the tributaries. Nevertheless, these are strongly depending on other, direct anthropogenic interventions, such as land use, hydraulic engineering, and population development. This anthropogenic influence may superpose climate change effects in the catchment. Luft and Ihringer (2011) analysed the long-term behaviour of the water level of Lake Constance. They could not clearly distinguish between climate and other anthropogenic influence. Therefore, in this study, all inflow boundary conditions are kept stable in all scenarios. Here, only the direct climate (i.e. meteorological) influence at the lake surface is studied, and all changes observed in the simulations can be attributed to climatic reasons.

4.1 Meteorological Boundary Conditions

The meteorological driving forces are the main boundary conditions of the lake model in this study. A weather generator is used to produce time series of meteorological variables with changed climatic characteristics.
The weather generator is data-driven, i.e. it needs measurement data to analyse the statistical properties. Based on the cross- and autocorrelations, i.e. the dependencies between the different variables, and the dependencies on the preceding time steps, data sets are generated with the same properties. In a second step, disturbances can be introduced, to change

the climatic conditions. The cross- and autocorrelations are still preserved, i.e., a change in air temperature will result in changing radiation and humidity.

4.1.1 The Vector-autoregressive weather-Generator VG

Schlabing et al. (2013) developed the **V**ector-autoregressive weather-**G**enerator (VG) for generating artificial meteorological time series as boundary conditions for hydrodynamic and ecological modelling of lakes. It is able to produce artificial time series, conserving the seasonal cycle, correlations, cross-correlations, autocorrelations and wind direction distributions of the input data.

VG is available online: https://bitbucket.org/iskur/vg/src

In the following, VG shall be explained briefly. For more detailed information on VG, the reader is referred to Schlabing et al. (2013).

VG uses a conventional vector autoregressive (VAR) process. The VAR process requires variables following standard-normal distributions. The meteorological variables are transformed to standard normal marginals by using quantile-quantile transformations. During this transformation, a de-seasonalisation of the variables takes place. The weather generation process first produces time series with standard-normal distributions without any seasonality. The simulated time series is then back-transformed to the original marginal distributions with the original seasonality. The annual cycle of the marginals is described by fitting Fourier series to the seasonally changing distribution parameters and used in the transformation to and from the standard-normal distributions.

The conventional VAR process has the form:

$$y_t = \sum_{i=1}^{p} (A_i \cdot y_{t-i}) + \epsilon_t + m \tag{4.1}$$

where
- y_t: K-dimensional vector of variables at time step t
- p: order of the autoregressive process
- A_i: $K \times K$ matrices containing the parameters of the VAR process
- ϵ_t: white noise
- m: K-dimensional disturbance vector

The set of meteorological variables y_t at time step t is determined by a linear combination of the values of the previous p time steps, plus white noise (ϵ_t). This means, that the weather on day t is depending on the weather of the preceding days, plus some random residual. The disturbance vector m can be used to generate scenarios. In the standard setting, all elements of m are zero.

VG is working on a daily basis. If sub-daily resolution is needed, scenario data can be further disaggregated after the generation process. The disaggregation procedure depends on the meteorological variable. For short-wave radiation, an idealized daily cycle is applied depending on the day of year and latitude. For the other variables, disaggregation is done

by resampling the deviations between daily and sub-daily values in the measured data of the respective variable.

For this study, VG was applied on the data set of meteorological measurements at the DWD measurement station in Konstanz in the years 1980-2000. The same data was used for modelling in chapter 3.3.
The simulated variables are:

- Air temperature θ
- Wind: westward (u) and northward (v) wind speed component
- Short wave (global) radiation Q_{sw}
- Incident long wave radiation $Q_{lw(incident)}$
- Relative humidity ϕ

Precipitation was deemed as of minor importance to the thermal budget of the lake, and therefore not simulated with the weather generator.

The order of the VAR process was set to $p = 3$. This value was found to represent the autocorrelation of the measured data best, while still being considered parsimonious under various information criteria (Akaike Information Criterion, Hannan-Quinn, Final Prediction Error) (Schlabing et al., 2013).

Wind and short-wave radiation were disaggregated to hourly values, as daily average values would lead to errors in the lake model simulation results. For wind, daily average values would lead to considerably lower energy input. Input of kinetic energy grows quadratic with wind speed, and the turbulent energy input even cubic. Solar radiation has to be given in hourly resolution for the water quality model, as the phytoplankton development depends on the daily cycle.
The other variables were used in daily resolution.

4.1.2 Generation of Climate Scenarios

VG gives the user the possibility to change the mean or variability of the primary variable (most often air temperature θ) to create user-defined climate scenarios.
The disturbance vector m is used to produce scenario simulations. It can be constant over time, simulating warmer climate. But it can also be time-dependant for non-uniform changes of the climatic conditions.
To obtain the disturbance vector m, the desired changes in air temperature have to be transformed to standard-normal world, transferred to the other variables according to the respective cross-correlations and scaled according to the parameters of the auto-regressive process.

The user-defined change in the primary variable (here θ) is passed to the other variables y_i according to their covariance $\sigma_{\theta^{tr} y_i^{tr}}$.
This is applied on the transformed variables:

$$\overline{y}_i^{tr} = \overline{y}_\theta^{tr} \frac{\sigma_{\theta^{tr} y_i^{tr}}}{\sigma^2_{\theta^{tr}}} \tag{4.2}$$

where $\overline{y}_i^{tr}$: process-mean of variable i, transformed to standard-normal
$\overline{y}_\theta^{tr}$: process-mean of air temperature, transformed to standard-normal
$\sigma_{\theta^{tr} y_i^{tr}}$: covariance of θ^{tr} and y_i^{tr}
$\sigma^2_{\theta^{tr}}$: variance of θ^{tr}

The resulting vector of process means $\overline{y}$ is converted to the disturbance vector m, accounting for the parameters of the VAR process using Schlabing's law:

$$m = \left(I - \sum_{i=1}^{p} A_i \right) \overline{y}. \tag{4.3}$$

where m: K-dimensional disturbance vector
I: $K \times K$-dimensional identity matrix
p: order of the autoregressive process
A_i: $K \times K$ matrices containing the parameters of the VAR process
$\overline{y}$: K-dimensional vector of process means

4.1.2.1 Increased Mean Air Temperature

For changing the mean temperature, m_θ is set to a constant value.

		median		range (90th - 10th percentile)	
		measured	simulated	measured	simulated
θ	[°C]	9.7	13.6	8.0	7.9
percentile in measured		50	86.1		
Q_{sw}	[W/m^2]	133.3	151.1	130.0	118.9
percentile in measured		50	62.5		
$Q_{lw(incident)}$	[W/m^2]	310.6	327.6	59.3	58.3
percentile in measured		50	74.5		
ϕ	[-]	0.79	0.76	0.24	0.24
percentile in measured		50	37.7		
u	[m/s]	0.37	0.47	2.71	2.87
percentile in measured		50	53.9		
v	[m/s]	0.03	0.29	2.48	2.66
percentile in measured		50	45.8		

Table 4.1: Statistical properties of the generated data with ΔT_{air}=4 °C: change in median compared to measured data and range between 10th and 90th percentile (averaged over yearly cycle).

Figure 4.1 shows the result of a simulation with + 4 °C increase in mean air temperature. Table 4.1 gives numbers for the median and 10-90 percentile range for the VG scenarios. To allow for the yearly cycle in the meteorological variables, all percentiles have first been

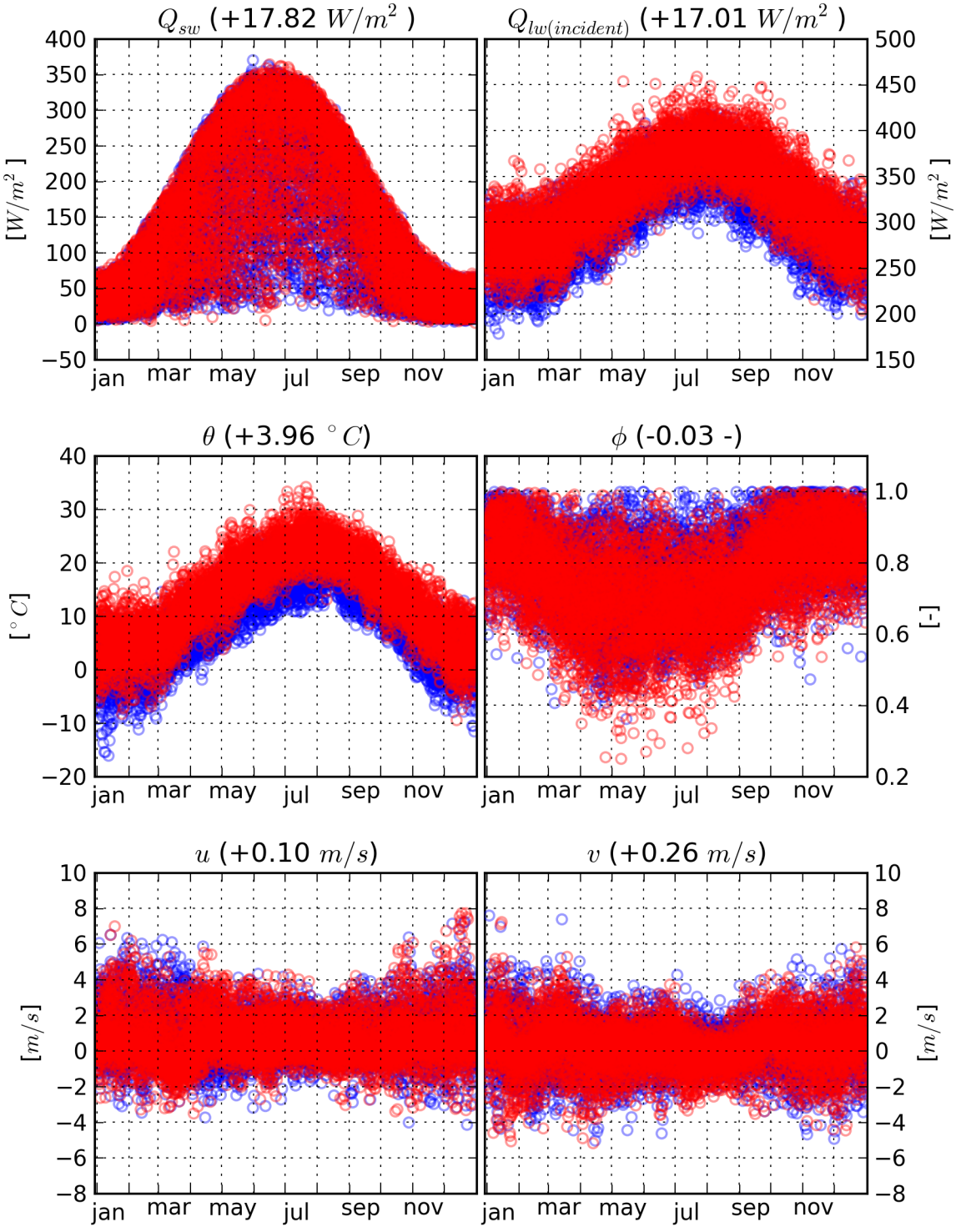

Figure 4.1: Measured meteorological data (blue circles) and output of a simulation with mean temperature increased by 4 °C (red circles). Numbers are given for the change in median compared to measured data (averaged over yearly cycle).

calculated for each day of year separately. The numbers in table 4.1 are the average values of these annual cycles. As a measure for the significance of the change in median, *percentile in measured* is given: It gives the percentile in the measured data that corresponds to the median in the specified scenario. The percentiles in the measured data were calculated using the distributions fitted to the data for the transformation.
The values of $Q_{lw(incident)}$, Q_{sw}, and wind speed components increased with increasing θ. ϕ decreased. Due to the physical upper limit, an increase in median short wave radiation has to decrease the range of Q_{sw}. The small absolute decrease in relative humidity of 0.03 makes the median in the + 4 °C scenario corresponding to the 38 - percentile in the unchanged scenario.

With VG, temperature increase for climate scenarios can be chosen freely. For the interpretation of the results, a comparison with the climate projections used in the IPCC AR4 (IPCC, 2007) shall be done.
For the A1FI scenario, global temperature increase is likely to be in the range of 2.4 - 6.4 °C within 100 years, for the A2 scenario the likely range is 2.0 - 5.4 °C. In Europe, the temperature increase is expected to be higher than the global increase. CH2011 (CH2011, 2011; Bosshard et al., 2011) gets for north-eastern Switzerland for the A2 scenario a range of 2.5 - 4.9 °C within 90 years, using GCM data and probabilistic downscaling. (The CH2011 data were obtained from the Center for Climate Systems Modeling (C2SM).)
The scenarios used in this study (+1, 2, 3, 4, 5 °C) thus all lie within the range these projections made fore the next 100 years for the Lake Constance region.

Changes in relative humidity under climatic change
The question, whether an increase in air temperature will rather lead to an increase in absolute humidity (moisture) or in a decrease of relative humidity, is of interest because of the high global warming potential of water vapour.
On a global scale, relative humidity seems to be rather independent of temperature. Temperature increases lead to increases in the air's moisture content, due to increased evaporation and the infinite water supply at the oceans' surface (Bony et al., 2006). Over the continents however, Ross et al. (2002) state a negative correlation between air temperature and relative humidity and a positive correlation between air temperature and moisture. This corresponds to the VG output: here, relative humidity decreased with increasing temperature, whereas vapour pressure increased (measurements: 10.1 hPa, + 4 °C scenario simulation: 12.5 hPa on average).

4.1.2.2 Changed Climate Variability

In the context of this study, climate variability is defined as episodes with daily average air temperatures deviating from the long-term average for this day of year (doy). The episodes can be described by their duration in days and their average amplitude in °C (figure 4.2). In the measured air temperatures of the reference period, episodes duration proved to be exponentially distributed with an average value of 5.3 days, and - apart from a pronounced bimodality - amplitudes are roughly normally distributed, with a standard deviation of 2.3 °C (see figure 4.3). Without any changes, VG reproduces these distributions (see figure 4.4).

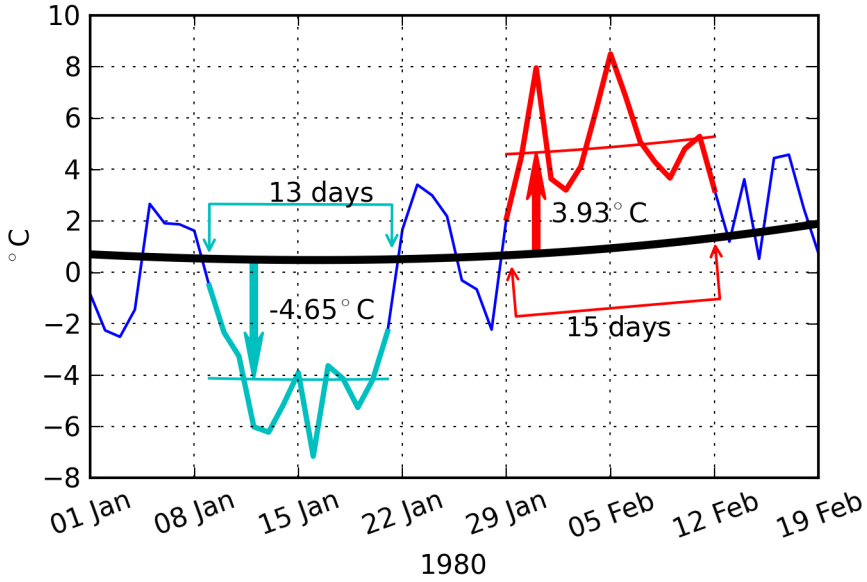

Figure 4.2: Climate variability: definition of cold and warm episodes.

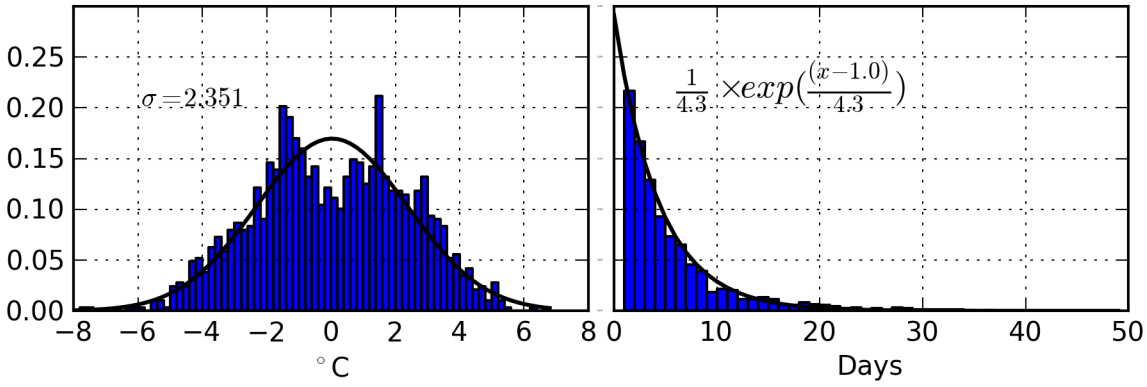

Figure 4.3: Climate variability of measured data: distribution of amplitude (left) and episode duration (right).

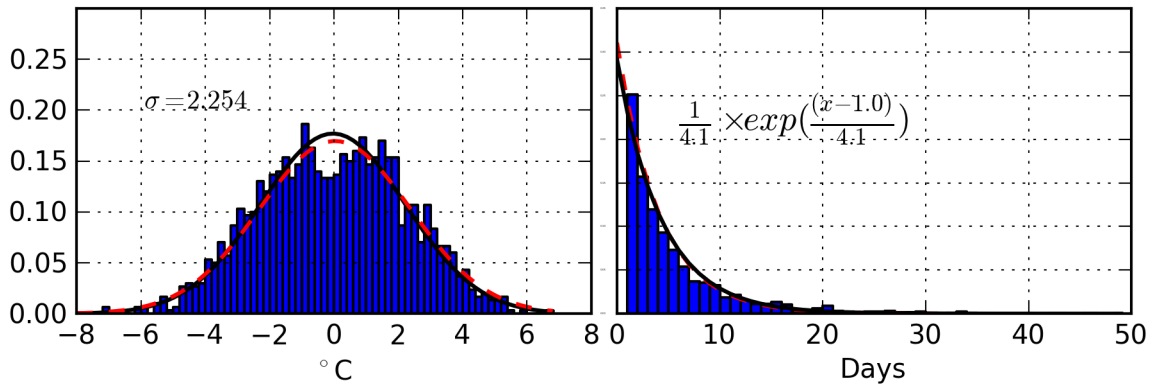

Figure 4.4: Climate variability of simulated data: distribution of amplitude (left) and episode duration (right). Dotted red lines indicate the distributions in the measured data.

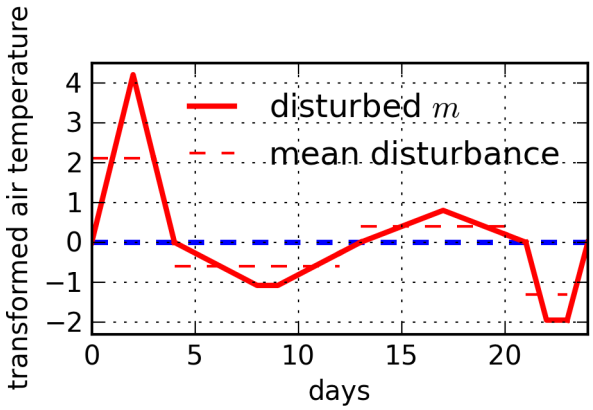

Figure 4.5: Artificial episodes generated by the Poisson process in VG to increase climate variability.

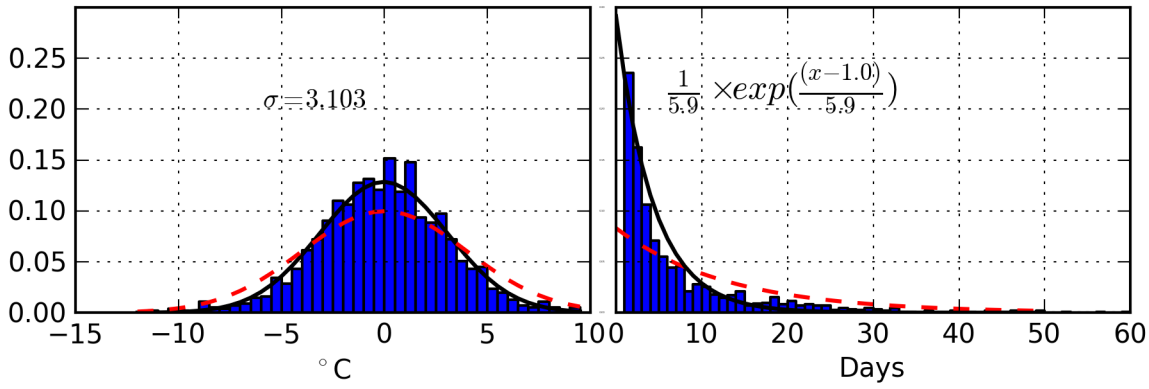

Figure 4.6: Increased climate variability: distribution of simulated amplitude (left) and episode duration (right). Dotted red lines indicate the distributions drawn from.

		median		range (90th - 10th percentile)	
		measured	simulated	measured	simulated
θ	[°C]	9.67	9.50	8.05	11.09
percentile in measured		50	49.0		
Q_{sw}	[W/m^2]	133.26	132.42	130.02	130.85
percentile in measured		50	50.9		
Q_{lw}	[W/m^2]	310.59	308.79	59.31	68.59
percentile in measured		50	48.1		
ϕ	[-]	0.79	0.79	0.24	0.24
percentile in measured		50	48.3		
u	[m/s]	0.37	0.39	2.71	2.82
percentile in measured		50	51.2		
v	[m/s]	0.03	0.19	2.48	2.66
percentile in measured		50	42.5		

Table 4.2: Statistical properties of the generated data with increased climate variability: change in median compared to measured data and range between 10th and 90th percentile (averaged over yearly cycle).

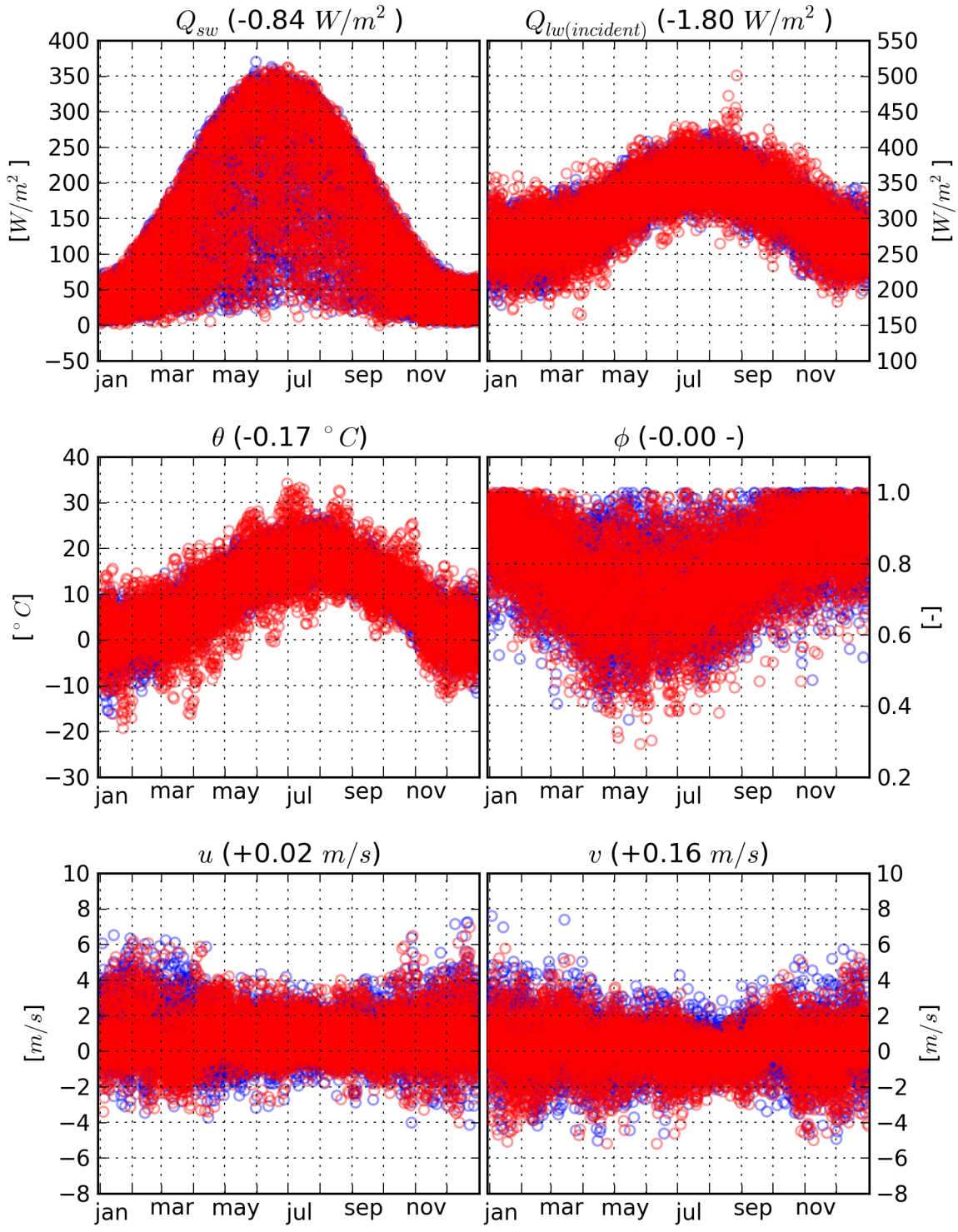

Figure 4.7: Measured meteorological data (blue circles) and output of a simulation with increased climate variability (red circles). Numbers are given for the change in median compared to measured data (averaged over yearly cycle).

Increasing climate variability means increasing duration and amplitude of the episodes. In VG, this is done with the help of a Poisson process. Enhanced variability is defined by the respective distributions with increased mean respectively standard deviation. During the weather generation process, amplitude and duration are sampled from these changed distributions, and the process-mean for air temperature m_{theta} (equation 4.1) is set to a triangular function with the drawn duration, and the drawn amplitude being the mean. Figure 4.5 shows an example for the disturbed m_{theta} with increased climate variability. With equation 4.2, the other elements of m are calculated.
As the stochasticity of the autoregressive process adds additional noise and autocorrelation, the episodes in the simulated time series do not fit the pre-defined distributions, but show shorter episodes with lower amplitudes.
Figure 4.6 shows the resulting episode statistics of a simulation with increased climate variability. Pre-defined mean episode length is 14 days and σ of amplitudes is 4 °C. In the simulated time series, mean episode length is 6.9 days and σ of amplitudes is 3.1°C. Figure 4.7 shows the results of the VG simulation with this increase in climate variability. Table 4.2 gives numbers for the median and 10-90 percentile range for the VG scenario.

Seasonality of episodes
In the measured data of the reference period, episodes are not evenly distributed all over the year, but exhibit a seasonal cycle. σ of amplitudes is highest in early winter (December: 2.627 °C, January: 2.599 °C) and lowest in late summer/early autumn (August: 1.972 °C, September: 1.832 °C, October: 1.974 °C). In episode duration, the seasonal differences are less pronounced. It is longer in winter (6.155 days in January, 6.266 days in February) than in the rest of the year.
In the simulation, some seasonality is added to the amplitudes during backtransformation of the simulated variables because of a seasonal cycle in the variance in θ. The duration of the episodes, however, are equally distributed throughout the year in the simulated time series.

4.1.2.3 Gradients in Air Temperature

m can also be used to define a temperature gradient in the simulated time series.
With VG, a temperature gradient for climate scenarios can be chosen freely. For the interpretation of the results, a comparison with the climate projections used in the IPCC AR4 (IPCC, 2007) shall be done. The climate projections of IPCC and CH2011 cited in section 4.1.2.1 yield average temperature gradients between 0.02 and 0.064 °C/a. For a simulation period of 20 years this would result in temperature increases of 0.4 - 1.3 °C. This is less than the temperature increase observed in the reference period (1.6 °C / 20 a. see figure 3.18), indicating the possibility of periods with stronger temperature increase.

4.1.2.4 Changes in Climatic Seasonality

To use VG for stochastic downscaling of GCM scenarios, there is the possibility to give a temperature time series to be used as m.

Besides that, a climate signal can be "sketched by hand", depending on the point of interest. This means, the influences of e.g. a changed yearly cycle, cold winters or hot summers can be addressed separately.

Fixing the randomness

VG gives the option to fix the random part ϵ_t (equation 4.1) for several simulations. This had been designed to run tests on the code, but might also be used to compare the influence of some effects in detail.

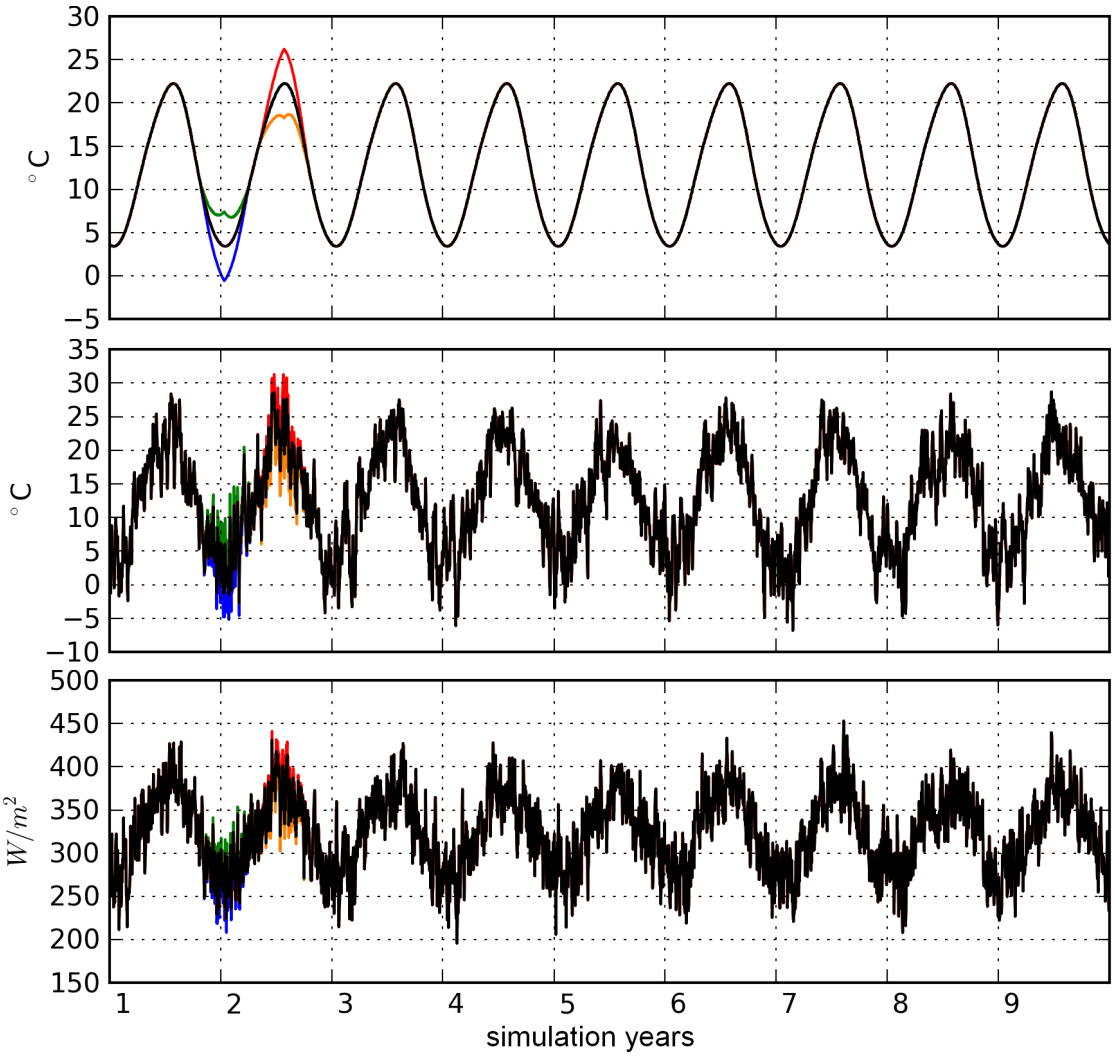

Figure 4.8: User-defined climate signal (upper panel) and simulated temperature (middle panel) and incident long wave radiation (lower panel) time series.

The upper panel of figure 4.8 shows the climate signals, in this case 5 lines indicating standard conditions with average θ increased by 3 °C, and scenarios with one cold winter, mild winter, cool summer or hot summer. In the middle panel, the corresponding simulated air temperature time series are shown. The lower panel shows simulated $Q_{lw(incident)}$.

All these five VG simulations were done with the same random state, i. e. the stochastic part of the simulation used the same random numbers.

4.2 Climate Scenario Simulations with ELCD

For lake model simulations with climate scenarios generated by VG, the same model set-up is used as in the simulation of the reference period in section 3.3. The simulation grid is the same coarse grid with 2000 m * 5000 m horizontal cell size. In- and outflow volumes and tributary water temperatures are the same as in the simulation of the reference period. Assuming a rather oligotrophic state of Lake Constance in most of the scenarios, the nutrient concentrations in the tributaries are calculated using the runoff - concentration - relationships obtained by Bührer et al. (2000) for the years 1996 and 1997.
Initial profiles of nutrient concentrations and water temperatures are chosen depending on the scenario.

4.2.1 Unchanged Climatic Conditions

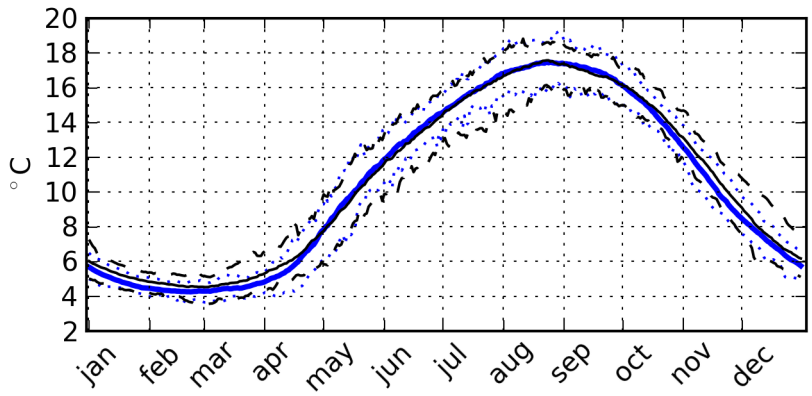

Figure 4.9: Average water temperature in the upper 20 m: comparison of VG unchanged conditions (blue line) to reference period (black line). Average (solid lines) and minimum/maximum values (dashed/dotted lines) of 19 years of simulation.

The scenario simulations with unchanged meteorological conditions should reproduce another possible reality. This means, these simulations could serve as an indirect validation of VG and its fitting. But, in contrast to reality, unchanged VG scenarios represent steady-state-climate without any gradients.
Figure 4.9 compares the results of the reference simulation (from section 3.3, black lines) to those of an ELCD simulation with artificial weather from VG with unchanged conditions (blue lines). The lines show the average water temperature of the upper 20 m; the average (solid lines) and the minimum and maximum values for each day of year over the 19 years of simulation.

In the summer half year (May - October), reference simulation and scenario agree almost perfectly, whereas in winter, the scenario simulation only covers the lower half of the measured temperature range.

Figure 4.10 shows the basin average water temperatures of reference simulation and sce-

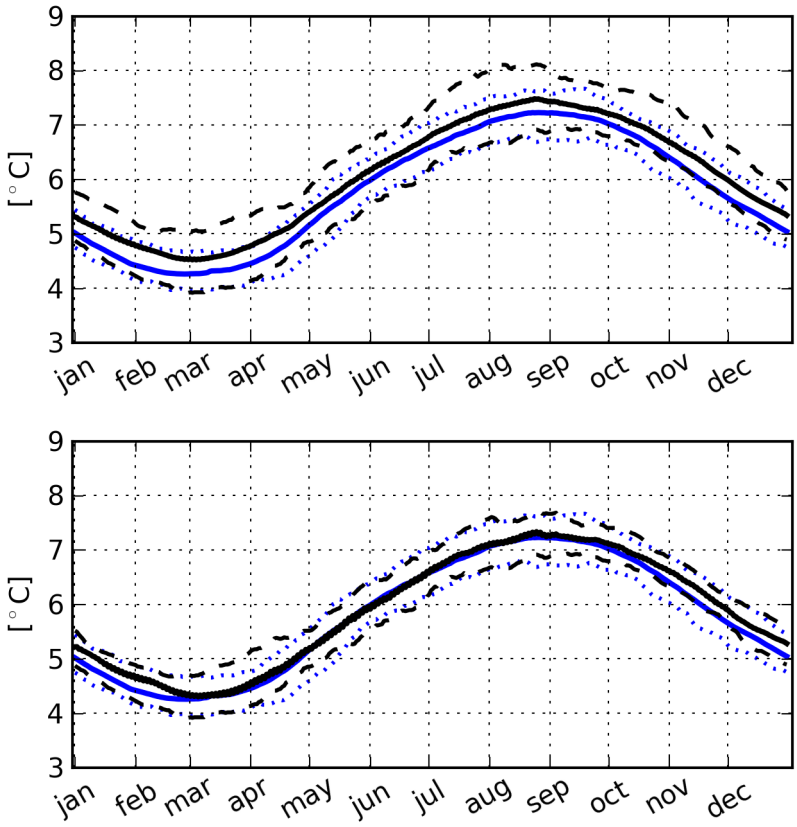

Figure 4.10: Basin average water temperature: comparison of VG unchanged conditions (blue line) to reference period (black line). Average (solid lines) and minimum/maximum values (dashed/dotted lines). Upper panel: complete time period, lower panel: reference period: 80ies only.

nario. Here, the scenario values tend to underestimate the reference simulation values for every day of the year. If only the measured data of the years 1980 - 1989 is considered (4.10, lower panel), water temperatures agree much better. Both average values and minimum-maximum range agree almost perfect, except for the autumn (September - November), where the minimum and the average in the scenario is lower.

Figure 4.11 shows times series of water temperature in the deep hypolimnion (below 200 m) in both simulations. Deep water temperatures in the scenario simulation (average: 4.28 °C), rather correspond to those simulated for the 1980ies (average: 4.325 °C) in the reference simulation than to those of the whole reference simulation (average: 4.46 °C).

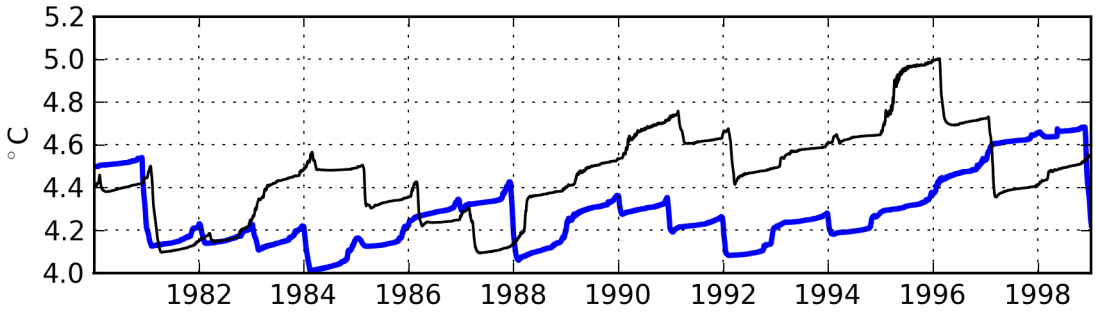

Figure 4.11: Hypolimnion water temperature: comparison of VG unchanged conditions (thin blue line) to reference period (thick black line).

The simulated residence time of water in the lake is $T_{1/2}$=4.1 years in the unchanged scenario and thus slightly shorter than that of the reference period (4.23 a).

4.2.2 Increased Mean Air Temperature

To evaluate the effects of a warmer climate, simulation runs with mean air temperature increase of 1, 2, 3, 4, 5 °C were performed. Sets of six scenarios of meteorological boundary conditions were produced by VG using the same random numbers for all six scenarios, to make sure that the warming is the only difference between them.
As in these simulations steady-state conditions should be considered, different initial conditions for both water temperature and water quality parameters were chosen. First, initial profiles were gained from simulations with air temperature gradients. Then, a 19 - years - simulation was run with steady-state boundary conditions with respectively increased air

			epilimnion 0 m - 20 m	hypolimnion below 200 m	basin average all
temperature	°C	unchanged	9.82	4.28	5.59
		+5 °C	13.80	7.08	8.58
		LR (°C/°C)	0.77	0.55	0.59
density	kg/m^3	unchanged	999.76	1000.21	1000.13
		+5 °C	999.29	1000.14	999.97
		LR (kg/m^3/°C)	-0.09	-0.01	-0.03
O_2 concentration	g/m^3	unchanged	10.53	9.40	10.24
		+5 °C	9.62	6.33	8.55
		LR (g/m^3/°C)	-0.17	-0.58	-0.32

Table 4.3: Average values for temperature, density and oxygen concentrations for unchanged and +5 °C simulations and linear regression parameters LR (b of $\hat{y} = a + b \cdot x$)

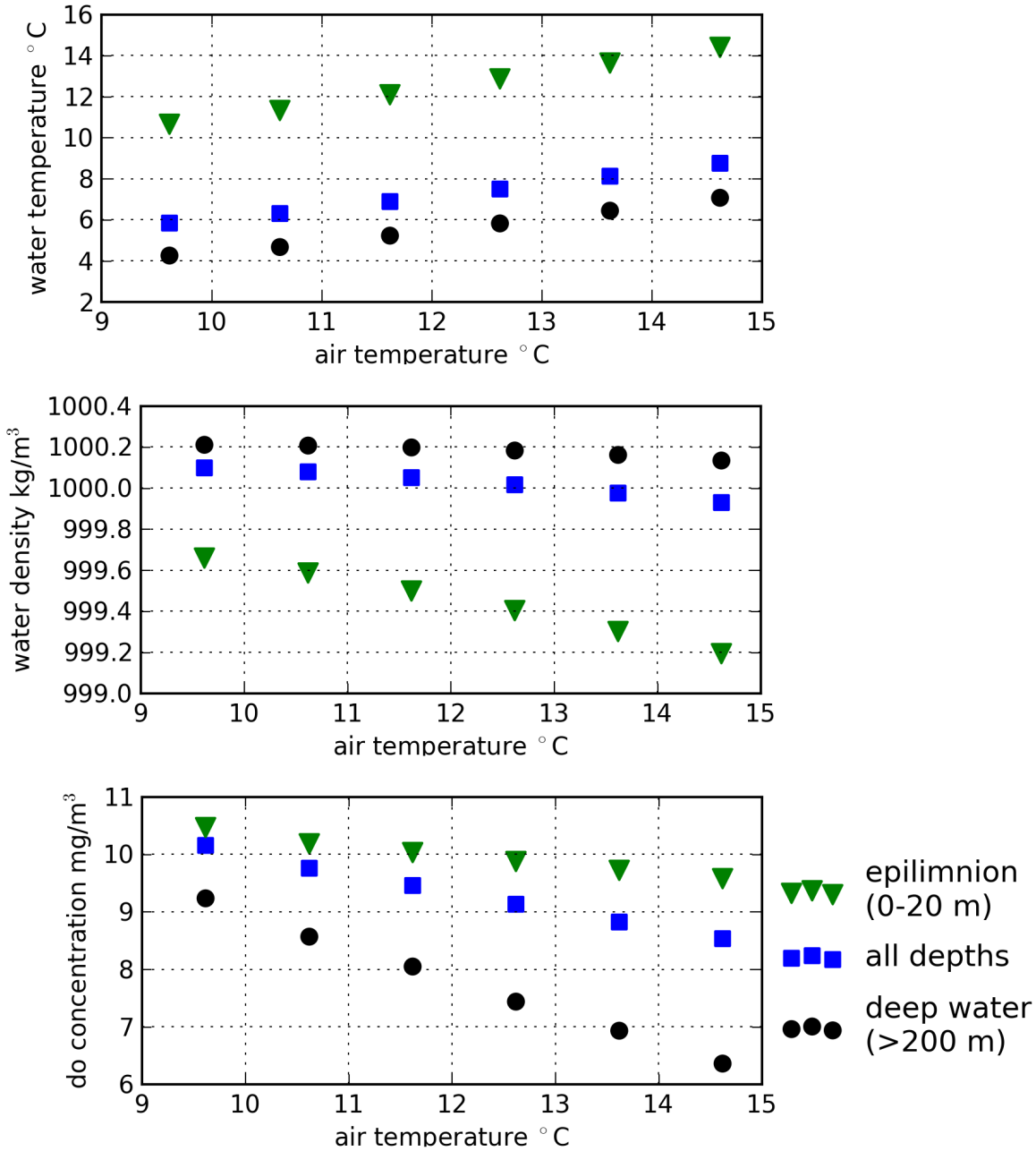

Figure 4.12: Water temperature, density, and oxygen concentration vs air temperature: simulation averages for epilimnion, deep hypolimnion and all-depth averages for simulations with mean air temperature increase of 0, 1, 2, 3, 4, 5 °C.

temperatures. The vertical profiles of water temperature and water quality parameters at the end of these simulations served as initial conditions for the scenario simulations in this chapter.

Figure 4.12 shows overall average values of water temperature, density and oxygen concentration for a set of five scenarios with increased mean air temperature and one scenario with unchanged conditions. A linear regression between average air temperature and average water temperature in the whole lake, the epilimnion (0-20 m) and the deep hypolimnion (below 200 m) results in different temperature increases in different layers (see table 4.3).
The heating of the epilimnion is stronger than that in the deep layers, resulting in 20 % increase in temperature difference between epi- and deep hypolimnion for the + 5 °C scenario compared to the unchanged conditions.
The increase in stability is even stronger than the increase in temperature difference: due to the polynomial shape of the temperature - density - curve, the density decrease in the epilimnion is faster than that in the hypolimnion, at the same temperature difference (see figure 4.12, middle panel). Thus, the enhanced temperature difference of 20 % for the + 5 °C scenario leads to an increase in density difference of 88 %.
For the oxygen concentrations (see figure 4.12, lower panel), there is also a clear trend visible in all depth. While there is just a minor decrease in epilimnetic oxygen concentration (mainly due to the temperature dependency of the oxygen saturation concentration), the average O_2 concentration in the deep hypolimnion decreases dramatically, from 9.4 mg/l to 6.3 mg/l.

Even though the air temperature increase in the considered scenarios is uniform throughout the year, the water temperature differences show an annual cycle: Increase in basin average water temperature is strongest in April and lowest in late summer and autumn (see figure 4.13). The absolute difference between April and October warming is up to 0.3 °C in the scenario with 5 °C mean air temperature increase.
The reason for the seasonal differences in warming lies in the surface energy loss.
Energy loss terms at the lake's surface are:

- sensible heat flux Q_{sh} [W/m^2]:

$$Q_s = c_{sh} \cdot \rho_{air} \cdot c_{p,air} \cdot v_{wind} \cdot (T_{air} - T_w) \tag{4.4}$$

  where c_s: sensible heat transfer coefficient ($1.3 \cdot 10^{-3}$)
  ρ_{air}: density of air [kg/m^3]
  $c_{p,air}$: specific heat of air at constant pressure (1003 J/(kg·K))
  v_{wind}: wind speed [m/s]
  $T_{air} - T_w$: temperature difference between air and lake surface [K]

- latent heat flux due to evaporation Q_{lh} [W/m^2]:

$$Q_{lh} = \frac{0.622}{P} \cdot c_L \cdot \rho_{air} \cdot L_E \cdot v_{wind} \cdot (e_a - e_s(T_w)) \tag{4.5}$$

  where P: atmospheric pressure [Pa]
  c_L: latent heat transfer coefficient ($1.3 \cdot 10^{-3}$)
  L_E: latent heat of evaporation of water ($2.453 \cdot 10^6$ J/kg)
  e_a: actual vapour pressure [Pa]
  $e_s(T_w)$: saturation vapour pressure at the water surface temperature T_w [Pa]

- long wave radiation Q_{lw} [W/m^2]:

$$Q_{lw} = \epsilon_w \cdot \sigma \cdot T_w^4 \tag{4.6}$$

where ϵ_w: emissivity of the water surface (0.96)
σ: Stefan-Boltzmann constant (5.6697$\cdot 10^{-8}$ W/(m$^2\cdot$K^{-4}))
T_w: lake surface temperature [K]

All energy loss terms at the surface are growing with increasing surface temperature.
During summer, in the stratified lake, the additional heat is added only to the epilimnion, whereas in winter, the heat is mixed to the entire water column (or at least to greater depths). Therefore, the increase in surface temperature for the same extra heat input is greater in summer, and the increase in energy loss is bigger during stratification. Maximum and minimum temperature difference hence appear at the end of the non-stratified respectively stratified period.
The maximum in spring is more pronounced than the minimum in autumn. While the beginning of stratification in spring is an abrupt change in mixed layer depth from very great depth in winter to minimal depth, the eroding thermocline in autumn gradually increases the mixing depth.

The averaged view is not suitable to analyse mixing events and stratification. In Figure 4.14, time series of water temperature and oxygen concentration below 200 m depth are shown for the six different scenarios.
With increasing air temperature, complete mixing events get more seldom, leading to longer periods of oxygen depletion. While in the unchanged scenario only in 5 out of 18 winters mixing is not strong enough to recover the deep water oxygen concentration, this number increases to 8, 10, 12 for the + 1, + 2, + 3 °C scenarios and 13 for the + 4 and + 5 °C scenarios. But even though the lake never cools down to temperature values close to the temperature of maximum density, complete mixing does take place, at higher isothermal temperatures. In the + 5 °C - simulation, the lake mixes at an average temperature of approximately 7 °C, 3 ° more than in the unchanged scenario.

In warmer water, the solubility of gases is lower. Maximum oxygen solubility is 12.6 mg/l at 4 °C and 11.6 mg/l at 7 °C. Hypolimnetic oxygen concentrations never reach these values of 100 % oxygen saturation. But maximum values are in the + 5 °C scenario approximately 1 mg/l lower than in the unchanged scenario (9.6 mg/l instead of 10.6 mg/l).
At the same time, as biogeochemical processes are temperature dependant, oxygen depletion is faster in warmer water.
During summer and autumn of year 12, oxygen concentration decreases linearly for all scenarios, starting from almost saturated conditions. A linear regression on these parts of the oxygen concentration time series yields 1.95 mg/l per year for the unchanged scenario. In the scenarios with increased air temperature, this value is 2.12, 2.37, 2.48, 2.54 mg/l per year, respectively. r^2-values of the linear regressions are higher than 0.99 for all scenarios. These values differ from year to year, but the gradient is always steeper in warmer water.

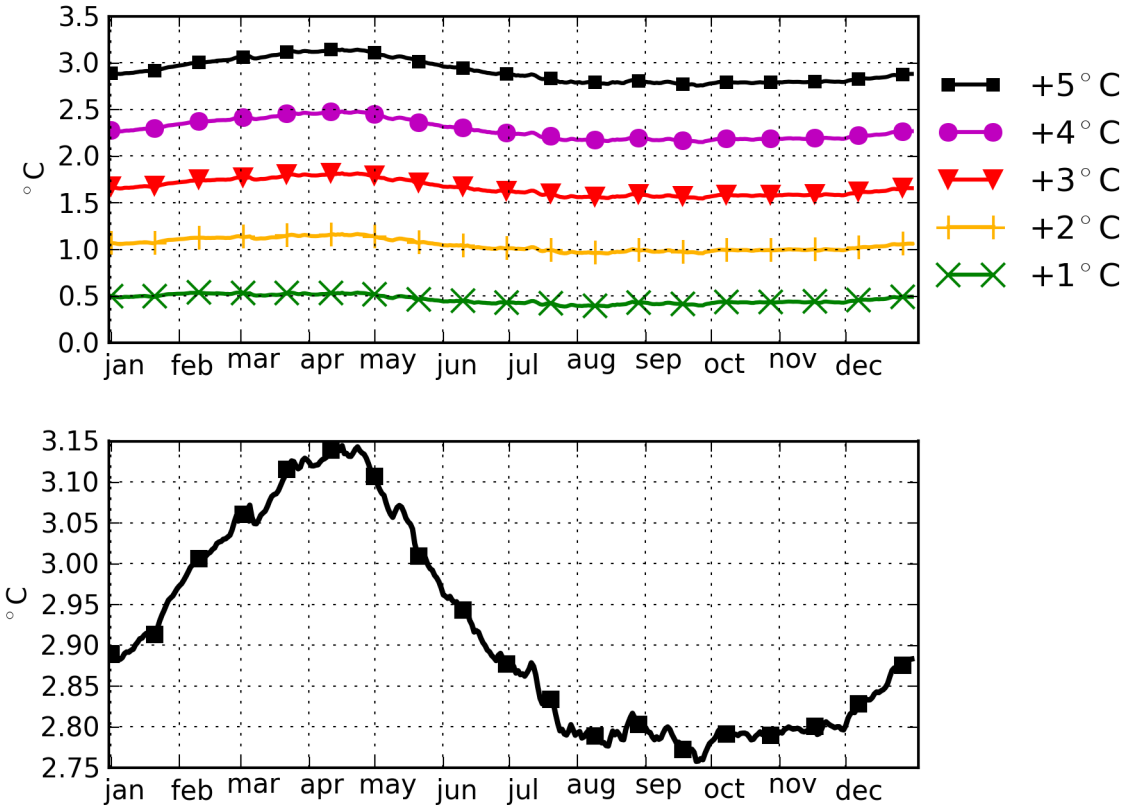

Figure 4.13: Differences of basin average water temperature between the scenarios with increased mean air temperature and the unchanged scenario.

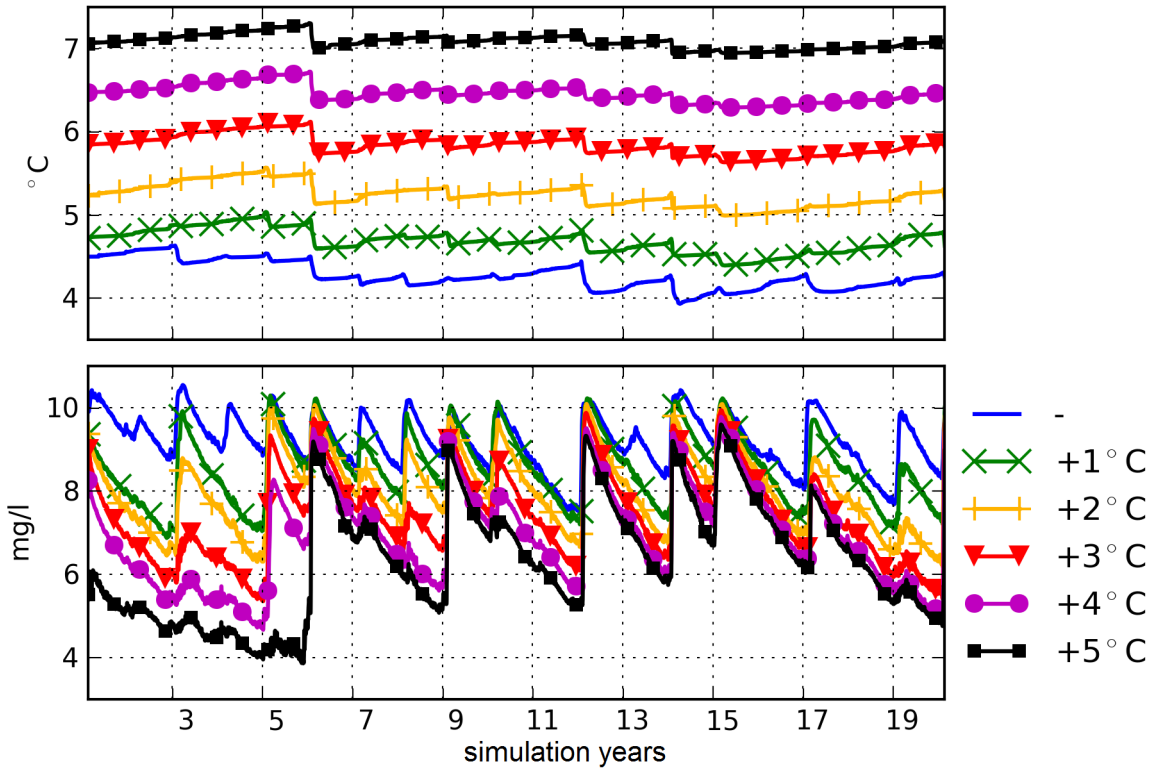

Figure 4.14: Temperature and oxygen concentration below 200 m in simulation with mean air temperature increased by 0, 1, 2, 3, 4, 5 °C.

Residence times
An increase in stratification stability, resulting in less deep mixing events, will certainly change the residence time of the water in the lake, at least in the hypolimnion. The half-life of water in the lake $T_{1/2}$ increases slightly from 4.1 years in the unchanged scenarios to 4.3 - 4.4 years in the scenarios with + 3 °C increase in air temperature. For the warmer scenarios, $T_{1/2}$ did not increase any more.
The residence time in the deep hypolimnion of the main basin clearly increased with increasing air temperature from 4.4-4.5 years in the unchanged scenarios to 5.4 - 5.7 years in the +5 °C - scenarios.

4.2.3 Changed Climate Variability

To evaluate the effects of a increased climate variability, simulation runs with mean air temperature increase of 1, 2, 3, 4, 5 °C and increased variability (pre-defined mean episode length: 14 d and σ of amplitudes: 4 °C) were performed. Sets of six scenarios of meteorological boundary conditions were produced by VG using the same random numbers for all six scenarios, to make sure that the warming is the only difference between them.
Initial conditions are the same as in the simulations with increased mean temperature in section 4.2.2.

Figure 4.15 shows overall average values of water temperature, and oxygen concentration for a set of six scenarios with increased climate variability and increased mean air temperature, and a set of six scenarios with standard climate variability and increased mean air temperature. In the scenarios with increased climate variability, the increase in deep water temperature is smaller for the same air temperature increase. In the epilimnion, both sets show a comparable gradient, but the absolute values are smaller in the simulations with increased climate variability.
The oxygen concentrations are the same for the epilimnion. In the hypolimnion, oxygen concentrations decrease faster with increasing air temperatures in the simulations with increased variability.

The increase in basin average water temperature in the simulations with increased climate variability and increased mean air temperature shows the same yearly cycle as in the simulations with standard climate variability (figure 4.16, compare to figure 4.13). The absolute water temperature increases are smaller, but the range of the yearly cycle is the same (0.3 °C).

Figure 4.17 compares the hypolimnetic conditions for four scenarios with standard and increased climate variability and 0 and 4 °C mean air temperature increase. In the scenarios with unchanged mean air temperature, the range of deep water temperature is the same for the two simulations with and without increased climate variability. The deep water temperature never falls below 3.9 °C. Oxygen concentrations reach lower values in the simulation with increased variability, but never fall below 6 mg/l. In the two +4 $^{\circ}C$-scenarios, the difference between unchanged and increased climate variability is larger: Deep water temperature is decreased by 0.7 $^{\circ}C$ on average, and deep water oxygen concentration by 0.3 mg/l due to the increased climate variability. While the minimum temperature is 6.3 °C in the unchanged variability scenario, it is 5.4 $^{\circ}C$ in the other.

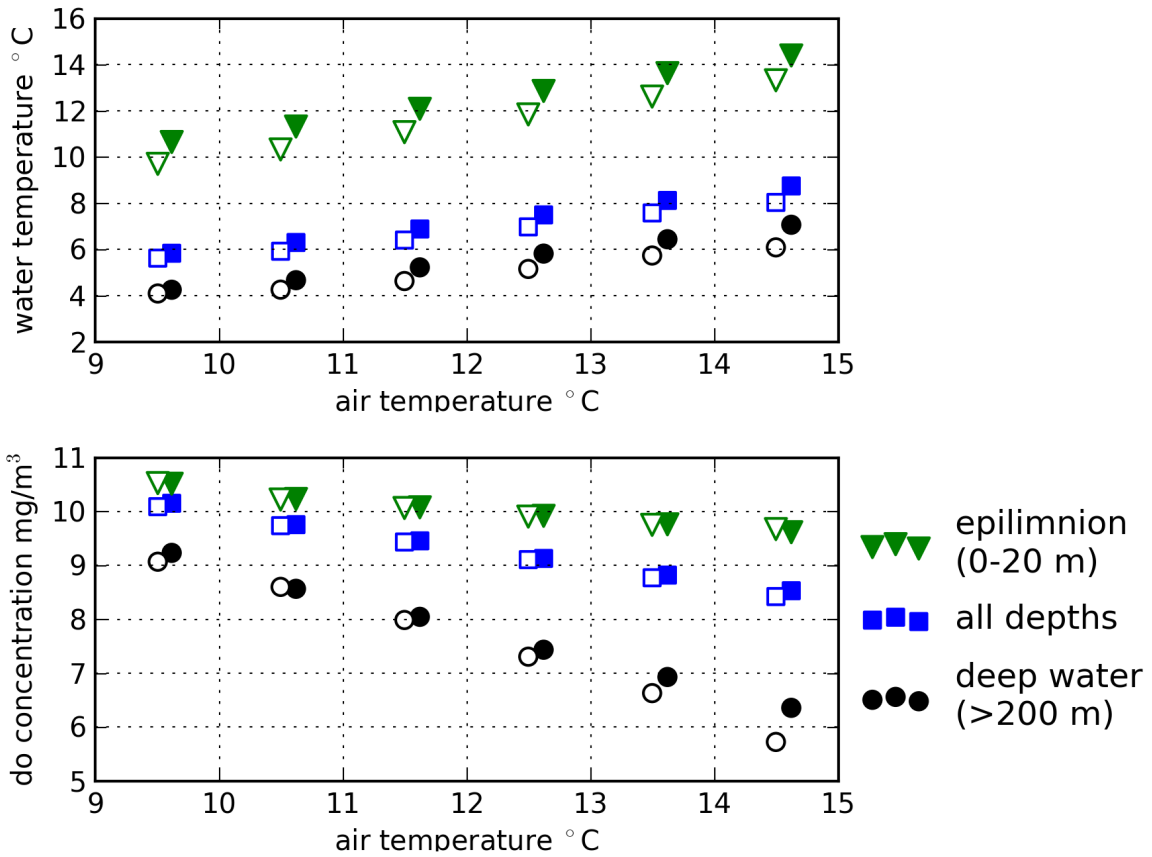

Figure 4.15: Water temperature, and oxygen concentration vs air temperature: simulation averages for epilimnion, deep hypolimnion and all-depth averages for simulation with unchanged conditions and mean air temperature increase of 1, 2, 3, 4, 5 °C (filled symbols), and the respective simulations with increased variability (empty symbols)

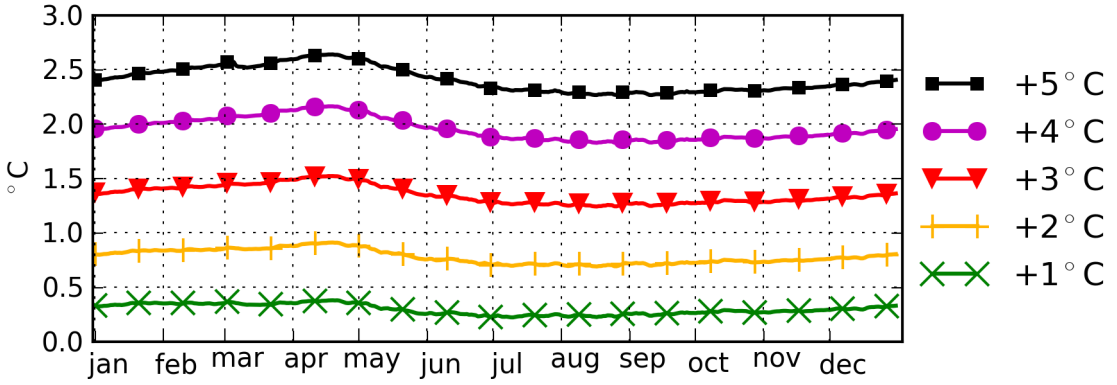

Figure 4.16: Differences of basin average water temperature between the scenarios with increased mean air temperature and increased variability and the unchanged scenario.

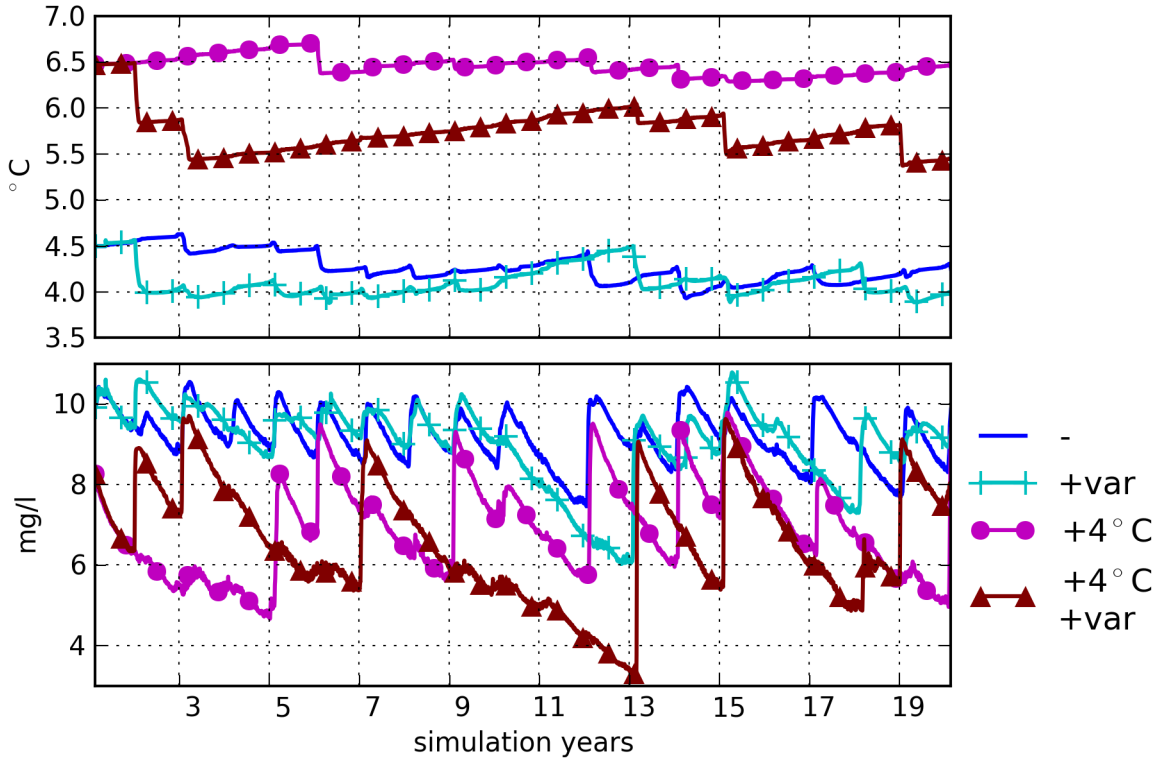

Figure 4.17: Water temperature and oxygen concentration below 200 m in simulation with and without increased climate variability.

Increasing the variability can have very different effects, depending on the average (air) temperature. As long as the average (winter) air temperature is such that the average isothermal temperatures during winter mixing are close to the temperature of maximum density,

both average hypolimnetic temperatures and oxygen concentration do not differ much from those resulting from simulations with standard variability. But the higher the deep water temperature normally is, the more pronounced the effect of single particularly cold winters can be. Even though the average air temperatures are the same for the scenarios with and without increased climate variability, simulated water temperatures are lower with increased climate variability in all depths (see figure 4.15). This indicates the larger importance of cold episodes: In a warm episode, water is heated at the surface. This stabilises the stratification, and the temperature change occurs mainly at the surface. The warmer surface leads to enhanced heat emission of the lake. A cold episode in contrast destabilises the stratification, letting the temperature change reach deeper regions. Remarkably cold winters cool down the whole water column, and produce an increased stability of the thermal stratification for the next time.

The half-life of water in the lake $T_{1/2}$ increases with increasing mean air temperature in the scenarios with increased climate variability from 4.01 years to 4.49 years. In the deep hypolimnion, $T_{1/2}$ increases by more than one year from 4.58 years to 5.88 years.

4.2.4 Temperature Gradients or Warming up the Lake

Up to now, this study analysed only steady-state scenarios, assuming both the climate and the lake to be in equilibrium. This assumption is not realistic for the near future. Even though global warming might experience periods of low or zero air temperature gradient, they are not likely to be long enough for the lake to reach equilibrium conditions for a longer time.
It is more likely, that air temperature will increase with varying gradient, forcing the lake to warm up as well.

As the warming climate influences the lake from the surface, the warming of the deeper layers lags behind the warming in the atmosphere.

A set of scenario simulations was run where the lake in the thermal conditions of 1980 suddenly meets the warmer climates of the scenarios with increased air temperatures from section 4.2.2. It takes a certain period until the water temperatures equal those of the equilibrium simulations. The duration of the warming period is depending on the air temperature increase. The difference in basin average water temperature decreases more or less exponentially. Strongest warming occurs during winter. In the deep hypolimnion, this seasonality is even more pronounced.

Table 4.4 gives numbers for the initial temperature differences ΔT_{max} and the warming time that is needed to decrease this basin average water temperature difference below 0.05 °C. The warming time varies from almost 5 years for ΔT_{air} = 1 °C to almost 18 years for ΔT_{air} = 4 °C. For ΔT_{air} = 5 °C, it is longer than the simulation time (19.2 years).

In a second set of scenario simulations, the ΔT_{air}s are applied in form of a gradient over the whole simulation period, resulting in gradients of 0.5, 1, 1.5, 2 and 2.5 °C per decade. In figure 4.18, the temperature differences to the equilibrium simulation of both the sudden-increase and the gradient simulation for a ΔT_{air} of 4 °C are given. In the gradient simulation,

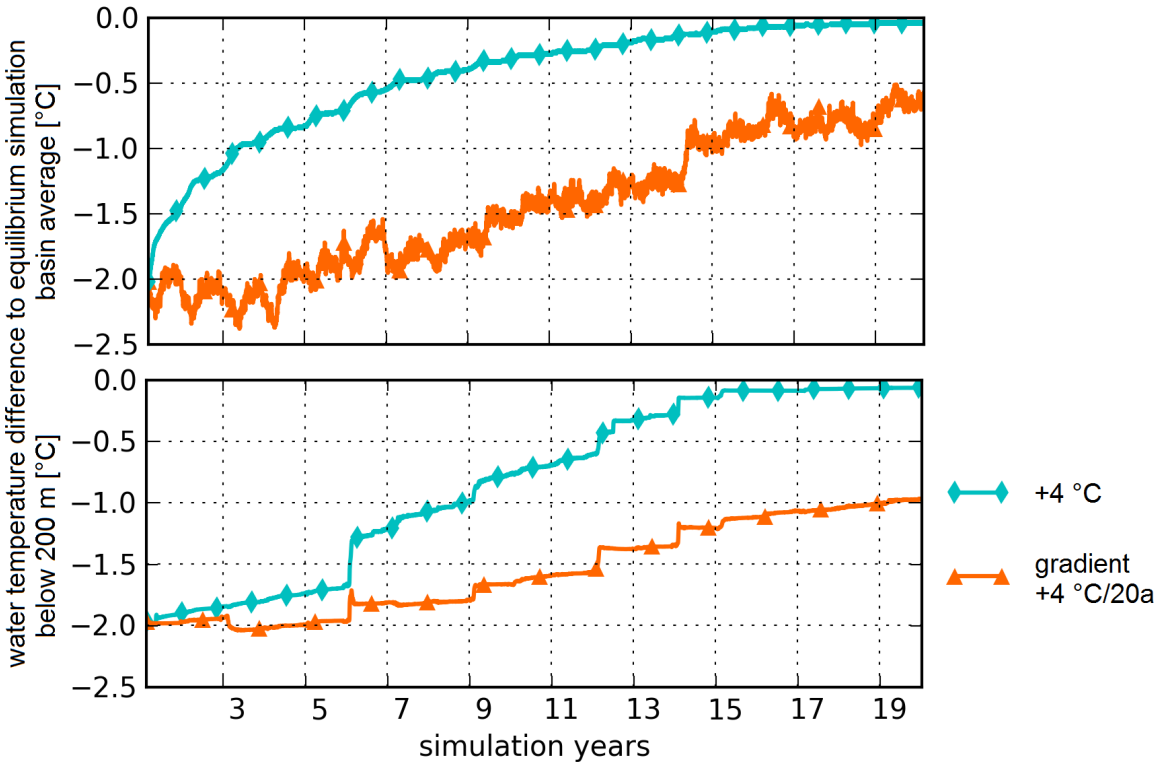

Figure 4.18: Water temperatures differences between two simulations with warmer climate starting from 1980 thermal conditions, and the equilibrium +4 °C simulation.

Table 4.4: Warming time lag of the lake: time in years the lake needs to acclimatise to a certain air temperature increase, and the corresponding increase in water temperature.

ΔT_{air}	[°C]	1	2	3	4	5
max. ΔT_{water}	[°C]	0.2	0.8	1.4	2.0	2.6
$\Delta T_{water} \leq 0.05$ °C after	[years]	4.9	8.9	13.0	17.9	>19.2

the difference in basin average water temperature is decreasing more or less linearly. The gradients in basin average water temperatures obtained by linear regression are given in table 4.5. The gradients in water temperature are smaller than those in the air temperature. The difference is decreasing with increasing air temperature gradient: For gradient T_{air} = 0.5 °C/10 years, the gradient in the water temperature is 0.38 times the air temperature gradient, while for gradient T_{air} = 2.5 °C/10 years, the factor is 0.52. The gradient measured in the air temperature in the reference period (1980-2000) is 0.75 °C per decade, and the measured gradient in basin average water temperature is 0.28 °C per decade.

Table 4.5: Gradients in basin average water temperature caused by air temperature gradients.

gradient T_{air}	[°C/10 years]	0.5	1	1.5	2	2.5
gradient in T_{water}	[°C/10 years]	0.19	0.43	0.66	0.90	1.3

4.2.5 Changes in Climatic Seasonality

To quantify the effect of extremely cold and warm winters and summers, the meteorological time series described in section 4.1.2.4 are used: approx. 3 °C anomaly for one season in a time series with + 3 °C increase in average air temperature. All five scenarios were produced using the same random state.

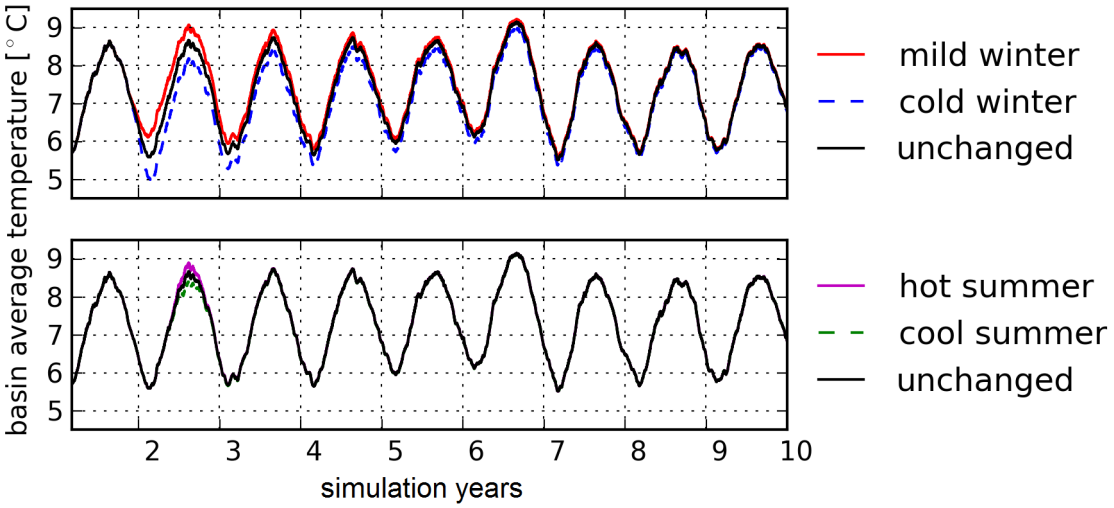

Figure 4.19: Basin average water temperature. Simulations with disturbed summer/winter.

In figure 4.19, the basin average water temperature is shown for the five simulations. Even though the air temperature differences are the same, the water temperature differences are much stronger and last longer for the simulations with disturbed winter (upper panel) than for those with disturbed summer. This is even more obvious in figure 4.20, where the differences in basin-average water temperatures between the disturbed and undisturbed simulations are shown.

Similar to the exponential function in equation 3.9, which was used in chapter 3.3.3 to get a residence time of water in the lake from tracer concentration decay, equation 4.7 was fitted to the temperature differences, in order to obtain a thermal residence time, i.e., the time, a temperature signal effects the lake:

$$\Delta T(t) = \Delta T_0 \cdot e^{-t \cdot \lambda} \tag{4.7}$$

where $\Delta T(t)$: temperature difference at time t [K]
ΔT_0: initial temperature difference [K]
t: time [years]
λ: decay constant [1/a]

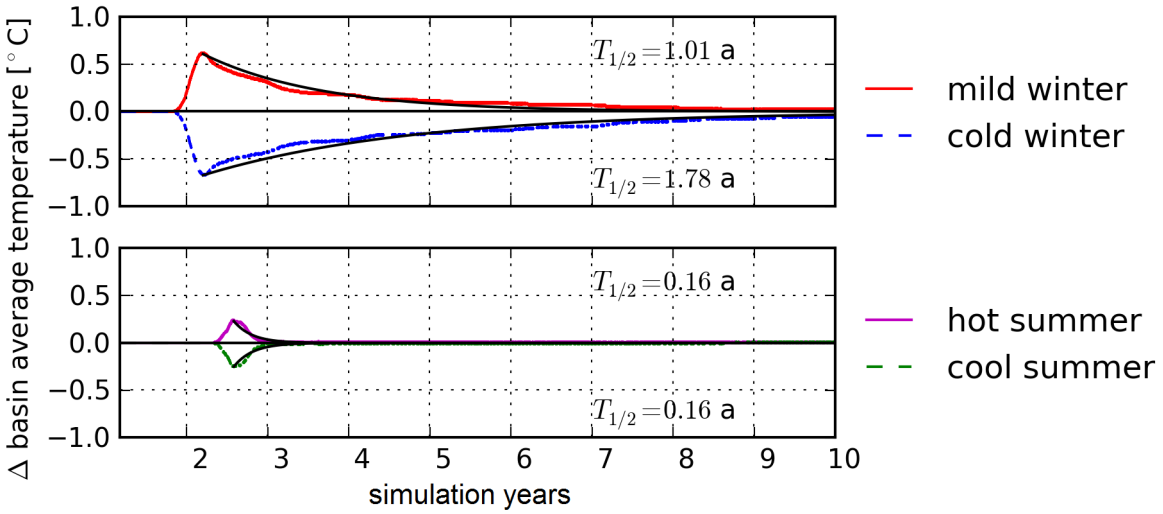

Figure 4.20: Thermal residence time: difference in basin average water temperature. Simulations with disturbed summer/winter.

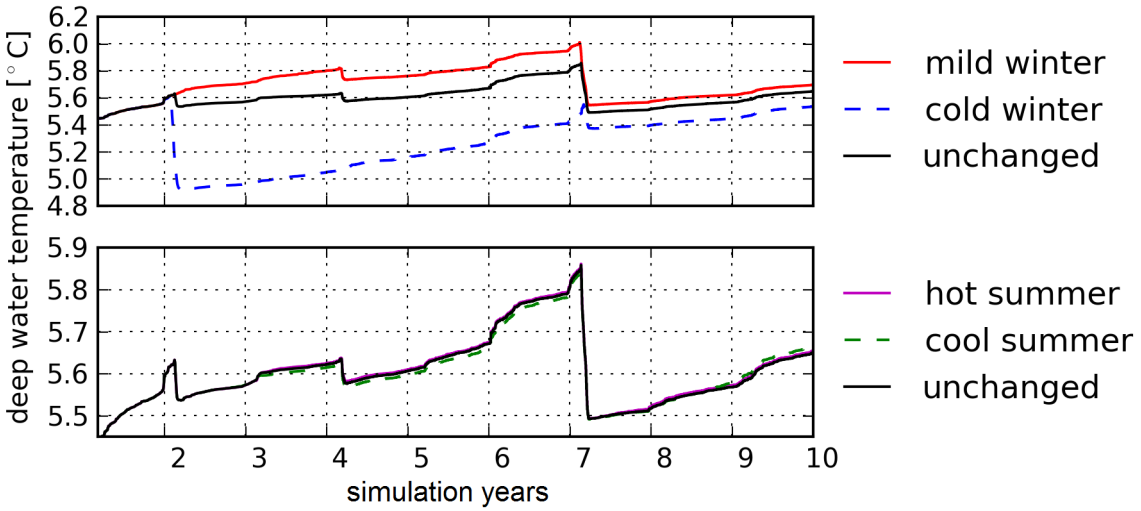

Figure 4.21: Deep water temperature. Simulations with disturbed summer/winter.

For the simulations with disturbed summer, the perturbations in basin average water temperature are small, and they disappear almost completely during the next winter. Both absolute magnitude and duration of the perturbation are the same for the cold and the warm summer. Initial temperature differences ΔT_0 are -0.25 K and 0.23 K and the half-life of the thermal signal is approximately 2 months.
In winter, cold and warm air temperature anomalies yield approximately the same magnitude of water temperature perturbation ΔT_0 of -0.67 K respective 0.61 K. But the thermal residence time for the cold anomaly ($T_{1/2}$=1.8 a) is considerably longer than that for the mild winter ($T_{1/2}$=1.0 a).

In the deep water temperatures (figure 4.21), differences are even more pronounced:

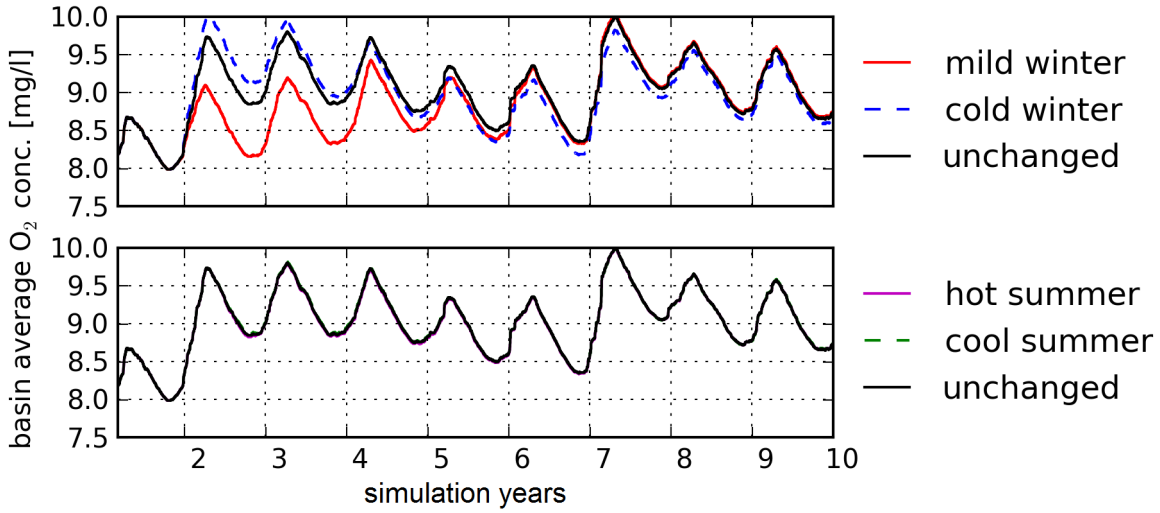

Figure 4.22: Basin average O_2 concentrations. Simulations with disturbed summer/winter.

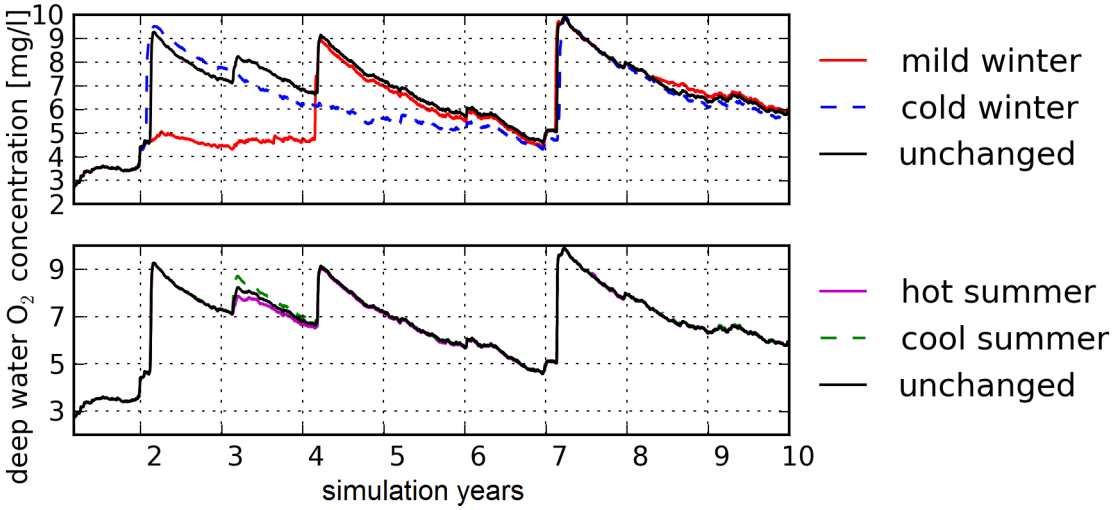

Figure 4.23: Deep water O_2 concentrations. Simulations with disturbed summer/winter.

The disturbed summer air temperatures show almost no effect on deep water temperatures. The mild winter increases deep water temperatures by approximately 0.1 °C. This difference is slightly increasing to 0.2 °C. The next reasonably cold winter four years later (in year seven) reduces this difference to 0.05 °C.
The cold winter decreases deep water temperatures by more than 0.6 °C. Two years later, winter four is just cold enough to mix the lake in the unchanged and mild winter scenarios, but not in the cold winter scenario, where stratification is stabilised by the colder hypolimnion. In the following years, the hypolimnion is constantly heating up, and the cold winter in year seven mixes the lake even in the cold winter scenario. As the decrease in hypolimnetic temperature in that winter in the cold winter scenario is small compared to that in the other scenarios, the temperature difference is reduced from 0.38 to 0.12 °C.

Basin-average oxygen concentrations (figure 4.22) show no visible differences for the disturbed summer scenarios.
The mild winter decreases the concentration by 0.7 mg/l. The difference decreases in the next years and vanishes in cold winter seven.
The cold winter first increases oxygen concentration by 0.3 mg/l, but two years later the concentration is lower than in the unchanged scenario.
The reason for that can be seen in the hypolimnetic oxygen concentrations in figure 4.23: In winter four, hypolimnetic oxygen is recovering in the unchanged and in the mild winter scenario, but not in the cold winter scenario, where complete mixing does not take place.

Changes in meteorological conditions in different times of the year show different effects on the lake's energy budget. As seen in section 4.2.2, is for homogeneous temperature increase throughout the year the increase in water temperature bigger during non-stratified conditions. Here, the reactions of the lake to changes in the yearly air temperature cycle are evaluated.

A set of five climate scenarios was produced:

- unchanged conditions
- warmer summer: air temperature increased by $\Delta T = + 3$ °C from April 15 to October 15. At the beginning and the end of the warm period, ΔT increased respectively decreased linearly within four weeks. All-year average air temperature increase is 1.7 °C.
- $\Delta T = + 1.7$ °C homogeneously throughout the year.
- warmer winter: air temperature increased by $\Delta T = + 3$ °C from November 03 to March 24. At the beginning and the end of the warm period, ΔT increased respectively decreased linearly. All-year average air temperature increase is 1.7 °C.
- $\Delta T = + 3$ °C homogeneously throughout the year.

All meteorological scenarios were produced using the same random numbers.

Figure 4.24 shows the simulated hypolimnetic conditions for these scenario simulations. Even though the average air temperature is the same, the lake's reaction to the +1.7 °C, winter +3 °C and summer +3 °C scenarios is very different. While the +1.7 °C scenario lies for both hypolimnetic temperature and O_2 conditions well between the unchanged and the +3 °C scenario, the summer +3 °C scenario behaves almost exactly as the unchanged scenario, and the winter +3 °C is very close to the homogeneous +3 °C scenario.
The water temperatures below 200 m depth differ at most by 0.09 °C for the + 3 °C and the winter +3 °C scenario, and 0.11 °C for the summer + 3 °C and the unchanged scenario. In the oxygen concentrations in the deep hypolimnion, the differences do not exceed 0.4 respectively 0.3 mg/l.
The hypolimnion is not affected significantly by changes in the meteorological conditions in summer.

Systematic change of yearly cycle
To analyse the seasonal differences in warming efficiency, simulations were performed with systematic changes in the seasonal warming of air temperature. A warming window of

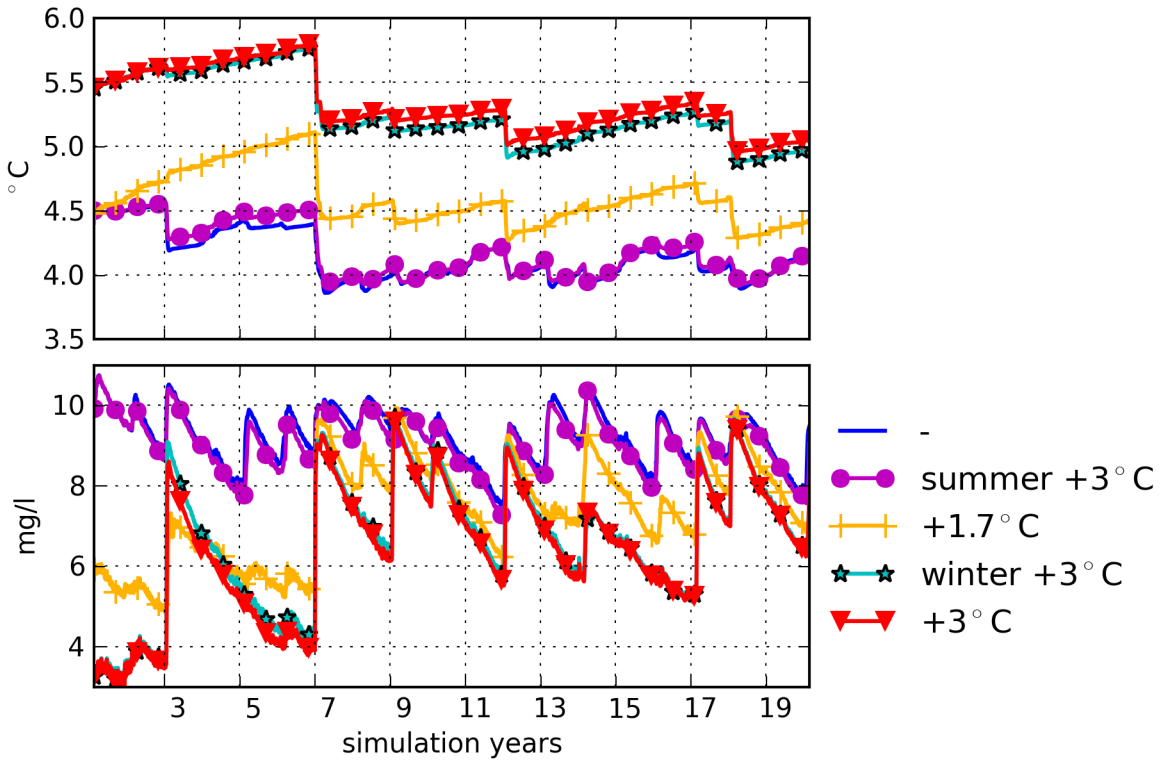

Figure 4.24: Water temperatures and O_2 concentrations below 200 m. Simulations with air temperature increase only in summer / winter.

120 days length, maximum ΔT of 3 °C and average increase of 1.6 °C was moved through the year. A set of twelve scenarios was produced, with average air temperature increase between 0.64 and 0.68 °C, using the same random numbers for all scenarios. Additionally, one scenario with unchanged conditions was generated using the same random numbers.

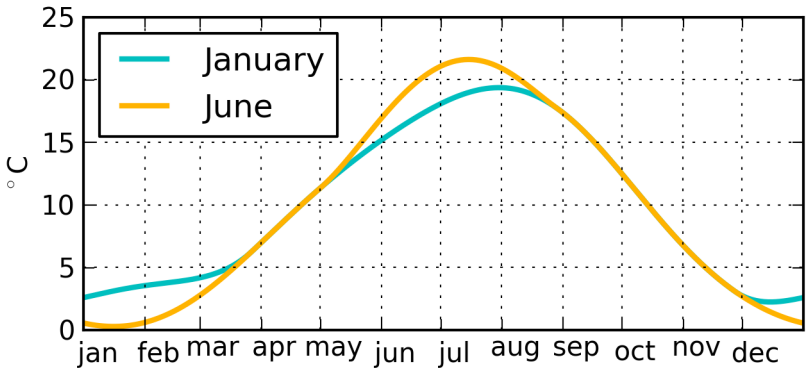

Figure 4.25: Annual cycles in air temperature: scenarios with maximum air temperature increase in January respectively June.

Figure 4.25 shows exemplarily the annual cycle in the air temperature for the scenarios with peak air temperature increase in January and June.

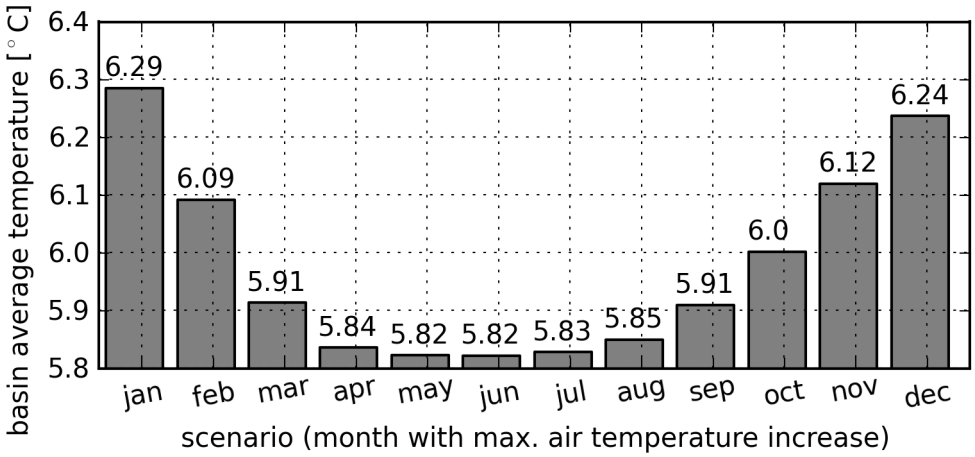

Figure 4.26: Simulation averages of basin average water temperatures.

Figure 4.26 shows the average water temperatures for the twelve scenarios with warming window. Average water temperature in the unchanged scenario is 5.80 °C. The most effective warming occurred in the scenario with maximum air temperature increase in January, (warming window between November 26 and March 26). The basin average water temperature increased in this simulation on average by 0.48 °C. The increase is biggest in February and March, and smallest in November and December (figure 4.27). The smallest warming effect showed the June-window: basin-average water temperature increased only by 0.02 °C (all-simulation average) and 0.16 °C in July. In winter, there is even a slight decrease in water temperature visible.

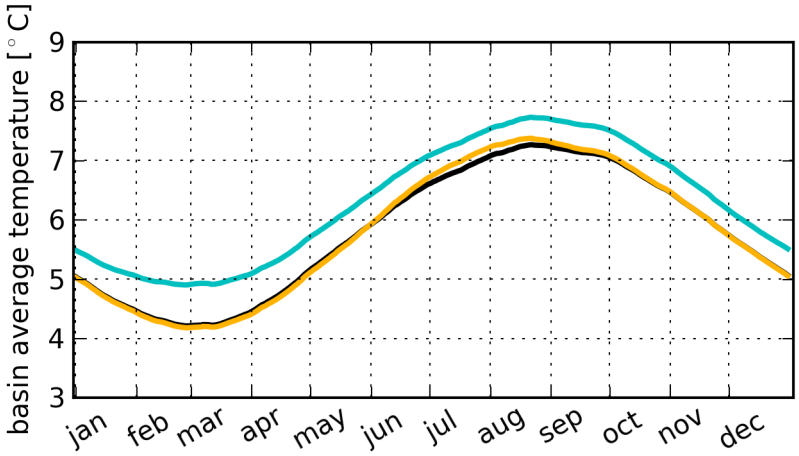

Figure 4.27: Annual cycles in basin average water temperatures: scenarios with maximum air temperature increase in January and June and unchanged scenario

In the deep hypolimnion (figure 4.28), water temperature increased on average by 0.42 °C in the January-scenario, and decreased by 0.02 °C in the June-scenario. Oxygen concentration decreased by 0.97 mg/l in the January-scenario, and increased by 0.04 mg/l in the June-scenario.

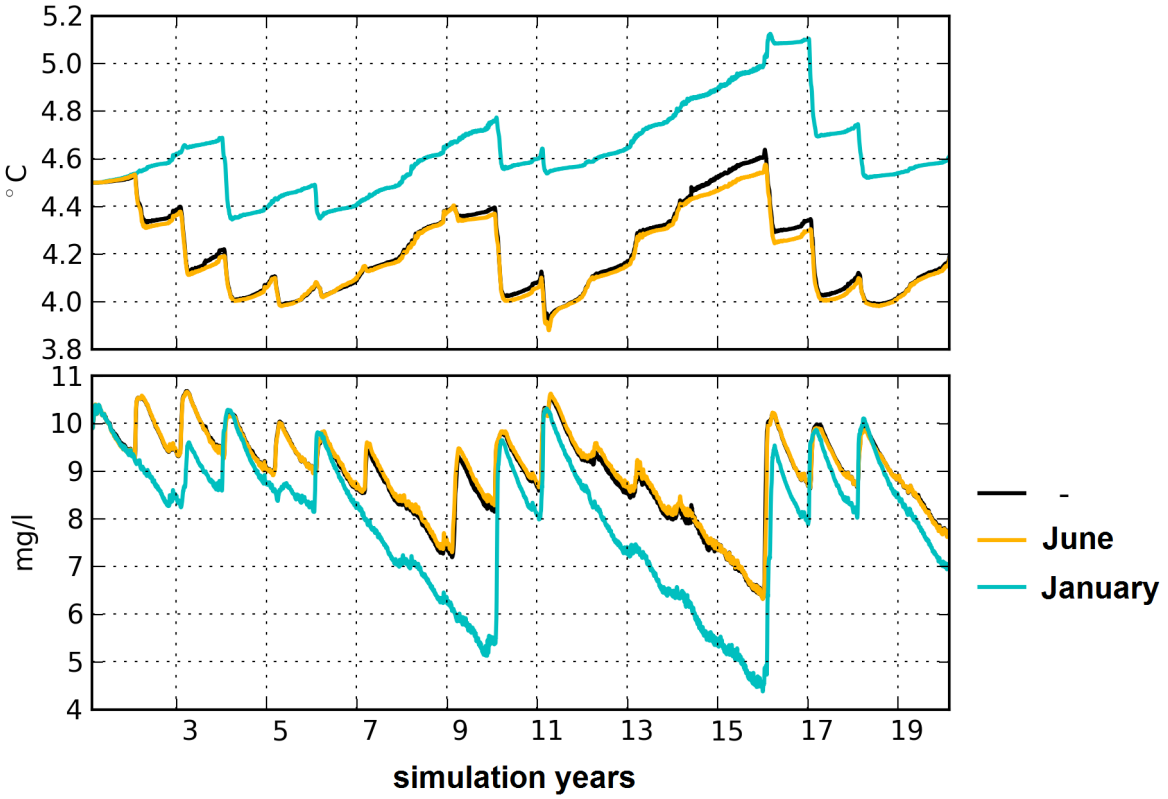

Figure 4.28: Water temperature and oxygen concentration below 200 m: scenarios with maximum air temperature increase in January respectively June and unchanged scenario.

The decrease in deep water temperature in the June-scenario, as well as the winterly decrease in basin average water temperature, can be explained with the enhanced stratification stability due to the additional warming in summer: The warming of the surface layer increases the density difference between epi- and hypolimnion and thus decreases the vertical heat transport.

4.3 Simulating Mesotrophic Conditions in a Warmer Climate

4.3.1 Nutrients, Oxygen and Fishery

The oligotrophic, i.e. low-productivity state of the lake is the natural state for Lake Constance, as for most deep (peri-) alpine lakes. Therefore, in terms of nature protection, this

state is the desired result of water protection efforts. But benefiting of the lake's products, one group of Lake Constance users might be interested in a higher productivity of the lake: the fishermen. A meso- or eutrophic lake with higher primary production can feed more fish, and therefore seems to guarantee for higher catches of the fishermen. Nowadays, 120 commercial fishermen are fishing in Lake Constance.
The commercially most important fish species in Lake Constance are the whitefish ≫Blaufelchen≪ (*Coregonus lavaretus wartmanii*) and European perch (*Perca fluviatilis*).
As the European perch is favouring mesotrophic water bodies, it was clearly profiting from eutrophication. Its yield in the years 1910 - 2004 is significantly correlated to total phosphorus concentrations TP, event though there are other influences, such as changes in fishing techniques. The decadal mean ($\pm$ standard deviation) yield was highest in the 1970ies (516 $\pm$ 175 t), and decreased to 274 $\pm$ 104 t in the 1990ies, and is still decreasing (Eckmann et al., 2006). As in the middle of the 20. century perch made up to 50-60 % of the total catch, this means also a decrease in total fishery yield in Lake Constance (Eckmann and Rösch, 1998).
Seeing this relationship, some commercial fishermen are asking for higher phosphorus concentrations in the lake.

The Blaufelchen also showed a decreasing growth rate during reoligotrophication, i.e. their growth rate is correlated to phosphorus concentrations in the lake. Thomas and Eckmann (2007) show, that the growth rate of Blaufelchen is also correlated to the standing stock. The more Blaufelchen there are in the lake, the slower they grow, due to intra-specific competition. In addition, size-selecting fishery causes an evolution towards slower growth: those fish that are growing more slowly reach the legal minimum size later and thus have more time to reproduce.

Blaufelchen depend on sufficient oxygen concentrations in the hypolimnion for reproduction. They spawn in late November / early December in the pelagic zone over water depths of 60 m - 250 m. The eggs sink down to the lake bottom, where the larvae hatch after 70 - 80 days in mid-February (Eckmann and Rösch, 1998).
During egg development a sufficiently high oxygen concentration is needed. Wahl and Löffler (2009) state, that oxygen concentrations 1 m above the lake bottom should not fall below 6 mg/l, otherwise almost all Blaufelchen eggs may be lost. Negative effects on the egg survival can be seen at concentrations below 8 mg/l.

Beginning in the end of the 19th century, and up to today, Blaufelchen eggs are harvested from adult fish caught in the lake and reared in hatcheries (Löffler, personal communication). Starting in a small scale, the amount of fry reared in the hatcheries increased significantly from the 1950ies on, which may have helped to overcome the problems with low oxygen concentrations in the hypolimnion during the years of intense eutrophication. The Kilch (*Coregonus acronius*, sometimes also *Coregonus pidschian* or *Coregonus pidschian acronius*), another Lake Constance whitefish spawning in the pelagic zone, became extinct in the 1960ies, maybe because it was not supported by hatcheries (Wahl and Löffler, 2009). But as the Kilch was spawning in water depths of 30 - 50 m, it might not have vanished due to lack of oxygen. Another possible reason is outcrossing: in the past, the hatcheries did not distinguish between the whitefish subspecies (Löffler, personal communication).

Since 1995, minimum oxygen concentrations in Upper Lake Constance did not fall below

6 mg/l (Internationale Gewässerschutzkommission für den Bodensee (IGKB), 2012). The Blaufelchen thus should have been able to reproduce naturally. Nevertheless, rearing in the hatcheries has been done all the time, and it is not clear, which percentage of the juvenile fish in the lake originates from the hatcheries and what percentage comes from natural reproduction.

4.3.2 Lake Model Simulations and Results

To evaluate the combined effects of a warmer climate and mesotrophic nutrient conditions on hypolimnetic oxygen, the simulations with increased mean air temperature from section 4.2.2 have been re-run with higher nutrient conditions. Initial conditions were measured values from March 1994, and nutrient concentrations in the tributaries were calculated using the relationships obtained from measurements in 1985/1986 (Wagner and Bührer, 1989). This results in basin-average PO_4 concentrations between 20 and 23 μg/l, which is low compared to the peak eutrophication values of 80 μg/l, but still much higher than the values in the oligotrophic scenarios, which lie around 5 μg/l (see figure 4.29).

The difference in primary production caused by this difference in nutrients is shown in

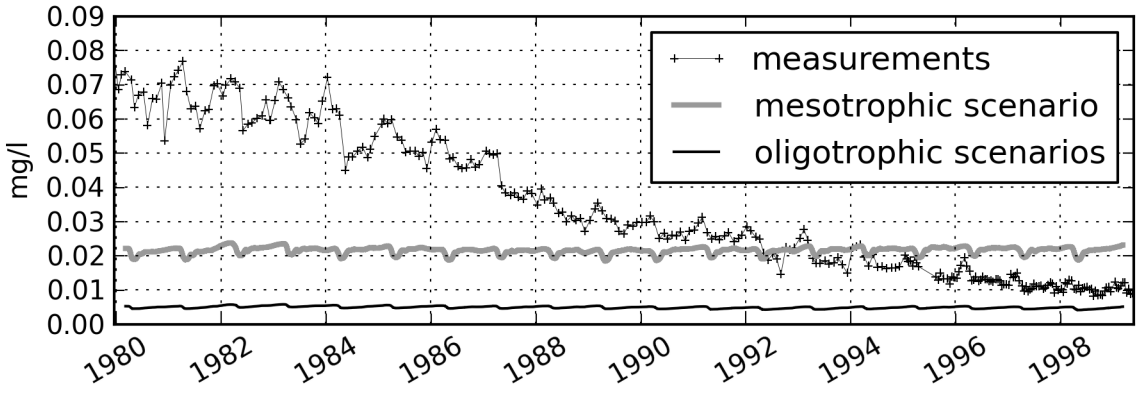

Figure 4.29: Basin-average PO_4 concentration in measurements and oligo- and mesotrophic + 3 °C scenario.

figure 4.30. The epilimnetic phytoplankton concentrations in the mesotrophic simulation show values between 2.5 and 3.7 μg/l. This is approximately twice as high as those in the oligotrophic scenario, which are around 1.5 μg/l, and corresponds to the values in the late 1980ies and early 1990ies in the reference simulation. The phytoplankton productivity in the mesotrophic simulation and in the first half of the reference simulation shows stronger year-to-year variability than that in the oligotrophic simulation and in the last years of the reference simulation.

As the physical boundary conditions are the same, the deep water oxygen concentration in the mesotrophic scenario shows the same pattern of reduction in stratified periods and recovery during mixing events, but the consumption of oxygen in the hypolimnion is faster in the mesotrophic scenario. This leads after two years without mixing to up to 1.5 mg/l lower oxygen concentrations in the mesotrophic scenario (Figure 4.31).

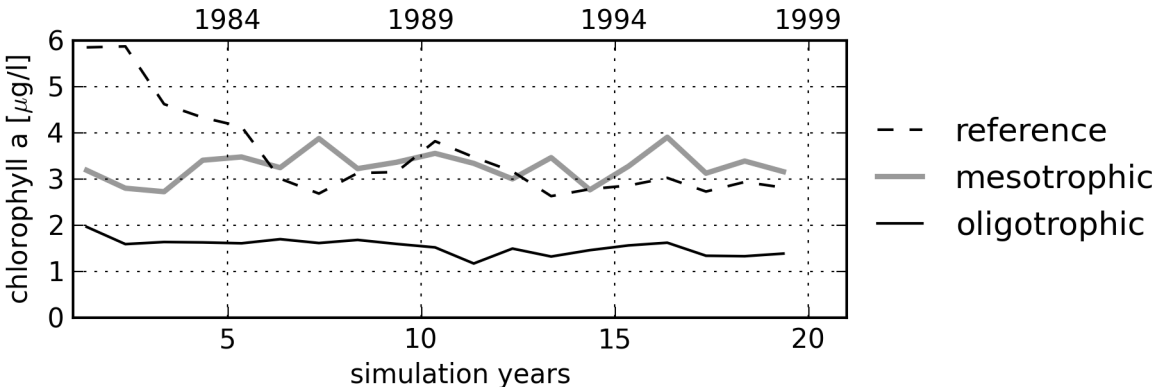

Figure 4.30: Yearly averages in phytoplankton concentration in the upper 20 m in reference simulation, oligo- and mesotrophic + 3 °C scenario.

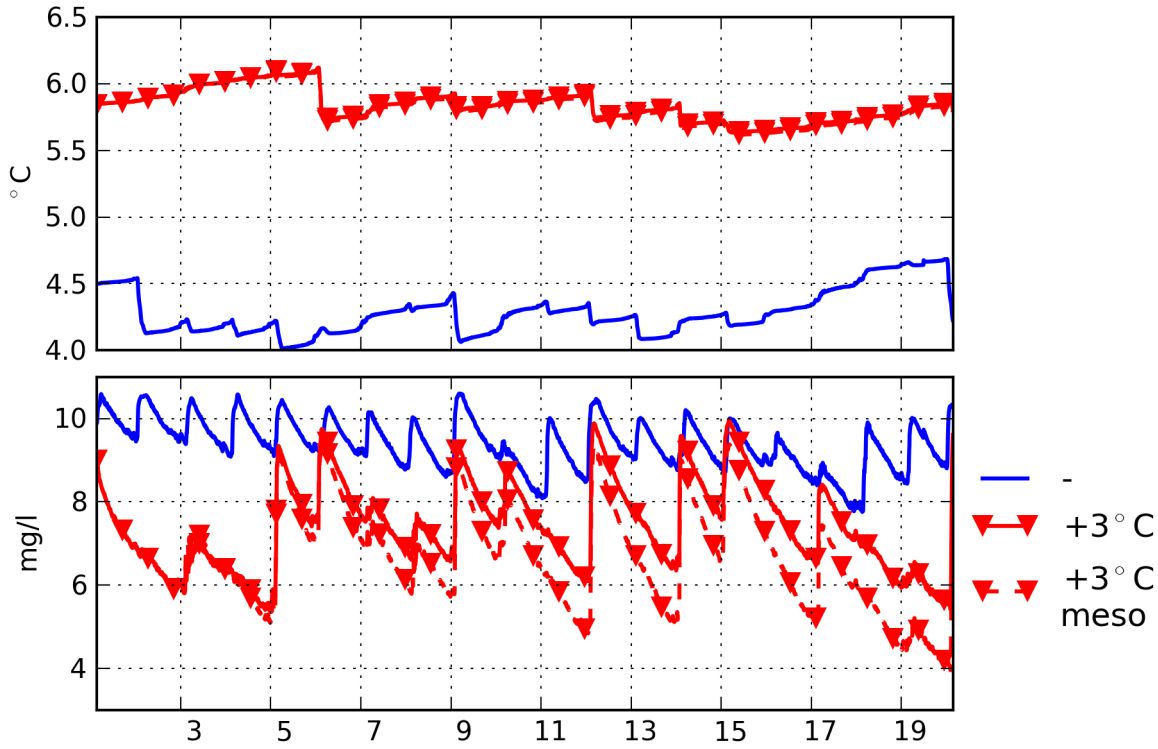

Figure 4.31: Water temperature and oxygen concentration below 200 m: comparison of oligo- and mesotrophic + 3 °C scenario

Possible implications for the Felchen

In the coarse grid with cell size of 10 km^2 (2 km * 5 km), 24 cells, e.g. 240 km^2, in the main basin are deeper than 60 m and thus potential spawning ground for the Blaufelchen.
In the following, simulation results shall be used to estimate how much of that area is lost due to oxygen deficiency (concentrations below 6 mg/l, values determined by Wahl and

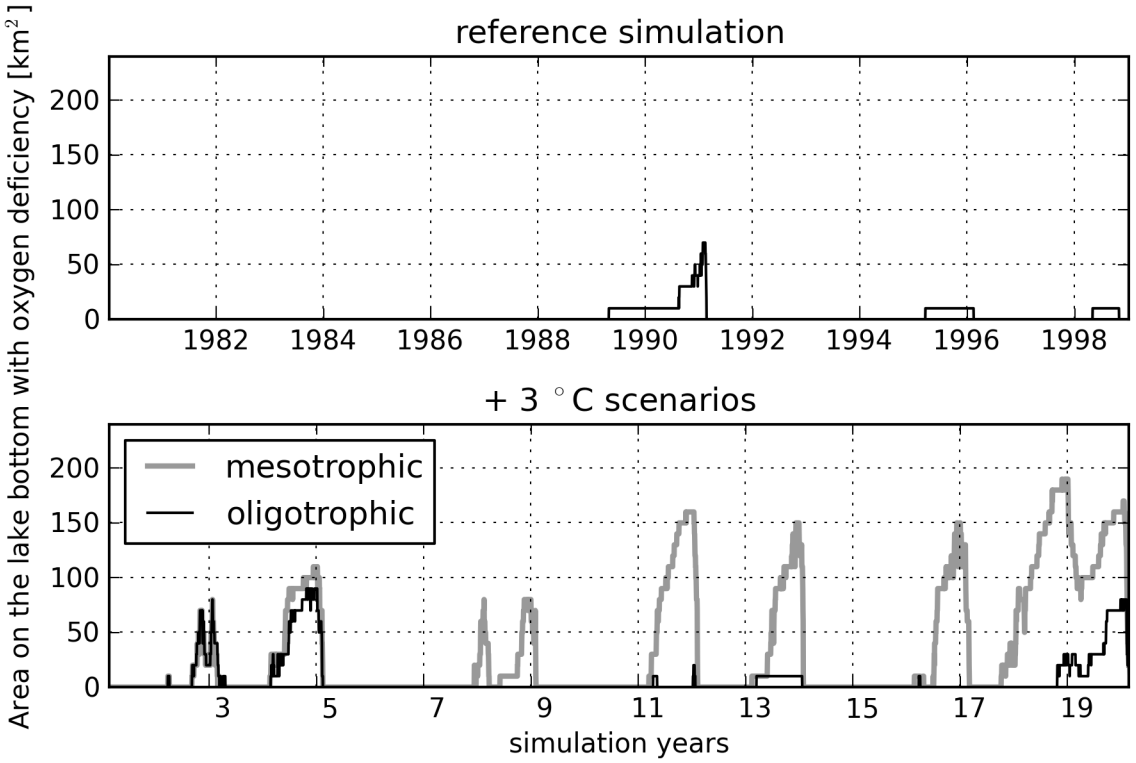

Figure 4.32: Area in the main basin with O_2 concentration below 6 mg/l at the lake bottom in reference simulation, oligo- and mesotrophic + 3 °C scenario.

Löffler (2009)).
In the reference simulation (see figure 4.32, upper panel), there are three periods where oxygen deficiency occur: 1989-91, 1995/96 and 1998. The maximum area with oxygen deficiency in the reference simulation is 70 km^2 in January and February 1991. In the other periods with oxygen deficiency it affects just one cell, i. e. 10 km^2.
In the oligotrophic + 3 °C - simulation (see figure 4.32, lower panel), oxygen deficiency occurs in 7 out of 19 winters, and the maximum affected area is 90 km^2 in the winter 4/5. On average, the oxygen deficiency area in those winters is 34 km^2.
In the mesotrophic + 3 °C - simulation, oxygen deficiency occurs in 13 out of 19 winters, and the maximum affected area is 190 km^2 in winter 18/19. On average, the oxygen deficiency area is 85 km^2.

Both the frequency of occurrence and the extent of oxygen deficiency area increased with increasing nutrient concentrations in the lake. It should be noted that some of the limitations of the lake model set-up that are explained in section 4.5, are of greater importance in a meso- or even eutrophic system: phosphorus release from the sediments is not considered, biogenic stabilisation of the stratification is ignored, and the parametrisation of the oxygen consumption has been done for a period where hypolimnetic oxygen concentrations were mostly on a higher level. This simulations are thus giving a rather conservative estimate concerning stratification stability and oxygen deficiency.

4.4 Climate Scenario based on GCM Projection

General Circulation Models (GCMs) simulate the global climate system numerically based on physical laws. Due to computational constraints, they are using grid cells of several degrees. To bring their output in a local context, downscaling is necessary. One option is **dynamic downscaling** by using a model chain of global and regional and / or local climate models. All those models base on more or less the same equations reproducing the physics of the climate, just the discretisation is different.
Empirical downscaling methods in contrast are data-driven approaches: **Statistic downscaling** is using the statistical description of the connection between large-scale features (modelled by the GCM) and locally measured weather. **Stochastic downscaling** methods are using weather generators and thus include randomness.

4.4.1 Stochastic Downscaling of GCM Output using VG

In VG, the option to determine a climate signal (used in section 4.2.5 for creating user-defined scenarios) was developed for stochastic downscaling of GCM scenarios: m (in equation 4.1) is defined using the bias-corrected GCM time series.

The air temperature simulated for the years 2070-79 by an A1B scenario simulation with the model ECHAM5/MPI-OM for the model cell containing the Lake Constance region was stochastically downscaled using VG to run simulations with ELCD.
The GCM simulation was done on the T63 horizontal resolution. Model cell width in the T63 resolution is 1.9 °, that is for Lake Constance region approximately 140 km * 200 km.
The model cell containing Lake Constance is thus also containing parts of the Alps with elevations up to 3000 m a.s.l. as well as pre-alpine regions with elevations around 300 m.
The temperature time was bias-corrected by using a reanalysis run of the same model, and station data from Konstanz, and performing a seasonal (day-of-year-specific) Q-Q-transformation. From this bias-corrected time-series, an average yearly cycle for the 2070ies decade was obtained by inverting the first four frequencies obtained by Fourier transformation.
Figure 4.33 shows the 2070ies annual cycle compared to that of the reference period.
The maximum daily average temperature in the reference period annual cycle is 19.4 °C and occurs at July 30th, whereas in the 2070ies the temperature slightly increases to 21.1 °C and occurs four days earlier on July 26th. The minimum daily average temperature in the reference period annual cycle is 0.3 °C and occurs at January 16th, whereas in the 2070ies the temperature increases to 4.9 °C and occurs two days earlier on January 14th.
The average difference between the two annual cycles is 3.27 °C. The warming itself shows a clear annual cycle (see Figure 4.34): Temperature rise is higher in winter and lower in summer. Highest increases of more than 4.5 °C can be found in January and February, the peak is 4.7 °C on February 9. Lowest warming (below 2 °C) can be found during summer school holidays in southern Germany (mid of July to begin of September), the absolute minimum is 1.5 °C on August 16th.

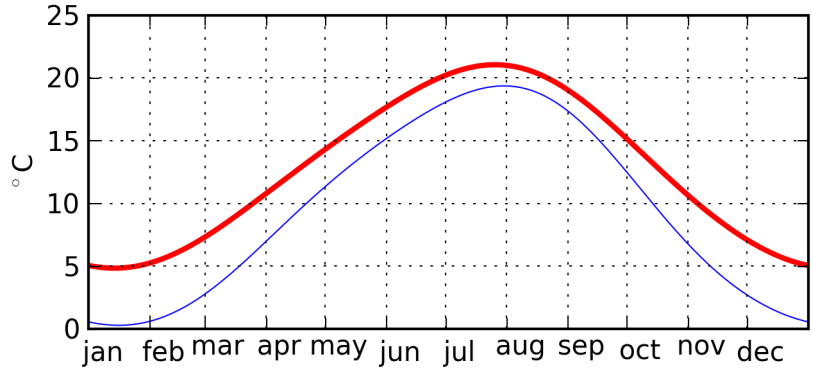

Figure 4.33: Average annual cycle in air temperature from bias-corrected GCM-output for 2070-79 (thick red line), and from the reference period measurement data (thin blue line)

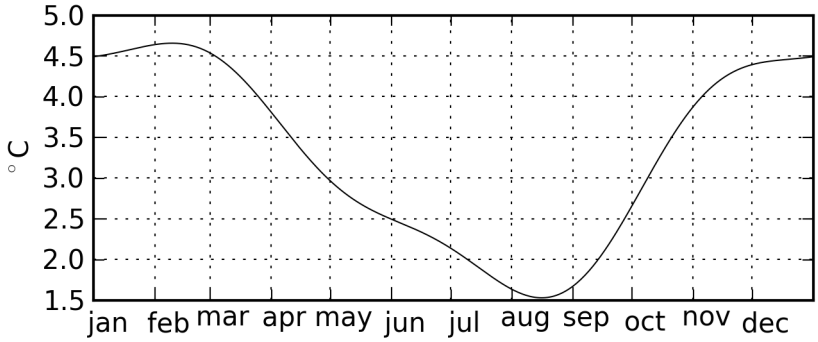

Figure 4.34: Difference in average annual cycle in air temperature from bias-corrected GCM-output for 2070-79 and from the reference period measurement data

This annual cycle was used as m.
Another option of passing a seasonal climate signal to a weather generator is using monthly values, as done for example by Wilks (2009) and Fatichi et al. (2011). In contrast to this method, the annual cycle obtained by Fourier transformation gives a smooth signal, and can show also sub-monthly shifts of the curve's minima and maxima.
Doing downscaling of GCM data by just running VG with this annual cycle as climate signal assumes the cross- and autocorrelations of the meteorological variables to stay the same in the scenario period as in the reference period. The autocorrelation of daily average air temperature is defining the climate variability defined in section 4.1.2.2 by length and amplitude of anomality episodes. Episodes in the bias corrected times series for the 2070ies show an average episode length of 4.5 days, and the standard deviation of the amplitudes is 2.1 °C. In the measured data of the reference period the average episode length is 4.3 days, and the standard deviation of the amplitudes is 2.4 °C.

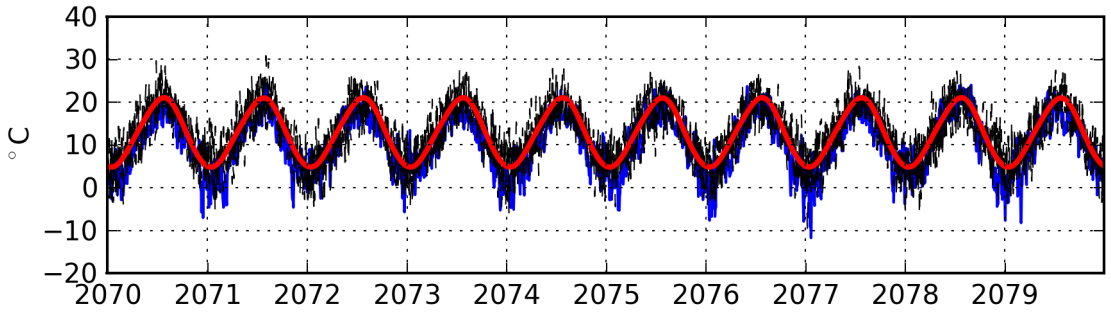

Figure 4.35: Average annual cycle (thick red line), bias-corrected GCM output (blue) and four VG realisations for daily average air temperatures in the 2070ies (dashed black lines)

Stochastic downscaling by using VG produces different realisations of the GCM projection (see Figure 4.35): All the simulated air temperature time series follow the average annual cycle but show different short-time fluctuations.

4.4.2 Lake Model Simulation Results

Four ELCD simulations were performed with four realisations of stochastically downscaled data from the ECHAM5 A1B projection for the period 2070-79.
Initial conditions are the same for all four realisations.

Figure 4.36 shows the annual cycles of basin-average water temperatures obtained by the four ELCD simulations with the downscaled ECHAM5 scenario compared to scenario simulations with unchanged conditions. The lake water temperature is increased by approximately 2 °C. The minimum of water temperature tends to be shifted to an earlier time in the year, by 1 - 2 weeks from end of February/ begin of march to mid of February. The annual cycle of water temperature is slightly flattened for the ECHAM5-scenarios: The range between the winterly minimum water temperatures and the maximum water temperatures in summer decreased from 3.0 °C in the unchanged conditions scenarios to 2.7 °C in the ECHAM5-scenarios.

Figure 4.37 shows the differences between the scenario simulations. Average temperature difference is 2.0 - 2.3 °C. Minimum difference is 1.7 - 2.0 °C in August or September. Maximum difference is 2.3 - 2.6 °C in March.
Compared to the scenarios with uniform temperature increase (Figure 4.13 in section 4.2.2), the annual cycle is stronger (inter-annual differences in heating are $\geq$ 0.5 °C here and up to 0.3 °C in the +3 and +4 °C scenarios in section 4.2.2). The minimum in summer is more pronounced in the downscaled scenarios, and the maximum occurs earlier.

Deep water temperatures and oxygen concentrations (figure 4.38) indicate 4 - 5 complete mixing events in the downscaled scenarios for the simulation period of 19 years. In the

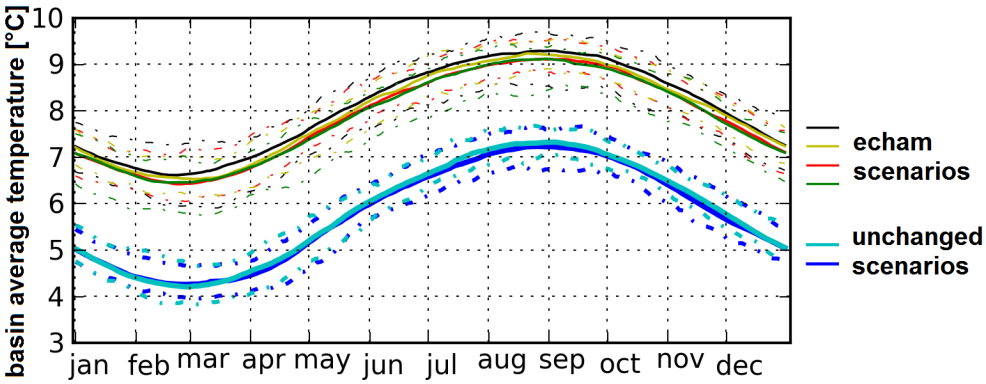

Figure 4.36: Basin-average water temperature: Simulation results for unchanged and downscaled scenarios. Solid lines indicate the average, dashed lines the 10- and 90-percentiles for the respective doy.

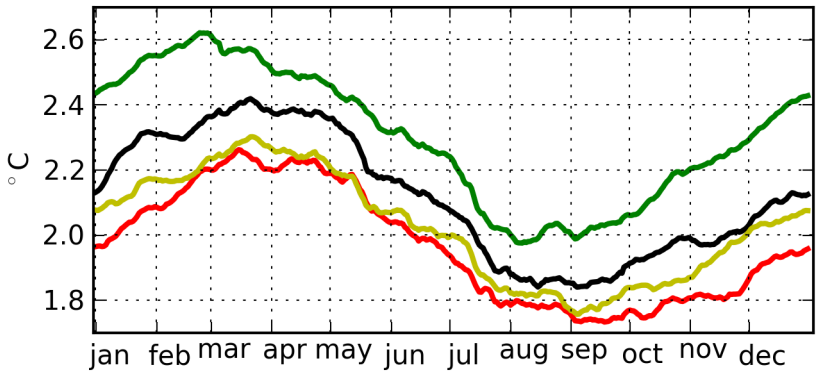

Figure 4.37: Difference between basin-average water temperatures in unchanged and downscaled scenarios.

scenarios with uniform temperature increase, this number is 5 - 6 for a comparable air temperature increase. Hypolimnetic oxygen concentrations decrease for several years down to values of 3 mg/l and below.
The simulation averages of water temperatures (figure 4.39) are higher than those with homogeneous temperature increase, while the oxygen concentrations are lower.

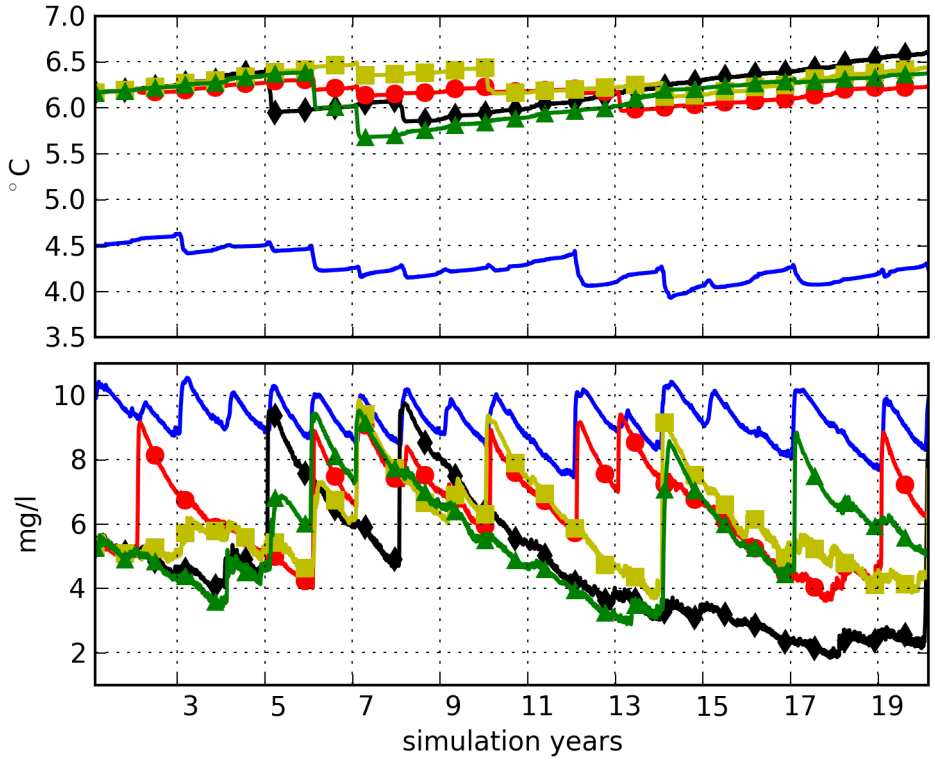

Figure 4.38: Temperature and oxygen concentration below 200 m in unchanged (blue line) and downscaled scenario simulations (4 realisations).

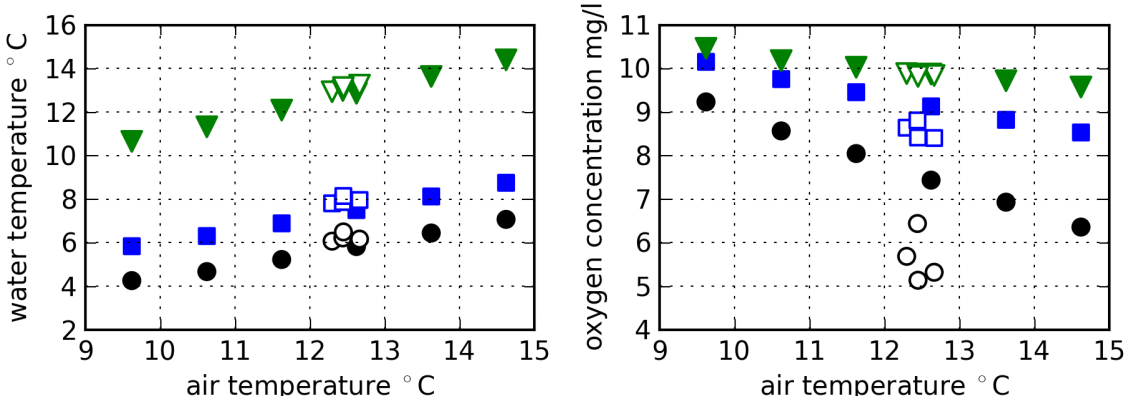

Figure 4.39: Water temperature (left) and O_2 concentration (right)vs air temperature: simulation averages for epilimnion 0-20 m (green triangles), deep hypolimnion below 200 m (black circles) and all-depth averages (blue squares) for simulation with unchanged conditions and uniform air temperature increase (filled symbols) and downscaled scenarios (empty symbols)

4.4.3 Conclusions

The annual cycle of temperature change (figure 4.33), used as perturbation for VG scenarios, shows a pronounced annual cycle with maximum temperature increase in winter. Thus, the effects on the lake's energy budget, the thermal stratification and the hypolimnion are stronger as in comparable simulations with homogeneous temperature increase.
This annual cycle in local temperature change is thus of some importance. But its shape strongly depends on the chosen downscaling method.

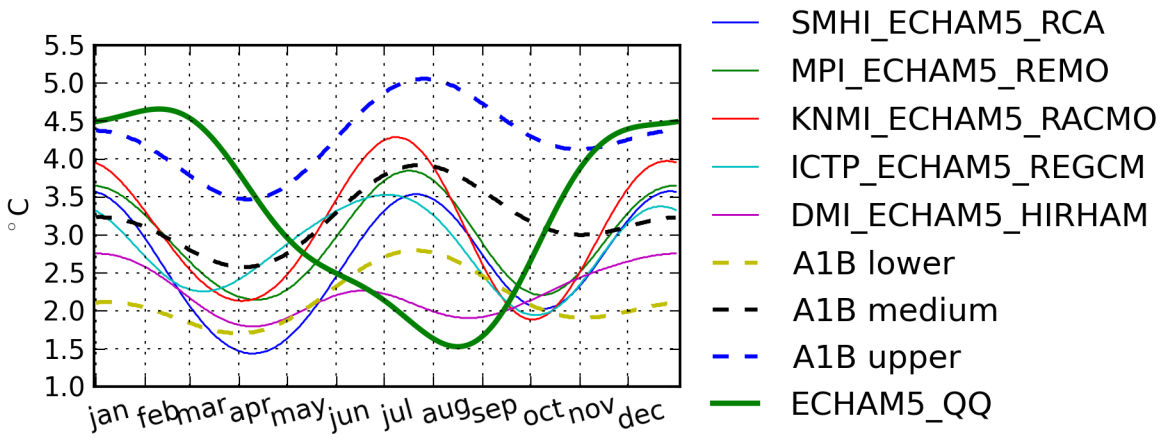

Figure 4.40: Downscaled air temperature from CH2011 for Güttingen (thin solid lines) or north-eastern Switzerland (dashed lines) for different model chains

CH2011 (CH2011, 2011; Bosshard et al., 2011) produced annual cycles of temperature increase using two different approaches:

1. Local scenarios at daily resolution based on individual model chains:
   Annual cycles of temperature change at station-scale were produced by GCM-RCM – model chains.

2. Regional scenarios based on the probabilistic method:
   Seasonal means of model ensembles were used to obtain annual cycles in the regional scale.

Figure 4.40 shows the daily temperature differences obtained by different downscaling methods. ECHAM5_QQ is the time series for 2070-79 obtained by QQ-transformation (see section 4.4.1). All other lines depict data from CH2011 for the scenario period 2070-79. Reference period for the CH2011 time series is 1980-2009. Thin lines are local scenarios for Güttingen, using the GCM ECHAM5 and different RCMs. Güttingen is situated at the Swiss shore of Lake Constance, approximately 10 km south-east of Konstanz. Dashed lines are regional scenarios based on the probabilistic method for north-eastern Switzerland. *Upper* and *lower* are standing for the 97.5 - and 2.5 -percentile, respectively.

While for the QQ–bias correction the output of one single GCM cell was used, CH2011 averaged values of four neighbouring RCM cells for their local scenarios. No station-data – based bias-correction was performed for the CH2011 scenarios.
Unlike the time series downscaled by QQ-transformation in section 4.4.1, most of the scenarios in figure 4.40 show a maximum in temperature increase during summer. DMI - ECHAM5 - HIRHAM produces at least a local minimum in temperature increase for August. Average temperature increases range from 2.2 - 3.1 °C for the local scenarios and 2.1 - 4.3 °C for the regional scenarios. So the increase of 3.3 °C obtained for ECHAM5_QQ is well within the range of the regional scenarios, but above the range of local scenarios for Güttingen. (The CH2011 data were obtained from the Center for Climate Systems Modeling (C2SM).)

4.5 Limits of this Study

Due to deficiencies in the models as well as in the setup of the study, several questions have to remain open.

4.5.1 Lake Models (ELCOM-CAEDYM)

The coarse resolution of the model grid (2 km * 5 km) enables long term simulations in reasonable computation times. But it neglects the details of the bathymetry. The shallow areas in the littoral zone thus are under-represented in the model.
These shallow areas are of considerable importance for the lake's ecosystem. The littoral zone is a highly dynamic system. The annual cycle of the water level moves the shoreline in some areas by several meters. The lake's surface area is in July on average 8 km^2 larger than in February. In the model, the water level changes, but this does not cause any changes in surface area.

The model is not simulating ice cover in cold winters. Ice cover reduces energy loss at the surface. But total ice cover is very seldom. Even in cold winters, the fraction of the surface that is covered by ice is negligible.

For some scenarios, the model simulations revealed stratified periods of several years duration. But even after eight years of oxygen depletion, the simulated oxygen concentration in the deepest cell does not fall below 1.5 mg/l. The parametrisation of the water quality model has been optimized to simulate the reference period. In the reference period, no oxygen concentration below 4.3 mg/l was measured.
In this parametrisation, under oxygen deficiency conditions, oxygen consumption is strongly decreasing. In the natural system of the lake, the microbial community might adopt to the decreasing oxygen concentration, and the decrease in oxygen consumption might be smaller.There is thus the potential of underestimating the risk of anoxia due to the fact that the parametrisation of the water quality model does not consider microbia favouring low-oxygen conditions.

The biochemic decomposition of organic material in the hypolimnion produces dissolved substances that increase the density of the water. When the density difference gets large

enough, the stratification is not destroyed in winter. Biogenic (or endogenic) meromixis has developed (Hakala, 2004; Boehrer and Schultze, 2008). A chemocline now seperates the mixolimnion on top from the monimolimnion below. This process becomes more important, the more productive the lake is, as more organic material is decomposed. If the lake does not mix for several years due to climatic reasons, differences in density have more time to develop, and a biogenic stabilisation of meromimixis might develop even in oligotrophic Lake Constance.
The water quality model CAEDYM does not consider the influence of dissolved products of the decomposition of organic material on the density of water. The model is thus not able to consider the possibility of biogenic stabilisation of meromixis.

Under anoxic conditions in lakes, phosphorus can be released from the sediments. This results in a self-fertilisation of the lake, leading to higher productivity and enhanced oxygen consumption in the hypolimnion. The parametrisation of the sediments in this study does not consider the release of phosphorus from the lake bottom. The oxygen consumption during long periods of stratified conditions thus might be underestimated by the model.

The effects of discretisation and missing ice coverage on the main questions of this study are negligible. But the other three points (oxygen consumption parametrisation, biogenic meromixis, and phosphorus release) are all concerning stratification stability and hypolimnetic oxygen concentration. All three of them lead to an underestimation of the severity of the projected reactions to changes in the climate. The magnitude of the underestimation might be small for oligotrophic conditions, but will increase with increasing nutrient supply. Especially the extent of oxygen deficiency in the mesotrophic scenario in section 4.3 is thus a conservative estimate.

4.5.2 Weather Generator (VG)

VG assumes the marginal distributions of the meteorological variables to remain the same for all scenarios. The seasonally changing distributions are fitted to the measured data and used for back-transformation for all scenarios.
In the data used for this study, air temperature for each day of the year is normally distributed. Mean and standard deviation are changing throughout the year: The mean is higher in summer and lower in winter, whereas the standard deviation is highest in winter and lower in summer. In the scenarios, this heteroscedasticity remains the same, regardless of the change of mean temperature. This is not necessarily true. Maybe climate change will also change the heteroscedasticity.
Even the choice of the normal distribution is not suitable for all climate zones: Measured air temperature data from Lake Kinneret in Israel shows no normal distribution for daily air temperature. Especially in summer, the distribution is clearly skewed to the warm extremes. If climate change means pushing Lake Constance closer to subtropical or Mediterranean climate conditions, the assumption of unchanged transformation function might not be suitable any more.

The generation of scenarios is done for transformed variables, where the seasonal cycles have been removed. The generation process thus is blind for all seasonal differences. The

cross- and autocorrelations are the same for the whole year.

In the current version of VG, rain is not simulated. Together with the fact that changes in the inflows and thus in the precipitation in the catchment are neglected, this leads to the fact that changes in the water budget and in the water level are not considered.

For the disaggregation of daily to hourly wind velocity values, a resampling algorithm is used. The use of resampling techniques for scenarios bears the problem, that only values measured in the past can emerge. In this case this means, that the ratio of hourly to daily average wind sped can not exceed the highest value from the reference period.

In contrast to a physically based approach, in the data-based approach it is assumed that generated time series are physically valid only because the measured time series on which the statistical model was fitted was valid. Certain properties like natural lower or upper bounds (radiation, humidity) are enforced in VG, but in general the statistical abstraction does not honour physical laws directly.

4.5.3 General Setup of Model Study

Due to the limited availability of long measurement time series, the study is based on the meteorological data from one single measurement station. However, especially for the wind, the measurements from Konstanz are not necessarily representative for the whole lake.

The study is focussing on the direct influence of the meteorology on the lake and thus neglects any influences of changes in the catchment.
Nutrient concentrations in the tributaries are calculated with the relationships from the 1990ies for all scenarios. Changes in the catchment in land use and population might change the loads and relationships.
The hydrology of the tributaries is very likely to change in a changing climate. The area covered by glaciers is expected to decrease down to 12 % of the current value by 2100 in the Alps (Huss, 2011). So the rivers which nowadays have glacial runoff regimes will turn to more nival regimes, meaning that the maximum runoff occurs earlier in the year. The snow cover season in the alpine catchments will shorten. This means, that river with nowadays nival runoff regime will turn to more pluvial regimes, where the seasonal cycle is much less pronounced (Laghari et al., 2012). This increases the risk of floods in the tributaries during winter (CH2011, 2011).
Besides those changes in the yearly cycle, some studies indicate an increasing probability for extreme precipitation events (CH2011, 2011; Frei et al., 2006).

5 Conclusions and Outlook

5.1 Conclusions

The climate sensitivity of a large monomictic lake was evaluated using the three-dimensional coupled hydrodynamic and ecological model ELCOM-CAEDYM.
Lake Constance was chosen as an example, because it is a well-studied system. Numerous measurement data exists from long-term monitoring. Furthermore, intensive field campaigns on selected topics give a comprehensive picture of the physical and biological processes in the lake and their reactions to external forcings.

The three-dimensional coupled hydrodynamic and ecological model was validated for different processes observed in the lake. Three sets of measurement data were used to validate the model: Observations on an underflow after a flood in the main tributary, measurements from a field campaign on the three-dimensional distribution of plankton and temperature in the lake, and long-term measurement data on temperature and oxygen in the hypolimnion.

The model system proved to be able to reproduce the effects of a flood flow in the largest tributary, the Alpine Rhine. A huge turbid underflow was observed flowing into the main basin after an intense rain event in the Alps in August 2005. A numerical experiment showed the influence of the earth's rotation on the flow path of the riverine water within the lake.

The model also reproduced the temperature evolution and distribution and to some extent the phytoplankton patchiness measured in spring 2007 during an intensive field campaign. The patchiness in the biological variables that resulted from physical drivers, such as gradients in the water temperature and wind-induced surface currents emerged in the simulation as well. Beyond that, the measured plankton distribution showed additional patterns, that might be attributed to internal reasons in the ecosystem, or to randomness. This part of the patchiness could not exactly be reproduced by the model.

The model reproduced the measured time series of temperature and oxygen in the deep hypolimnion measured in the years 1980-2000. This indicates, that the vertical mixing and the lake's cycle of mixing and stratification was reproduced correctly. During this period the lake was influenced both by re-oligotrophication and climate warming. The increasing trend in the air temperature induced an increasing trend in the water temperatures in the lake, which was correctly simulated by the model. The effects of the oligotrophication on the lake's ecosystem was less linear, but was to some extend also reproduced by the simulations. The residence time of water in the lake was estimated with the help of a conservative tracer.

Climate scenario simulations were run with the lake model, using the model set-up validated for the years 1980-2000. The main focus was on temperature and oxygen concentrations in the hypolimnion, the cycle of stratification and mixing, and the heat budget

of the lake. The meteorological boundary conditions for the climate scenario simulations were generated using a weather generator instead of downscaling climate projections from GCMs. This approach gives the possibility to change different characteristics of the climate independently. The resulting lake model simulations are »what-if«-scenarios rather than predictions, helping to obtain a deeper understanding of the processes in the lake.
The main results can be summarized as follows:

An **increase in air temperature** leads to an increase in water temperature, especially in the upper layers. The deep water temperature increases as well, but not to the same extent as the temperature of the epilimnion. This results in an increased vertical temperature difference. Due to the non-linear shape of the temperature-density curve (UNESCO, 1981), the difference in density grows even stronger than the temperature difference. This results in enhanced stratification stability, and consequently in less mixing. Complete mixing of the lake becomes more seldom in a warmer climate, but even in the scenario simulations with air temperature increased by 5 °C, full circulation took place every 3-4 years.
Less complete mixing events lead to less oxygen in the hypolimnion. Additionally, as many biogeochemical processes are temperature dependant, the oxygen consumption rate is larger in warmer water. Gases dissolve less in warmer water. Therefore, the oxygen concentration decreases with increasing temperature even in the surface layers.
The residence time of water in the lake tends to increase with warming climate. The half-life $T_{1/2}$ of water in the deep hypolimnion increased by more than one year with air temperature increased by 5 °C.

In the context of this study, **climate variability** is defined as episodes with daily average air temperatures deviating from the long-term average for this day of year. The episodes can be described by their duration in days and their amplitude in °C.
Changes in climate variability can have very different effects, depending on the average air and water temperatures. The effects are stronger in lakes with higher water temperatures: As long as the average isothermal temperatures during winter mixing are close to the temperature of maximum density, both water temperatures and oxygen concentrations are similar in simulations with standard and with increased climate variability. This is due to the buffering effect of density maximum: When the water temperature equals the temperature of maximum density, and the surface layers are cooled down further, inverse stratification is established. The cooling takes places only at the surface. Surface heat fluxes from the lake to the atmosphere decrease.
But the higher the deep water temperature normally is, the more pronounced the effect of increased climate variability can be. For the same average air temperatures, simulated water temperatures are lower in those scenarios with increased climate variability. This indicates the larger importance of cold episodes: In a warm episode, water is heated at the surface. This stabilises the stratification, and the temperature change occurs mainly at the surface. The warmer surface leads to enhanced heat emission of the lake. A cold episode in contrast destabilises the stratification, letting the temperature change reach deeper regions. Remarkably cold winters cool down the whole water column, and produce an increased stability of the thermal stratification when the surface layer warm up again.

For the hypolimnetic conditions, the **seasonality** in warming is important: Increasing winter

air temperatures have a much stronger effect on the water temperatures in the lake than increasing summer temperatures. The most efficient warming takes place in December and January. The least efficient warming takes place in the months May - July. The reasons for the seasonal differences lie in the stratification in summer and in the non-linear temperature dependence of surface thermodynamics.

The combined effects of a warmer climate and **higher nutrient concentrations** enhances oxygen depletion in the hypolimnion.

5.2 Transferability of Results to other Lakes

This study has been carried out for Lake Constance, but the results are to a large extent transferable to other lakes. In this chapter it shall be discussed, which parts of the results can be transferred under which circumstances.

The reactions of Lake Constance on climate change are determined by its physical, geographical and ecosystem characteristics, such as mixing type, water temperatures, residence time, salinity and trophic state.
The hydrodynamic reactions are primarily controlled by the mixing type, which is determined by morphology and present climate. With a depth of about 250 m, Lake Constance is classified as a deep lake. The deeper a lake is, the more the thermal reactions are lagged.
Due to its depth and the temperate climate of the region the lake is situated in, it is classified as warm monomictic or oligomictic. Warm monomictic lakes show a thermal stratification most of the year, and experience one period of mixing in winter (Lewis Jr, 1983). In an oligomictic lake, complete mixing does not occur every year, but only in cold winters (Boehrer and Schultze, 2008).
Complete ice coverage is very seldom at Lake Constance. Lakes that experience complete ice coverage are sheltered from atmospheric influences during that period. A change in winter meteorological conditions thus are much less important for those lakes, as long as they still permit the maintenance of a stable ice cover. In contrast to that, for ice-free monomictic Lake Constance, winter meteorological conditions are especially important for the heat budget.
Winters nowadays are generally cold enough to cool the water of Lake Constance down to temperatures close to the temperature of the density maximum. The reaction of the lake on a changed climate variability is different when the minimum water temperatures are considerably above 4 °C.
The residence time of the water in a lake determines the relative importance of catchment processes compared to lake-internal processes. It depends on the volume of in- and outflows compared to the lake volume.
Salinity does not play a major role in Lake Constance. Vertical differences in salinity in a lake influence the density and stratification.
The oligotrophic state of the lake determines the biogeochemical reactions to climate change. Especially the oxygen concentrations depend on the productivity. Biological processes can also have feedbacks on the physical processes, for example via light extinction (Rinke et al., 2010) or density effects (Boehrer and Schultze, 2008; Hakala, 2004).

Results of this study thus might be transferred to other deep, warm monomictic, oligotrophic fresh water lakes in temperate climate zones with a comparable residence time. Below, those lakes in the world shall be identified that fit best to that description.

Comparable to Lake Constance are at first of course the lakes in its direct neighbourhood, i.e., the other perialpine lakes of glacial origin.
The larger northern perialpine lakes in Germany (Nixdorf et al., 2004) and Austria (Beiwl and Mühlmann, 2008) (Ammersee, Starnberger See, Walchensee, Chiemsee, Königssee, Mondsee, Attersee, Traunsee) all have a smaller volume than Lake Constance (Mondsee and Königssee 0.5 km^3, Attersee 3.9 km^3). Their depth is also smaller, ranging from 68 m (Mondsee) to 190 m (Walchensee, Königssee, Traunsee). Only Traunsee and Attersee show a clearly monomictic behaviour. The others are dimictic or mono- to dimictic, and experience complete ice cover at least in cold winters. Walchen- and Königssee, which are deep compared to their surface area, and sheltered by the surrounding mountains of the Alps, are both meromictic in most years. The trophic state of all these lakes is oligotrophic. Total phosphorus concentrations do not exceed 10 μg/l. Theoretical water renewal times are smaller than in Lake Constance (1 - 2.7 years), except for Attersee (7.1 years) and Starnberger See (21 years). These lakes are experiencing roughly the same climate and the same climate change as Lake Constance. Their trophic states are comparable. Differences in the reactions to climate change will derive from their smaller sizes and different mixing regime. The smaller depths ensure for most of them regular complete mixing events and thus also good oxygen supply for the hypolimnion also in a warming climate. The oligotrophic state supports this.

At the southern boundary of the Alps, the lakes Maggiore, Como and Garda are in volume comparable to Lake Constance (37.5, 22.4, 49 km^3, respectively) and even deeper (370, 410, 346 m, respectively). Total phosphorus concentrations are slightly higher than those in northern perialpine lakes, ranging from 10 (Maggiore) to 23 μg/l (Como). All three lakes show an oligomictic behaviour, undergoing complete mixing only in cold winters. As they are situated in the warmer climate of the southern perialpine region, the average water temperature during complete mixing, and thus the water temperature in the deep hypolimnion, in those lakes does not reach the temperature of maximum density, but lies between 6 °C in Lake Maggiore and 8 °C in Lake Garda (Salmaso, 2005; Salmaso et al., 2012). Due to their greater depths and the warmer climate, complete mixing occurs more seldom in those lakes already nowadays, leading to greater oxygen deficiencies in the hypolimnion. The fact that the productivity is higher than that in the northern perialpine lakes enhances this further. As those lakes experience a warmer climate already nowadays, their actual state could be to some extend considered to be a possible future for Lake Constance. The actual deep water temperature of around 6 °C in Lake Maggiore corresponds to the deep water temperatures simulated in this study for Lake Constance in a 3-4 °C warmer climate.

Lake Geneva is the largest lake of the Alpine region. Its surface area is 580.1 km^2, the volume 88.9 km^3 and the maximum depth 309.7 m. Theoretical retention time is 11.3 a (CIPEL, 2011). Air temperatures on the shores of Lake Geneva are generally 1 - 1.5 °C higher than in Konstanz. Measured annual average temperatures from 1980-2001 show a trend comparable to that observed in Konstanz (Quetin, 2011). Hypolimnetic water temperatures increased from values close to the temperature of maximum density in the 1960ies to 5.6-6 °C nowadays.

Total phosphorus concentration in Lake Geneva is nowadays around 22 μg/l (Lazzarotto et al., 2011). Lake Geneva is likely to show quite similar reaction to a changing climate as Lake Constance. Differences might arise from its slightly larger depth and the higher productivity.

In north-eastern Europe in the landscapes formed during and after the last ice age by the Scandinavian ice shield, many large lakes can be found. The largest lake in Europe, Lake Ladoga, can be found here. But these lakes all freeze over in winter for a long period, and thus show very different responses to climate warming. Climate change studies for lakes in this region are focusing on changes in the duration of ice coverage period and summer stratification period (Karetnikov and Naumenko, 2008; Ventelä et al., 2011). Some of the fjord lakes in Norway are so deep that they do not freeze every winter despite their northern location. Lake Mjøsa (369 km^2, 55.3 km^3, 453 m, 5.5 a) is the largest lake in Norway. The frequency of complete ice cover in winter on Lake Mjøsa shows a decreasing trend: between 1950-69, the lake was frozen in 18 winters, but only in seven winters in 1990-2009 (Hobæk et al., 2012).
For this region, climate warming might bring the lakes into a state closer to the actual state of Lake Constance.

In North America, the Great Laurentian Lakes, and most other Canadian lakes also are completely ice covered during winter. Only in the very south-west of Canada monomictic lakes can be found, for example Kennedy Lake (64 km^2, 2.136 km^3, <2 a) on Vancouver Island (Stockner and Shortreed, 1988). Lake Tahoe in California and Nevada (501 km^2, 157 km^3, 500 m, 650 a) is oligotrophic and oligomictic. Mixing depends rather on wind conditions than on air temperatures (Coats et al., 2006).

Lake Biwa in Japan consists of the eutrophic shallow southern basin and the mesotrophic deep northern basin. Total surface area is 674 km^2 and maximum depth 104 m (Gurung and Urabe, 1999). The volume is 27.5 km^3, theoretical residence time is 5.5 a (Rimmer et al., 2006). Hypolimnetic water temperatures are 6-7 °C (Nagata, 1988).

In the lake district (Regió de los Lagos) in Chile several large oligotrophic warm monomictic lakes, called the Araucanian Lakes, can be found (Geller, 1992). Situated at the foot of the Andes, they are of glacial origin. In size comparable to Lake Constance are for example Lake Ranco (surface area 401 km^2, volume 54 km^3, maximum depth 199 m, theoretical residence time 4.1 a) and Lake Todos los Santos (178.5 km^2, 34.4 km^3, 337 m, 4 a). Both are situated between 41 and 42° south. Their deep water and winter water temperatures are 10 - 10.5 °C. The southernmost large lake in the world (besides sub-ice freshwater reservoirs in the Antarctica) is Lake Fagagno (600 km^2, 41 km^3, 204 m) in Tierra del Fuego in Argentina and Chile (Richter et al., 2010). It is situated at 54° 30′ south. The lake is of tectonic origin. It is a warm monomictic, oligotrophic lake. Winterly water temperatures reach values around 4 °C.

In Australia not many large freshwater lakes can be found due to the dry climate. The deepest lake in Australia is the oligotrophic and monomictic Lake St. Clair in Tasmania with 180 m depth (Haworth and Tyler, 1993). The lake's volume is 1.7 km^3 (Derbyshire, 1971).

In New Zealand are several large monomictic oligotrophic lakes. Lake Taupo (612 km^2, 59 km^3, 163 m, 12 a) on the northern island has approximately the size of Lake Constance. Winterly water temperature is 10.5 °C (Vincent, 1983).
The deepest lakes are on the southern island. Deepest lake of New Zealand is Lake Hauroko with a depth of 462 m at the southern end of the southern island. Its winterly water temperature was determined to be 8.25±0.10 °C (Sander et al., 2013).

Most of the lakes on the southern hemisphere are already at a higher temperature level than Lake Constance, and might therefore react different on further warming.

Even though every lake is a different system, there are some lakes that might react in a comparable way as Lake Constance. This are at first the other lakes in the Alpine regions, but to some extent also lakes in other regions of the world with moderate climate.

5.3 Outlook

The study on climate impact on Lake Constance can be extended in several aspects. Including the catchment in the scenarios will bring more input both considering nutrient input and the water balance. When focussing on the water balance, rain has to be taken into account and included in the weather generator simulations.
Wind is an important factor for the mixing of Lake Constance (Roßknecht et al., 2007). Up to now, wind conditions were not changed much in the scenarios. It would be interesting to run wind scenarios.

For a more detailed look at water quality and ecosystem, the water quality model has to be enhanced to include dynamic sediment processes, especially the re-suspension of phosphorus from the lake bottom under oxygen deficiency conditions.

Bibliography

R. Adrian, C. M. OReilly, H. Zagarese, S. B. Baines, D. O. Hessen, W. Keller, D. M. Livingstone, R. Sommaruga, D. Straile, E. Van Donk, et al. Lakes as sentinels of climate change. *Limnology and Oceanography*, 54(6):2283, 2009.

J. Appt. *Analysis of basin-scale internal waves in upper Lake Constance*. PhD thesis, Universität Stuttgart, Stuttgart, 2003.

J. Appt, J. Imberger, and H. Kobus. Basin-scale motion in stratified Upper Lake Constance. *Limnology and Oceanography*, 49(4):919–933, 2004.

F. Arnaud, M. Revel, E. Chapron, M. Desmet, and N. Tribovillard. 7200 years of Rhone river flooding activity in Lake Le Bourget, France: a high-resolution sediment record of NW Alps hydrology. *The Holocene*, 15(3):420–428, 2005.

E. Bäuerle. Some meteorological, hydrological, and hydrodynamical aspects of upper Lake Constance (with 30 figures and 2 tables). In E. Bäuerle and U. Gaedke, editors, *Lake Constance: characterization of an ecosystem in transition*, volume 53 of *Special issues: Ergebnisse der Limnologie*, pages 31–83. Schweizerbart, Stuttgart, 1998.

C. Beiwl and H. Mühlmann. Atlas der natürlichen Seen Österreichs mit einer Fläche $\geq$ 50 ha: Morphometrie - Typisierung - Trophie. Stand 2005, 2008.

T. Blenckner, R. Adrian, D. M. Livingstone, E. Jennings, G. A. Weyhenmeyer, D. George, T. Jankowski, M. Järvinen, C. N. Aonghusa, T. Nõges, et al. Large-scale climatic signatures in lakes across Europe: a meta-analysis. *Global Change Biology*, 13(7):1314–1326, 2007.

B. Boehrer and M. Schultze. Stratification of lakes. *Reviews of Geophysics*, 46(2):RG2005, 2008.

S. Bony, R. Colman, V. M. Kattsov, R. P. Allan, C. S. Bretherton, J.-L. Dufresne, A. Hall, S. Hallegatte, M. M. Holland, W. Ingram, et al. How well do we understand and evaluate climate change feedback processes? *Journal of Climate*, 19(15):3445–3482, 2006.

T. Bosshard, S. Kotlarski, T. Ewen, and C. Schär. Spectral representation of the annual cycle in the climate change signal. *Hydrology and Earth System Sciences*, 15(9):2777–2788, 2011.

E. Braun and K. Schärpf. *Internationale Bodensee-Tiefenvermessung 1990: Eine Dokumentation über die von 1985 bis 1990 durchgeführte Tiefenvermessung der Internationalen Gewässerschutzkommission für den Bodensee*. Landesvermessungsamt Baden-Württemberg, Stuttgart, 1994.

L. C. Bruce, D. Hamilton, J. Imberger, G. Gal, M. Gophen, T. Zohary, and K. D. Hambright. A numerical simulation of the role of zooplankton in C, N and P cycling in Lake Kinneret, Israel. *Ecological Modelling*, 193(3):412–436, 2006.

H. Bührer, P. K. Kirner, and G. Wagner. Dem Bodensee in den Abflussjahren 1996 und 1997 zugeführte Stofffrachten, 2000.

H. Bührer and G. Wagner. Die Belastung des Bodensees mit Phosphor- und Stickstoffverbindungen und organischem Kohlenstoff im Abflussjahr 1978/79, 1982.

CH2011. Swiss Climate Change Scenarios 2011, 2011.

S. Chung, M. Hipsey, and J. Imberger. Modelling the propagation of turbid density inflows into a stratified lake: Daecheong Reservoir, Korea. *Environmental Modelling & Software*, 24 (12):1467–1482, 2009.

CIPEL. Fiche signalétique du Léman et de son bassin versant. *Rapports sur les études et recherches entreprises dans le bassin lémanique, programme quinquennal 2006-2010, campagne 2010*, pages 7–9, 2011.

R. Coats, J. Perez-Losada, G. Schladow, R. Richards, and C. Goldman. The warming of lake Tahoe. *Climatic change*, 76(1-2):121–148, 2006.

M. Czymzik, P. Dulski, B. Plessen, U. von Grafenstein, R. Naumann, and A. Brauer. A 450 year record of spring-summer flood layers in annually laminated sediments from Lake Ammersee (southern Germany). *Water Resources Research*, 46(11), 2010.

E. Derbyshire. The bathymetry of Lake St Clair, western central Tasmania. In *Papers and Proceedings of the Royal Society of Tasmania*, volume 105, pages 49–58, 1971.

R. Eckmann, S. Gerster, and A. Kraemer. Yields of European perch from Upper Lake Constance from 1910 to present. *Fisheries Management and Ecology*, 13(6):381–390, 2006.

R. Eckmann and R. Rösch. Lake Constance fisheries and fish ecology. In E. Bäuerle and U. Gaedke, editors, *Lake Constance: characterization of an ecosystem in transition*, volume 53 of *Special issues: Ergebnisse der Limnologie*, pages 285–301. Schweizerbart, Stuttgart, 1998.

M. M. Eder and M. Wessels. Underflows affected by Coriolis Force in Lake Constance - Modeling and Observation. In preperation, 2013.

S. Fatichi, V. Y. Ivanov, and E. Caporali. Simulation of future climate scenarios with a weather generator. *Advances in Water Resources*, 34(4):448–467, 2011.

S. A. Forbes. The Lake as a Microcosm. *Bulletin of the Scientific Association of Peoria, Illinois*, pages 77–87, 1887.

G. Foster and S. Rahmstorf. Global temperature evolution 1979–2010. *Environmental Research Letters*, 6(4):044022, 2011.

M. A. Frassl, K. Rinke, and K.-O. Rothhaupt. Internal nutrient dynamics of algae determine the vertical distribution of phosphorus in a large lake. In preperation, 2013.

C. Frei, R. Schöll, S. Fukutome, J. Schmidli, and P. L. Vidale. Future change of precipitation extremes in europe: Intercomparison of scenarios from regional climate models. *Journal of Geophysical Research: Atmospheres (1984–2012)*, 111(D6), 2006.

M. Gasser, R. Sivetz, A. Pfefferkorn, and J. Kanonier. Das Starkregen- und Hochwasserereignis des August 2005 in Vorarlberg: Ein Bericht des Amtes der Vorarlberger Landesregierung, 2005.

W. Geller. The temperature stratification and related characteristics of chilean lakes in midsummer. *Aquatic Sciences*, 54(1):37–57, 1992.

C. R. Goldman and A. Jassby. Spring mixing depth as a determinant of annual primary production in lakes. In M. M. Tilzer and C. Serruya, editors, *Large Lakes*, pages 125–132. Springer Berlin Heidelberg, 1990.

A. Gómez-Giraldo, J. Imberger, and J. P. Antenucci. Spatial structure of the dominant basin-scale internal waves in Lake Kinneret. *Limnology and Oceanography*, 51(1):229, 2006.

H. Güde, H. Hetzenauer, R. Kümmerlin, H.-G. Schröder, H.-B. Stich, and M. Wessels. Bodensee–Untersuchung–Seeboden: Forschungsprojekt von 2003 bis 2006, 2009.

H. Güde, H. Roßknecht, and G. Wagner. Anthropogenic impacts on the trophic state of Lake Constance during the 20th century (with 7 figures and 2 tables). In E. Bäuerle and U. Gaedke, editors, *Lake Constance: characterization of an ecosystem in transition*, volume 53 of *Special issues: Ergebnisse der Limnologie*, pages 85–108. Schweizerbart, Stuttgart, 1998.

T. Gurung and J. Urabe. Temporal and vertical difference in factors limiting growth rate of heterotrophic bacteria in Lake Biwa. *Microbial ecology*, 38(2):136–145, 1999.

A. Hakala. Meromixis as a part of lake evolution; observations and a revised classification of true meromictic lakes in Finland. *Boreal Environment Research*, 9(1):37–53, 2004.

E. Haworth and P. Tyler. Morphology and taxonomy of Cyclotella tasmanica spec. nov, a newly described diatom from Tasmanian lakes. *Hydrobiologia*, 269(1):49–56, 1993.

I. Hillmer, P. van Reenen, J. Imberger, and T. Zohary. Phytoplankton patchiness and their role in the modelled productivity of a large, seasonally stratified lake. *Ecological Modelling*, 218(1):49–59, 2008.

M. R. Hipsey and D. P. Hamilton. Computational aquatic ecosystem dynamics model: CAEDYM v3: Science Manual, 2008.

A. Hobæk, J. E. Løvik, T. Rohrlack, S. J. Moe, M. Grung, H. Bennion, G. Clarke, and G. T. Piliposyan. Eutrophication, recovery and temperature in Lake Mjøsa: detecting trends with monitoring data and sediment records. *Freshwater Biology*, 57(10):1998–2014, 2012.

B. R. Hodges and C. Dallimore. Estuary, Lake and Coastal Ocean Model: ELCOM - v2.2: Science Manual, 2006.

B. R. Hodges, J. Imberger, A. Saggio, and K. B. Winters. Modeling basin-scale internal waves in a stratified lake. *Limnology and Oceanography*, 45(7):1603–1620, 2000.

E. Hollan. Mögliche Auswirkungen einer Klimaveränderung auf größere Binnenseen. In *Klimaveränderungen und Konsequenzen für die Wasserwirtschaft*, number 1 in KLIWA Klimaveränderung und Wasserwirtschaft, pages 213–235. Karlsruhe, 2001.

R. Hornung. Numerical Modelling of Stratification in Lake Constance with the 1-D hydrodynamic model DYRESM. Master's thesis, Universität Stuttgart, Holzgartenstr. 16, 70174 Stuttgart, 2002.

N. E. Huang, Z. Shen, S. R. Long, M. C. Wu, H. H. Shih, Q. Zheng, N.-C. Yen, C. C. Tung, and H. H. Liu. The empirical mode decomposition and the Hilbert spectrum for nonlinear and non-stationary time series analysis. *Proceedings of the Royal Society of London. Series A: Mathematical, Physical and Engineering Sciences*, 454(1971):903–995, 1998.

M. Huss. Present and future contribution of glacier storage change to runoff from macroscale drainage basins in Europe. *Water Resources Research*, 47(7), 2011.

S. B. Idso. On the concept of lake stability. *Limnology and Oceanography*, 18(4):681–683, 1973.

J. Imberger and J. C. Patterson. Dynamic reservoir simulation model- dyresm: 5. In *Transport Models for Inland and Coastal Waters, Academic Press New York. 1981. Proceedings of a Symposium on Predictive Ability, Berkeley, California, August 18-20, 1980. p 310-361, 12 fig, 36 ref.*, 1980.

Internationale Gewässerschutzkommission für den Bodensee (IGKB). Jahresbericht der Internationalen Gewässerschutzkommission für den Bodensee: Limnologischer Zustand des Bodensees Nr. 39 (2011), 2012.

IPCC. Climate Change 2007: The Physical Science Basis. Contribution of Working Group I to the Fourth Assessment Report of the Intergovernmental Panel on Climate Change, 2007.

M. G. Iziomon, H. Mayer, and A. Matzarakis. Downward atmospheric longwave irradiance under clear and cloudy skies: Measurement and parameterization. *Journal of Atmospheric and Solar-Terrestrial Physics*, 65(10):1107–1116, 2003.

J. Janse, T. Aldenberg, and P. Kramer. A mathematical model of the phosphorus cycle in Lake Loosdrecht and simulation of additional measures. In *Restoration and Recovery of Shallow Eutrophic Lake Ecosystems in The Netherlands*, pages 119–136. Springer, 1992.

K. D. Jöhnk, D. Straile, and W. Ostendorp. Water level variability and trends in Lake Constance in the light of the 1999 centennial flood. *Limnologica-Ecology and Management of Inland Waters*, 34(1):15–21, 2004.

S. G. Karetnikov and M. A. Naumenko. Recent trends in Lake Ladoga ice cover. *Hydrobiologia*, 599(1):41–48, 2008.

R. K. Kaufmann, H. Kauppi, M. L. Mann, and J. H. Stock. Reconciling anthropogenic climate change with observed temperature 1998–2008. *Proceedings of the National Academy of Sciences*, 108(29):11790–11793, 2011.

M. G. Kendall. *Rank correlation methods*. Griffin, London, 4. ed. edition, 1970.

O. Kerimoglu, D. Straile, and F. Peeters. Seasonal, inter-annual and long term variation in top–down versus bottom–up regulation of primary production. *Oikos*, 122(2):223–234, 2013.

A. Laghari, D. Vanham, and W. Rauch. To what extent does climate change result in a shift in Alpine hydrology? A case study in the Austrian Alps. *Hydrological Sciences Journal*, 57 (1):103–117, 2012.

U. Lang, H. Kobus, H. Mehlhorn, R. Schick, T. Paul, M. Eder, K. Rinke, K.-O. Rothhaupt, S. Kempke, W. Scheuermann, F. Schmidt, C. Krass, A. Huber, and T. Wolf. Verbundforschungsvorhaben BodenseeOnline: Ein Informationssystem zur Vorhersage der Hydrodynamik und der Wasserqualität von Seen am Beispiel des Bodensees: Abschlussbericht, 2008.

U. Lang and T. Paul. Description of up to date situation and forecast using the data and method base Bodenseeonline. *Wasserwirtschaft*, 98(10):39–44, 2008.

J. R. Lanzante. Resistant, robust and non-parametric techniques for the analysis of climate data: Theory and examples, including applications to historical radiosonde station data. *International Journal of Climatology*, 16(11):1197–1226, 1996.

J. Lazzarotto, P. Nirel, and F. Rapin. Évolution physico-chimique des eaux du Léman. *Rapports sur les études et recherches entreprises dans le bassin lémanique, programme quinquennal 2006-2010, campagne 2010*, pages 31–63, 2011.

W. M. Lewis Jr. A revised classification of lakes based on mixing. *Canadian Journal of Fisheries and Aquatic Sciences*, 40(10):1779–1787, 1983.

D. M. Livingstone. Impact of secular climate change on the thermal structure of a large temperate central European lake. *Climatic Change*, 57(1-2):205–225, 2003.

H. Löffler. 2012, personal communication.

G. Luft and J. Ihringer. Langzeitverhalten der Bodensee-Wasserstände. Auswertezeitspanne: 1888 bis 2007, 2011.

J. McManus, E. Heinen, and M. Baehr. Hypolimnetic oxidation rates in Lake Superior: Role of dissolved organic material on the lake's carbon budget. *Limnology and Oceanography*, 48 (4):1624–1632, 2003.

D. Mironov, L. Rontu, E. Kourzeneva, and A. Terzhevik. Towards improved representation of lakes in numerical weather prediction and climate models: Introduction to the special issue of boreal environment research. *Boreal Environment Research*, 15(2):97–99, 2010.

W. Mooij, J. Janse, L. D. S. Domis, S. Hülsmann, and B. Ibelings. Predicting the effect of climate change on temperate shallow lakes with the ecosystem model PCLake. In *Shallow Lakes in a Changing World*, pages 443–454. Springer, 2007.

W. M. Mooij, D. Trolle, E. Jeppesen, G. Arhonditsis, P. V. Belolipetsky, D. B. Chitamwebwa, A. G. Degermendzhy, D. L. DeAngelis, L. N. D. S. Domis, A. S. Downing, et al. Challenges and opportunities for integrating lake ecosystem modelling approaches. *Aquatic Ecology*, 44(3):633–667, 2010.

T. Mulder and J. P. Syvitski. Turbidity currents generated at river mouths during exceptional discharges to the world oceans. *The Journal of Geology*, pages 285–299, 1995.

G. Müller and U. Förstner. General relationship between suspended sediment concentration and water discharge in the Alpenrhein and some other rivers. *Nature*, 217:244–245, 1968.

T. Nagata. The microflagellate-picoplankton food linkage in the water column of Lake Biwa. *Limnology and Oceanography*, 33(4):504–517, 1988.

H. Niemann, A. Stadnitskaia, S. Wirth, A. Gilli, F. Anselmetti, J. S. Damsté, S. Schouten, E. Hopmans, and M. Lehmann. Bacterial GDGTs in Holocene sediments and catchment soils of a high Alpine lake: application of the MBT/CBT-paleothermometer. *Climate of the Past*, 8:889–906, 2012.

B. Nixdorf, M. Hemm, A. Hoffmann, and P. Richter. Dokumentation von Zustand und Entwicklung der wichtigsten Seen Deutschlands, Teil 11 Bayern, 2004.

F. Peeters, D. Straile, A. Lorke, and D. M. Livingstone. Earlier onset of the spring phytoplankton bloom in lakes of the temperate zone in a warmer climate. *Global Change Biology*, 13(9):1898–1909, 2007a.

F. Peeters, D. Straile, A. Lorke, and D. Ollinger. Turbulent mixing and phytoplankton spring bloom development in a deep lake. *Limnology and Oceanography*, 52(1):286–298, 2007b.

V. Putyrskaya, E. Klemt, and S. Röllin. Migration of ^{137}Cs in tributaries, lake water and sediment of Lago Maggiore (Italy, Switzerland)–analysis and comparison with Lago di Lugano and other lakes. *Journal of environmental radioactivity*, 100(1):35–48, 2009.

P. Quetin. Météorologie. *Rapports sur les études et recherches entreprises dans le bassin lémanique, programme quinquennal 2006-2010, campagne 2010*, pages 19–30, 2011.

A. Richter, J. Luis Hormaechea, R. Dietrich, R. Perdomo, M. Fritsche, D. Del Cogliano, G. Liebsch, and L. Mendoza. Lake-level variations of Lago Fagnano, Tierra del Fuego: observations, modelling and interpretation. *Journal of Limnology*, 69(1):29–41, 2010.

A. Rimmer, M. Boger, Y. Aota, and M. Kumagai. A lake as a natural integrator of linear processes: Application to Lake Kinneret (Israel) and Lake Biwa (Japan). *Journal of Hydrology*, 319(1):163–175, 2006.

K. Rinke, M. Eder, F. Peeters, R. Kümmerlin, G. Gal, and K.-O. Rothaupt. Simulating phytoplankton community dynamics in Lake Constance with a coupled hydrodynamic-ecological model. In *Proceedings of the International Society of Limnology 30*, pages 701–704. Universität Konstanz, 2009a.

K. Rinke, A. M. Huber, S. Kempke, M. Eder, T. Wolf, W. N. Probst, K.-O. Rothhaupt, et al. Lake-wide distributions of temperature, phytoplankton, zooplankton, and fish in the pelagic zone of a large lake. *Limnology and Oceanography*, 54(4):1306, 2009b.

K. Rinke, P. Yeates, and K.-O. Rothhaupt. A simulation study of the feedback of phytoplankton on thermal structure via light extinction. *Freshwater Biology*, 55(8):1674–1693, 2010.

H. Roßknecht, B. Wahl, H. Güde, H. Hetzenauer, and T. Wolf. Auswirkungen des Klimawandels auf das Zirkulationsverhalten des Bodensee-Obersees. In *Zum Einfluss des Klimas auf den Bodensee*, number 11 in KLIWA Klimaveränderung und Wasserwirtschaft. 2007.

R. J. Ross, W. P. Elliott, D. J. Seidel, and A.-I. Participating. Lower-tropospheric humidity-temperature relationships in radiosonde observations and atmospheric general circulation models. *Journal of Hydrometeorology*, 3(1):26–38, 2002.

N. Salmaso. Effects of climatic fluctuations and vertical mixing on the interannual trophic variability of Lake Garda, Italy. *Limnology and Oceanography*, 50(2):553–565, 2005.

N. Salmaso, F. Buzzi, L. Garibaldi, G. Morabito, and M. Simona. Effects of nutrient availability and temperature on phytoplankton development: a case study from large lakes south of the Alps. *Aquatic sciences*, 74(3):555–570, 2012.

P. Samuelsson, E. Kourzeneva, and D. Mironov. The impact of lakes on the European climate as simulated by a regional climate model. *Boreal environment research*, 15(2):113–129, 2010.

S. G. Sander, B. Anderson, M. R. Reid, J. P. Kim, and K. A. Hunter. Trace Metal Chemistry in the Pristine Freshwater Lake Hauroko, Fiordland, New Zealand. *Microchemical Journal*, 2013.

D. Schlabing, M. A. Frassl, M. M. Eder, K. Rinke, and A. Bárdossy. Use of a weather generator for simulating climate change effects on ecosystems: A case study on Lake Constance. Submitted to Ecological Modelling and Software, 2013.

W. Schmidt. Über den Energiegehalt der Seen. Mit Beispielen vom Lunzer Untersee nach Messungen mit einem einfachen Temperaturlot. *Internationale Revue der gesamten Hydrobiologie und Hydrographie*, 6(S1):1–25, 1914.

W. Schmidt. Über die Temperatur-und Stabilitätsverhältnisse von Seen. *Geografiska annaler*, 10:145–177, 1928.

P. Schneider, S. Hook, R. Radocinski, G. Corlett, G. Hulley, S. Schladow, and T. Steissberg. Satellite observations indicate rapid warming trend for lakes in California and Nevada. *Geophysical Research Letters*, 36(22):L22402, 2009.

P. Schneider and S. J. Hook. Space observations of inland water bodies show rapid surface warming since 1985. *Geophysical Research Letters*, 37(22):L22405, 2010.

K. Shimizu, J. Imberger, and M. Kumagai. Horizontal structure and excitation of primary motions in a strongly stratified lake. *Limnology and Oceanography*, 52(6):2641, 2007.

D. A. Smith and G. Matisoff. Sediment oxygen demand in the central basin of Lake Erie. *Journal of Great Lakes Research*, 34(4):731–744, 2008.

J. T. Smith, N. V. Belova, A. A. Bulgakov, R. N. Comans, A. V. Konoplev, A. V. Kudelsky, M. J. Madruga, O. V. Voitsekhovitch, and G. Zibold. The "AQUASCOPE" simplified model for predicting Sr-89, Sr-90, I-131, and Cs-134, Cs-137 in surface waters after a large-scale radioactive fallout. *Health physics*, 89(6):628–644, 2005.

H.-B. Stich and A. Brinker. Oligotrophication outweighs effects of global warming in a large, deep, stratified lake ecosystem. *Global Change Biology*, 16(2):877–888, 2010.

J. G. Stockner and K. S. Shortreed. Response of anabaena and synechococcus to manipulation of nitrogen: phosphorus ratios in a lake fertilization experiment. *Limnology and Oceanography*, 33(6):1348–1361, 1988.

D. Straile, K. Jöhnk, and H. Roßknecht. Complex effects of winter warming on the physicochemical characteristics of a deep lake. *Limnology and Oceanography*, 48(4):1432–1438, 2003.

G. Thomas and R. Eckmann. The influence of eutrophication and population biomass on common whitefish (Coregonus lavaretus) growth - the Lake Constance example revisited. *Canadian Journal of Fisheries and Aquatic Sciences*, 64(3):402–410, 2007.

UNESCO. The practical salinity scale 1978 and the international equation of state of seawater 1980. Tenth report of the Joint Panel on Oceanographic Tables and standards,(JPOTS)., 1981.

A.-M. Ventelä, T. Kirkkala, A. Lendasse, M. Tarvainen, H. Helminen, and J. Sarvala. Climate-related challenges in long-term management of Säkylän Pyhäjärvi (SW Finland). *Hydrobiologia*, 660(1):49–58, 2011.

J. Vilar, R. Solé, and J. Rubı. On the origin of plankton patchiness. *Physica A: Statistical Mechanics and its Applications*, 317(1):239–246, 2003.

W. F. Vincent. Phytoplankton production and winter mixing: contrasting effects in two oligotrophic lakes. *The Journal of Ecology*, pages 1–20, 1983.

G. Wagner and H. Bührer. Die Belastung des Bodensees mit Phosphor- und Stickstoffverbindungen, organisch gebundenem Kohlenstoff und Borat im Abflußjahr 1985/86, 1989.

G. Wagner. Untersuchungen am zugefrorenen Bodensee (studies performed in frozen Lake Constance). *SCHWEIZ Z HYDROL*, 1964.

B. Wahl and H. Löffler. Influences on the natural reproduction of whitefish (coregonus lavaretus) in lake constance. *Canadian Journal of Fisheries and Aquatic Sciences*, 66(4):547–556, 2009.

M. Wessels. Geological history of the Lake Constance area. In E. Bäuerle and U. Gaedke, editors, *Lake Constance: characterization of an ecosystem in transition*, volume 53 of *Special issues: Ergebnisse der Limnologie*, pages 1–12. Schweizerbart, Stuttgart, 1998.

D. S. Wilks. A gridded multisite weather generator and synchronization to observed weather data. *Water Resources Research*, 45(10), 2009.

A. Zenger, W. Anker, J. Ilmberger, and K. Münnich. Die Untersuchung der Windverhältnisse im westlichen Teil des Bodensees und die Umrechnung von Landwinden auf Seebedingungen. *Meteorologische Rundschau*, 42(2):42–51, 1990.

Institut für Wasser- und Umweltsystemmodellierung
Universität Stuttgart

Pfaffenwaldring 61
70569 Stuttgart (Vaihingen)
Telefon (0711) 685 - 64717/64749/64752/64679
Telefax (0711) 685 - 67020 o. 64746 o. 64681
E-Mail: iws@iws.uni-stuttgart.de
http://www.iws.uni-stuttgart.de

Verzeichnis der Mitteilungshefte

5 Plate, Erich: *Beitrag zur Bestimmung der Windgeschwindigkeitsverteilung in der durch eine Wand gestörten bodennahen Luftschicht*,
und
Röhnisch, Arthur; Marotz, Günter: *Neue Baustoffe und Bauausführungen für den Schutz der Böschungen und der Sohle von Kanälen, Flüssen und Häfen; Gestehungskosten und jeweilige Vorteile*, sowie Unny, T.E.: *Schwingungsuntersuchungen am Kegelstrahlschieber*, 1967

6 Seiler, Erich: *Die Ermittlung des Anlagenwertes der bundeseigenen Binnenschiffahrtsstraßen und Talsperren und des Anteils der Binnenschiffahrt an diesem Wert*, 1967

7 *Sonderheft anläßlich des 65. Geburtstages von Prof. Arthur Röhnisch mit Beiträgen von* Benk, Dieter; Breitling, J.; Gurr, Siegfried; Haberhauer, Robert; Honekamp, Hermann; Kuz, Klaus Dieter; Marotz, Günter; Mayer-Vorfelder, Hans-Jörg; Miller, Rudolf; Plate, Erich J.; Radomski, Helge; Schwarz, Helmut; Vollmer, Ernst; Wildenhahn, Eberhard; 1967

8 Jumikis, Alfred: *Beitrag zur experimentellen Untersuchung des Wassernachschubs in einem gefrierenden Boden und die Beurteilung der Ergebnisse*, 1968

9 Marotz, Günter: *Technische Grundlagen einer Wasserspeicherung im natürlichen Untergrund*, 1968

10 Radomski, Helge: *Untersuchungen über den Einfluß der Querschnittsform wellenförmiger Spundwände auf die statischen und rammtechnischen Eigenschaften*, 1968

11 Schwarz, Helmut: *Die Grenztragfähigkeit des Baugrundes bei Einwirkung vertikal gezogener Ankerplatten als zweidimensionales Bruchproblem*, 1969

12 Erbel, Klaus: *Ein Beitrag zur Untersuchung der Metamorphose von Mittelgebirgsschneedecken unter besonderer Berücksichtigung eines Verfahrens zur Bestimmung der thermischen Schneequalität*, 1969

13 Westhaus, Karl-Heinz: *Der Strukturwandel in der Binnenschiffahrt und sein Einfluß auf den Ausbau der Binnenschiffskanäle*, 1969

14 Mayer-Vorfelder, Hans-Jörg: *Ein Beitrag zur Berechnung des Erdwiderstandes unter Ansatz der logarithmischen Spirale als Gleitflächenfunktion*, 1970

15 Schulz, Manfred: *Berechnung des räumlichen Erddruckes auf die Wandung kreiszylindrischer Körper*, 1970

16 Mobasseri, Manoutschehr: *Die Rippenstützmauer. Konstruktion und Grenzen ihrer Standsicherheit*, 1970

17 Benk, Dieter: *Ein Beitrag zum Betrieb und zur Bemessung von Hochwasserrückhaltebecken*, 1970

18 Gàl, Attila: *Bestimmung der mitschwingenden Wassermasse bei überströmten Fischbauchklappen mit kreiszylindrischem Staublech*, 1971, vergriffen

19 Kuz, Klaus Dieter: *Ein Beitrag zur Frage des Einsetzens von Kavitationserscheinungen in einer Düsenströmung bei Berücksichtigung der im Wasser gelösten Gase*, 1971, vergriffen

20 Schaak, Hartmut: *Verteilleitungen von Wasserkraftanlagen*, 1971

21 *Sonderheft zur Eröffnung der neuen Versuchsanstalt des Instituts für Wasserbau der Universität Stuttgart mit Beiträgen von* Brombach, Hansjörg; Dirksen, Wolfram; Gàl, Attila; Gerlach, Reinhard; Giesecke, Jürgen; Holthoff, Franz-Josef; Kuz, Klaus Dieter; Marotz, Günter; Minor, Hans-Erwin; Petrikat, Kurt; Röhnisch, Arthur; Rueff, Helge; Schwarz, Helmut; Vollmer, Ernst; Wildenhahn, Eberhard; 1972

22 Wang, Chung-su: *Ein Beitrag zur Berechnung der Schwingungen an Kegelstrahlschiebern*, 1972

23 Mayer-Vorfelder, Hans-Jörg: *Erdwiderstandsbeiwerte nach dem Ohde-Variationsverfahren*, 1972

24 Minor, Hans-Erwin: *Beitrag zur Bestimmung der Schwingungsanfachungsfunktionen überströmter Stauklappen*, 1972, vergriffen

25 Brombach, Hansjörg: *Untersuchung strömungsmechanischer Elemente (Fluidik) und die Möglichkeit der Anwendung von Wirbelkammerelementen im Wasserbau*, 1972, vergriffen

26 Wildenhahn, Eberhard: *Beitrag zur Berechnung von Horizontalfilterbrunnen*, 1972

27 Steinlein, Helmut: *Die Eliminierung der Schwebstoffe aus Flußwasser zum Zweck der unterirdischen Wasserspeicherung, gezeigt am Beispiel der Iller*, 1972

28 Holthoff, Franz Josef: *Die Überwindung großer Hubhöhen in der Binnenschiffahrt durch Schwimmerhebewerke*, 1973

29 Röder, Karl: *Einwirkungen aus Baugrundbewegungen auf trog- und kastenförmige Konstruktionen des Wasser- und Tunnelbaues*, 1973

30 Kretschmer, Heinz: *Die Bemessung von Bogenstaumauern in Abhängigkeit von der Talform*, 1973

31 Honekamp, Hermann: *Beitrag zur Berechnung der Montage von Unterwasserpipelines*, 1973

32 Giesecke, Jürgen: *Die Wirbelkammertriode als neuartiges Steuerorgan im Wasserbau*, und Brombach, Hansjörg: *Entwicklung, Bauformen, Wirkungsweise und Steuereigenschaften von Wirbelkammerverstärkern*, 1974

33 Rueff, Helge: *Untersuchung der schwingungserregenden Kräfte an zwei hintereinander angeordneten Tiefschützen unter besonderer Berücksichtigung von Kavitation*, 1974

34 Röhnisch, Arthur: *Einpreßversuche mit Zementmörtel für Spannbeton - Vergleich der Ergebnisse von Modellversuchen mit Ausführungen in Hüllwellrohren*, 1975

35 *Sonderheft anläßlich des 65. Geburtstages von Prof. Dr.-Ing. Kurt Petrikat mit Beiträgen von*: Brombach, Hansjörg; Erbel, Klaus; Flinspach, Dieter; Fischer jr., Richard; Gàl, Attila; Gerlach, Reinhard; Giesecke, Jürgen; Haberhauer, Robert; Hafner Edzard; Hausenblas, Bernhard; Horlacher, Hans-Burkhard; Hutarew, Andreas; Knoll, Manfred; Krummet, Ralph; Marotz, Günter; Merkle, Theodor; Miller, Christoph; Minor, Hans-Erwin; Neumayer, Hans; Rao, Syamala; Rath, Paul; Rueff, Helge; Ruppert, Jürgen; Schwarz, Wolfgang; Topal-Gökceli, Mehmet; Vollmer, Ernst; Wang, Chung-su; Weber, Hans-Georg; 1975

36 Berger, Jochum: *Beitrag zur Berechnung des Spannungszustandes in rotationssymmetrisch belasteten Kugelschalen veränderlicher Wandstärke unter Gas- und Flüssigkeitsdruck durch Integration schwach singulärer Differentialgleichungen*, 1975

37 Dirksen, Wolfram: *Berechnung instationärer Abflußvorgänge in gestauten Gerinnen mittels Differenzenverfahren und die Anwendung auf Hochwasserrückhaltebecken*, 1976

38 Horlacher, Hans-Burkhard: *Berechnung instationärer Temperatur- und Wärmespannungsfelder in langen mehrschichtigen Hohlzylindern*, 1976

39 Hafner, Edzard: *Untersuchung der hydrodynamischen Kräfte auf Baukörper im Tiefwasserbereich des Meeres*, 1977, ISBN 3-921694-39-6

40 Ruppert, Jürgen: *Über den Axialwirbelkammerverstärker für den Einsatz im Wasserbau*, 1977, ISBN 3-921694-40-X

41 Hutarew, Andreas: *Beitrag zur Beeinflußbarkeit des Sauerstoffgehalts in Fließgewässern an Abstürzen und Wehren*, 1977, ISBN 3-921694-41-8, vergriffen

42 Miller, Christoph: *Ein Beitrag zur Bestimmung der schwingungserregenden Kräfte an unterströmten Wehren*, 1977, ISBN 3-921694-42-6

43 Schwarz, Wolfgang: *Druckstoßberechnung unter Berücksichtigung der Radial- und Längsverschiebungen der Rohrwandung*, 1978, ISBN 3-921694-43-4

44 Kinzelbach, Wolfgang: *Numerische Untersuchungen über den optimalen Einsatz variabler Kühlsysteme einer Kraftwerkskette am Beispiel Oberrhein*, 1978, ISBN 3-921694-44-2

45 Barczewski, Baldur: *Neue Meßmethoden für Wasser-Luftgemische und deren Anwendung auf zweiphasige Auftriebsstrahlen*, 1979, ISBN 3-921694-45-0

46 Neumayer, Hans: *Untersuchung der Strömungsvorgänge in radialen Wirbelkammerverstärkern*, 1979, ISBN 3-921694-46-9

47 Elalfy, Youssef-Elhassan: *Untersuchung der Strömungsvorgänge in Wirbelkammerdioden und -drosseln*, 1979, ISBN 3-921694-47-7

48 Brombach, Hansjörg: *Automatisierung der Bewirtschaftung von Wasserspeichern*, 1981, ISBN 3-921694-48-5

49 Geldner, Peter: *Deterministische und stochastische Methoden zur Bestimmung der Selbstdichtung von Gewässern*, 1981, ISBN 3-921694-49-3, vergriffen

50 Mehlhorn, Hans: *Temperaturveränderungen im Grundwasser durch Brauchwassereinleitungen*, 1982, ISBN 3-921694-50-7, vergriffen

51 Hafner, Edzard: *Rohrleitungen und Behälter im Meer*, 1983, ISBN 3-921694-51-5

52 Rinnert, Bernd: *Hydrodynamische Dispersion in porösen Medien: Einfluß von Dichteunterschieden auf die Vertikalvermischung in horizontaler Strömung*, 1983, ISBN 3-921694-52-3, vergriffen

53 Lindner, Wulf: *Steuerung von Grundwasserentnahmen unter Einhaltung ökologischer Kriterien*, 1983, ISBN 3-921694-53-1, vergriffen

54 Herr, Michael; Herzer, Jörg; Kinzelbach, Wolfgang; Kobus, Helmut; Rinnert, Bernd: *Methoden zur rechnerischen Erfassung und hydraulischen Sanierung von Grundwasserkontaminationen*, 1983, ISBN 3-921694-54-X

55 Schmitt, Paul: *Wege zur Automatisierung der Niederschlagsermittlung*, 1984, ISBN 3-921694-55-8, vergriffen

56 Müller, Peter: *Transport und selektive Sedimentation von Schwebstoffen bei gestautem Abfluß*, 1985, ISBN 3-921694-56-6

57 El-Qawasmeh, Fuad: *Möglichkeiten und Grenzen der Tropfbewässerung unter besonderer Berücksichtigung der Verstopfungsanfälligkeit der Tropfelemente*, 1985, ISBN 3-921694-57-4, vergriffen

58 Kirchenbaur, Klaus: *Mikroprozessorgesteuerte Erfassung instationärer Druckfelder am Beispiel seegangsbelasteter Baukörper*, 1985, ISBN 3-921694-58-2

59 Kobus, Helmut (Hrsg.): *Modellierung des großräumigen Wärme- und Schadstofftransports im Grundwasser*, Tätigkeitsbericht 1984/85 (DFG-Forschergruppe an den Universitäten Hohenheim, Karlsruhe und Stuttgart), 1985, ISBN 3-921694-59-0, vergriffen

60 Spitz, Karlheinz: *Dispersion in porösen Medien: Einfluß von Inhomogenitäten und Dichteunterschieden*, 1985, ISBN 3-921694-60-4, vergriffen

61 Kobus, Helmut: *An Introduction to Air-Water Flows in Hydraulics*, 1985, ISBN 3-921694-61-2

62 Kaleris, Vassilios: *Erfassung des Austausches von Oberflächen- und Grundwasser in horizontalebenen Grundwassermodellen*, 1986, ISBN 3-921694-62-0

63 Herr, Michael: *Grundlagen der hydraulischen Sanierung verunreinigter Porengrundwasserleiter*, 1987, ISBN 3-921694-63-9

64 Marx, Walter: *Berechnung von Temperatur und Spannung in Massenbeton infolge Hydratation*, 1987, ISBN 3-921694-64-7

65 Koschitzky, Hans-Peter: *Dimensionierungskonzept für Sohlbelüfter in Schußrinnen zur Vermeidung von Kavitationsschäden*, 1987, ISBN 3-921694-65-5

66 Kobus, Helmut (Hrsg.): *Modellierung des großräumigen Wärme- und Schadstofftransports im Grundwasser*, Tätigkeitsbericht 1986/87 (DFG-Forschergruppe an den Universitäten Hohenheim, Karlsruhe und Stuttgart) 1987, ISBN 3-921694-66-3

67 Söll, Thomas: *Berechnungsverfahren zur Abschätzung anthropogener Temperaturanomalien im Grundwasser*, 1988, ISBN 3-921694-67-1

68 Dittrich, Andreas; Westrich, Bernd: *Bodenseeufererosion, Bestandsaufnahme und Bewertung*, 1988, ISBN 3-921694-68-X, vergriffen

69 Huwe, Bernd; van der Ploeg, Rienk R.: *Modelle zur Simulation des Stickstoffhaushaltes von Standorten mit unterschiedlicher landwirtschaftlicher Nutzung*, 1988, ISBN 3-921694-69-8, vergriffen

70 Stephan, Karl: *Integration elliptischer Funktionen*, 1988, ISBN 3-921694-70-1

71 Kobus, Helmut; Zilliox, Lothaire (Hrsg.): *Nitratbelastung des Grundwassers, Auswirkungen der Landwirtschaft auf die Grundwasser- und Rohwasserbeschaffenheit und Maßnahmen zum Schutz des Grundwassers*. Vorträge des deutsch-französischen Kolloquiums am 6. Oktober 1988, Universitäten Stuttgart und Louis Pasteur Strasbourg (Vorträge in deutsch oder französisch, Kurzfassungen zweisprachig), 1988, ISBN 3-921694-71-X

72 Soyeaux, Renald: *Unterströmung von Stauanlagen auf klüftigem Untergrund unter Berücksichtigung laminarer und turbulenter Fließzustände*,1991, ISBN 3-921694-72-8

73 Kohane, Roberto: *Berechnungsmethoden für Hochwasserabfluß in Fließgewässern mit überströmten Vorländern*, 1991, ISBN 3-921694-73-6

74 Hassinger, Reinhard: *Beitrag zur Hydraulik und Bemessung von Blocksteinrampen in flexibler Bauweise*, 1991, ISBN 3-921694-74-4, vergriffen

75 Schäfer, Gerhard: *Einfluß von Schichtenstrukturen und lokalen Einlagerungen auf die Längsdispersion in Porengrundwasserleitern*, 1991, ISBN 3-921694-75-2

76 Giesecke, Jürgen: *Vorträge, Wasserwirtschaft in stark besiedelten Regionen; Umweltforschung mit Schwerpunkt Wasserwirtschaft*, 1991, ISBN 3-921694-76-0

77 Huwe, Bernd: *Deterministische und stochastische Ansätze zur Modellierung des Stickstoffhaushalts landwirtschaftlich genutzter Flächen auf unterschiedlichem Skalenniveau*, 1992, ISBN 3-921694-77-9, vergriffen

78 Rommel, Michael: *Verwendung von Kluftdaten zur realitätsnahen Generierung von Kluftnetzen mit anschließender laminar-turbulenter Strömungsberechnung*, 1993, ISBN 3-92 1694-78-7

79 Marschall, Paul: *Die Ermittlung lokaler Stofffrachten im Grundwasser mit Hilfe von Einbohrloch-Meßverfahren*, 1993, ISBN 3-921694-79-5, vergriffen

80 Ptak, Thomas: *Stofftransport in heterogenen Porenaquiferen: Felduntersuchungen und stochastische Modellierung*, 1993, ISBN 3-921694-80-9, vergriffen

81 Haakh, Frieder: *Transientes Strömungsverhalten in Wirbelkammern,* 1993, ISBN 3-921694-81-7

82 Kobus, Helmut; Cirpka, Olaf; Barczewski, Baldur; Koschitzky, Hans-Peter: *Versucheinrichtung zur Grundwasser und Altlastensanierung VEGAS, Konzeption und Programmrahmen*, 1993, ISBN 3-921694-82-5

83 Zang, Weidong: *Optimaler Echtzeit-Betrieb eines Speichers mit aktueller Abflußregenerierung*, 1994, ISBN 3-921694-83-3, vergriffen

84 Franke, Hans-Jörg: *Stochastische Modellierung eines flächenhaften Stoffeintrages und Transports in Grundwasser am Beispiel der Pflanzenschutzmittelproblematik*, 1995, ISBN 3-921694-84-1

85 Lang, Ulrich: *Simulation regionaler Strömungs- und Transportvorgänge in Karstaquiferen mit Hilfe des Doppelkontinuum-Ansatzes: Methodenentwicklung und Parameteridentifikation*, 1995, ISBN 3-921694-85-X, vergriffen

86 Helmig, Rainer: *Einführung in die Numerischen Methoden der Hydromechanik*, 1996, ISBN 3-921694-86-8, vergriffen

87 Cirpka, Olaf: *CONTRACT: A Numerical Tool for Contaminant Transport and Chemical Transformations - Theory and Program Documentation* -, 1996, ISBN 3-921694-87-6

88 Haberlandt, Uwe: *Stochastische Synthese und Regionalisierung des Niederschlages für Schmutzfrachtberechnungen*, 1996, ISBN 3-921694-88-4

89 Croisé, Jean: *Extraktion von flüchtigen Chemikalien aus natürlichen Lockergesteinen mittels erzwungener Luftströmung*, 1996, ISBN 3-921694-89-2, vergriffen

90 Jorde, Klaus: *Ökologisch begründete, dynamische Mindestwasserregelungen bei Ausleitungskraftwerken*, 1997, ISBN 3-921694-90-6, vergriffen

91 Helmig, Rainer: *Gekoppelte Strömungs- und Transportprozesse im Untergrund - Ein Beitrag zur Hydrosystemmodellierung-*, 1998, ISBN 3-921694-91-4, vergriffen

92 Emmert, Martin: *Numerische Modellierung nichtisothermer Gas-Wasser Systeme in porösen Medien,* 1997, ISBN 3-921694-92-2

93 Kern, Ulrich: *Transport von Schweb- und Schadstoffen in staugeregelten Fließgewässern am Beispiel des Neckars*, 1997, ISBN 3-921694-93-0, vergriffen

94 Förster, Georg: *Druckstoßdämpfung durch große Luftblasen in Hochpunkten von Rohrleitungen 1997*, ISBN 3-921694-94-9

95 Cirpka, Olaf: *Numerische Methoden zur Simulation des reaktiven Mehrkomponententransports im Grundwasser*, 1997, ISBN 3-921694-95-7, vergriffen

96 Färber, Arne: *Wärmetransport in der ungesättigten Bodenzone: Entwicklung einer thermischen In-situ-Sanierungstechnologie*, 1997, ISBN 3-921694-96-5

97 Betz, Christoph: *Wasserdampfdestillation von Schadstoffen im porösen Medium: Entwicklung einer thermischen In-situ-Sanierungstechnologie*, 1998, ISBN 3-921694-97-3

98 Xu, Yichun: *Numerical Modeling of Suspended Sediment Transport in Rivers*, 1998, ISBN 3-921694-98-1, vergriffen

99 Wüst, Wolfgang: *Geochemische Untersuchungen zur Sanierung CKW-kontaminierter Aquifere mit Fe(0)-Reaktionswänden,* 2000, ISBN 3-933761-02-2

100 Sheta, Hussam: *Simulation von Mehrphasenvorgängen in porösen Medien unter Einbeziehung von Hysterese-Effekten*, 2000, ISBN 3-933761-03-4

101 Ayros, Edwin: *Regionalisierung extremer Abflüsse auf der Grundlage statistischer Verfahren*, 2000, ISBN 3-933761-04-2, vergriffen

102 Huber, Ralf: *Compositional Multiphase Flow and Transport in Heterogeneous Porous Media*, 2000, ISBN 3-933761-05-0

103 Braun, Christopherus: *Ein Upscaling-Verfahren für Mehrphasenströmungen in porösen Medien*, 2000, ISBN 3-933761-06-9

104 Hofmann, Bernd: *Entwicklung eines rechnergestützten Managementsystems zur Beurteilung von Grundwasserschadensfällen*, 2000, ISBN 3-933761-07-7

105 Class, Holger: *Theorie und numerische Modellierung nichtisothermer Mehrphasenprozesse in NAPL-kontaminierten porösen Medien,* 2001, ISBN 3-933761-08-5

106 Schmidt, Reinhard: *Wasserdampf- und Heißluftinjektion zur thermischen Sanierung kontaminierter Standorte*, 2001, ISBN 3-933761-09-3

107 Josef, Reinhold:, *Schadstoffextraktion mit hydraulischen Sanierungsverfahren unter Anwendung von grenzflächenaktiven Stoffen*, 2001, ISBN 3-933761-10-7

108 Schneider, Matthias: *Habitat- und Abflussmodellierung für Fließgewässer mit unscharfen Berechnungsansätzen*, 2001, ISBN 3-933761-11-5

109 Rathgeb, Andreas: *Hydrodynamische Bemessungsgrundlagen für Lockerdeckwerke an überströmbaren Erddämmen*, 2001, ISBN 3-933761-12-3

110 Lang, Stefan: *Parallele numerische Simulation instätionärer Probleme mit adaptiven Methoden auf unstrukturierten Gittern*, 2001, ISBN 3-933761-13-1

111 Appt, Jochen; Stumpp Simone: *Die Bodensee-Messkampagne 2001, IWS/CWR Lake Constance Measurement Program 2001*, 2002, ISBN 3-933761-14-X

112 Heimerl, Stephan: *Systematische Beurteilung von Wasserkraftprojekten,* 2002, ISBN 3-933761-15-8, vergriffen

113 Iqbal, Amin: *On the Management and Salinity Control of Drip Irrigation,* 2002, ISBN 3-933761-16-6

114 Silberhorn-Hemminger, Annette: *Modellierung von Kluftaquifersystemen: Geostatistische Analyse und deterministisch-stochastische Kluftgenerierung,* 2002, ISBN 3-933761-17-4

115 Winkler, Angela: *Prozesse des Wärme- und Stofftransports bei der In-situ-Sanierung mit festen Wärmequellen,* 2003, ISBN 3-933761-18-2

116 Marx, Walter: *Wasserkraft, Bewässerung, Umwelt - Planungs- und Bewertungsschwerpunkte der Wasserbewirtschaftung,* 2003, ISBN 3-933761-19-0

117 Hinkelmann, Reinhard: *Efficient Numerical Methods and Information-Processing Techniques in Environment Water,* 2003, ISBN 3-933761-20-4

118 Samaniego-Eguiguren, Luis Eduardo: *Hydrological Consequences of Land Use / Land Cover and Climatic Changes in Mesoscale Catchments*, 2003, ISBN 3-933761-21-2

119 Neunhäuserer, Lina: *Diskretisierungsansätze zur Modellierung von Strömungs- und Transportprozessen in geklüftet-porösen Medien*, 2003, ISBN 3-933761-22-0

120 Paul, Maren: *Simulation of Two-Phase Flow in Heterogeneous Poros Media with Adaptive Methods*, 2003, ISBN 3-933761-23-9

121 Ehret, Uwe: *Rainfall and Flood Nowcasting in Small Catchments using Weather Radar*, 2003, ISBN 3-933761-24-7

122 Haag, Ingo: *Der Sauerstoffhaushalt staugeregelter Flüsse am Beispiel des Neckars - Analysen, Experimente, Simulationen -,* 2003, ISBN 3-933761-25-5

123 Appt, Jochen: *Analysis of Basin-Scale Internal Waves in Upper Lake Constance,* 2003, ISBN 3-933761-26-3

124 Hrsg.: Schrenk, Volker; Batereau, Katrin; Barczewski, Baldur; Weber, Karolin und Koschitzky, Hans-Peter: *Symposium Ressource Fläche und VEGAS - Statuskolloquium 2003, 30. September und 1. Oktober 2003,* 2003, ISBN 3-933761-27-1

125 Omar Khalil Ouda: *Optimisation of Agricultural Water Use: A Decision Support System for the Gaza Strip,* 2003, ISBN 3-933761-28-0

126 Batereau, Katrin: *Sensorbasierte Bodenluftmessung zur Vor-Ort-Erkundung von Schadensherden im Untergrund*, 2004, ISBN 3-933761-29-8

127 Witt, Oliver: *Erosionsstabilität von Gewässersedimenten mit Auswirkung auf den Stofftransport bei Hochwasser am Beispiel ausgewählter Stauhaltungen des Oberrheins*, 2004, ISBN 3-933761-30-1

128 Jakobs, Hartmut: *Simulation nicht-isothermer Gas-Wasser-Prozesse in komplexen Kluft-Matrix-Systemen*, 2004, ISBN 3-933761-31-X

129 Li, Chen-Chien: *Deterministisch-stochastisches Berechnungskonzept zur Beurteilung der Auswirkungen erosiver Hochwasserereignisse in Flussstauhaltungen,* 2004, ISBN 3-933761-32-8

130 Reichenberger, Volker; Helmig, Rainer; Jakobs, Hartmut; Bastian, Peter; Niessner, Jennifer: *Complex Gas-Water Processes in Discrete Fracture-Matrix Systems: Upscaling, Mass-Conservative Discretization and Efficient Multilevel Solution,* 2004, ISBN 3-933761-33-6

131 Hrsg.: Barczewski, Baldur; Koschitzky, Hans-Peter; Weber, Karolin; Wege, Ralf: *VEGAS - Statuskolloquium 2004,* Tagungsband zur Veranstaltung am 05. Oktober 2004 an der Universität Stuttgart, Campus Stuttgart-Vaihingen, 2004, ISBN 3-933761-34-4

132 Asie, Kemal Jabir: *Finite Volume Models for Multiphase Multicomponent Flow through Porous Media*. 2005, ISBN 3-933761-35-2

133 Jacoub, George: *Development of a 2-D Numerical Module for Particulate Contaminant Transport in Flood Retention Reservoirs and Impounded Rivers,* 2004, ISBN 3-933761-36-0

134 Nowak, Wolfgang: *Geostatistical Methods for the Identification of Flow and Transport Parameters in the Subsurface,* 2005, ISBN 3-933761-37-9

135 Süß, Mia: *Analysis of the influence of structures and boundaries on flow and transport processes in fractured porous media*, 2005, ISBN 3-933761-38-7

136 Jose, Surabhin Chackiath: *Experimental Investigations on Longitudinal Dispersive Mixing in Heterogeneous Aquifers,* 2005, ISBN: 3-933761-39-5

137 Filiz, Fulya: *Linking Large-Scale Meteorological Conditions to Floods in Mesoscale Catchments,* 2005, ISBN 3-933761-40-9

138 Qin, Minghao: *Wirklichkeitsnahe und recheneffiziente Ermittlung von Temperatur und Spannungen bei großen RCC-Staumauern*, 2005, ISBN 3-933761-41-7

139 Kobayashi, Kenichiro: *Optimization Methods for Multiphase Systems in the Subsurface - Application to Methane Migration in Coal Mining Areas*, 2005, ISBN 3-933761-42-5

140 Rahman, Md. Arifur: *Experimental Investigations on Transverse Dispersive Mixing in Heterogeneous Porous Media,* 2005, ISBN 3-933761-43-3

141 Schrenk, Volker: *Ökobilanzen zur Bewertung von Altlastensanierungsmaßnahmen,* 2005, ISBN 3-933761-44-1

142 Hundecha, Hirpa Yeshewatesfa: *Regionalization of Parameters of a Conceptual Rainfall-Runoff Model*, 2005, ISBN: 3-933761-45-X

143 Wege, Ralf: *Untersuchungs- und Überwachungsmethoden für die Beurteilung natürlicher Selbstreinigungsprozesse im Grundwasser,* 2005, ISBN 3-933761-46-8

144 Breiting, Thomas: *Techniken und Methoden der Hydroinformatik - Modellierung von komplexen Hydrosystemen im Untergrund*, 2006, 3-933761-47-6

145 Hrsg.: Braun, Jürgen; Koschitzky, Hans-Peter; Müller, Martin: *Ressource Untergrund: 10 Jahre VEGAS: Forschung und Technologieentwicklung zum Schutz von Grundwasser und Boden,* Tagungsband zur Veranstaltung am 28. und 29. September 2005 an der Universität Stuttgart, Campus Stuttgart-Vaihingen, 2005, ISBN 3-933761-48-4

146 Rojanschi, Vlad: *Abflusskonzentration in mesoskaligen Einzugsgebieten unter Berücksichtigung des Sickerraumes,* 2006, ISBN 3-933761-49-2

147 Winkler, Nina Simone: *Optimierung der Steuerung von Hochwasserrückhaltebecken-systemen,* 2006, ISBN 3-933761-50-6

148 Wolf, Jens: *Räumlich differenzierte Modellierung der Grundwasserströmung alluvialer Aquifere für mesoskalige Einzugsgebiete*, 2006, ISBN: 3-933761-51-4

149 Kohler, Beate: *Externe Effekte der Laufwasserkraftnutzung*, 2006, ISBN 3-933761-52-2

150 Hrsg.: Braun, Jürgen; Koschitzky, Hans-Peter; Stuhrmann, Matthias: *VEGAS-Statuskolloquium 2006,* Tagungsband zur Veranstaltung am 28. September 2006 an der Universität Stuttgart, Campus Stuttgart-Vaihingen, 2006, ISBN 3-933761-53-0

151 Niessner, Jennifer: *Multi-Scale Modeling of Multi-Phase - Multi-Component Processes in Heterogeneous Porous Media*, 2006, ISBN 3-933761-54-9

152 Fischer, Markus: *Beanspruchung eingeerdeter Rohrleitungen infolge Austrocknung bindiger Böden,* 2006, ISBN 3-933761-55-7

153 Schneck, Alexander: *Optimierung der Grundwasserbewirtschaftung unter Berücksichtigung der Belange der Wasserversorgung, der Landwirtschaft und des Naturschutzes*, 2006, ISBN 3-933761-56-5

154 Das, Tapash: *The Impact of Spatial Variability of Precipitation on the Predictive Uncertainty of Hydrological Models,* 2006, ISBN 3-933761-57-3

155 Bielinski, Andreas: *Numerical Simulation of CO_2 sequestration in geological formations*, 2007, ISBN 3-933761-58-1

156 Mödinger, Jens: *Entwicklung eines Bewertungs- und Entscheidungsunterstützungssystems für eine nachhaltige regionale Grundwasserbewirtschaftung*, 2006, ISBN 3-933761-60-3

157 Manthey, Sabine: *Two-phase flow processes with dynamic effects in porous media - parameter estimation and simulation,* 2007, ISBN 3-933761-61-1

158 Pozos Estrada, Oscar: *Investigation on the Effects of Entrained Air in Pipelines,* 2007, ISBN 3-933761-62-X

159 Ochs, Steffen Oliver: *Steam injection into saturated porous media – process analysis including experimental and numerical investigations*, 2007, ISBN 3-933761-63-8

160 Marx, Andreas: *Einsatz gekoppelter Modelle und Wetterradar zur Abschätzung von Niederschlagsintensitäten und zur Abflussvorhersage, 2007,* ISBN 3-933761-64-6

161 Hartmann, Gabriele Maria: *Investigation of Evapotranspiration Concepts in Hydrological Modelling for Climate Change Impact Assessment*, 2007, ISBN 3-933761-65-4

162 Kebede Gurmessa, Tesfaye: *Numerical Investigation on Flow and Transport Characteristics to Improve Long-Term Simulation of Reservoir Sedimentation*, 2007, ISBN 3-933761-66-2

163 Trifković, Aleksandar: *Multi-objective and Risk-based Modelling Methodology for Planning, Design and Operation of Water Supply Systems*, 2007, ISBN 3-933761-67-0

164 Götzinger, Jens: *Distributed Conceptual Hydrological Modelling - Simulation of Climate, Land Use Change Impact and Uncertainty Analysis*, 2007, ISBN 3-933761-68-9

165 Hrsg.: Braun, Jürgen; Koschitzky, Hans-Peter; Stuhrmann, Matthias: *VEGAS – Kolloquium 2007,* Tagungsband zur Veranstaltung am 26. September 2007 an der Universität Stuttgart, Campus Stuttgart-Vaihingen, 2007, ISBN 3-933761-69-7

166 Freeman, Beau: *Modernization Criteria Assessment for Water Resources Planning; Klamath Irrigation Project, U.S.*, 2008, ISBN 3-933761-70-0

167 Dreher, Thomas: *Selektive Sedimentation von Feinstschwebstoffen in Wechselwirkung mit wandnahen turbulenten Strömungsbedingungen*, 2008, ISBN 3-933761-71-9

168 Yang, Wei: *Discrete-Continuous Downscaling Model for Generating Daily Precipitation Time Series*, 2008, ISBN 3-933761-72-7

169 Kopecki, Ianina: *Calculational Approach to FST-Hemispheres for Multiparametrical Benthos Habitat Modelling,* 2008*,* ISBN 3-933761-73-5

170 Brommundt, Jürgen: *Stochastische Generierung räumlich zusammenhängender Niederschlagszeitreihen*, 2008, ISBN 3-933761-74-3

171 Papafotiou, *Alexandros: Numerical Investigations of the Role of Hysteresis in Heterogeneous Two-Phase Flow Systems*, 2008, ISBN 3-933761-75-1

172 He, Yi: *Application of a Non-Parametric Classification Scheme to Catchment Hydrology*, 2008, ISBN 978-3-933761-76-7

173 Wagner, Sven: *Water Balance in a Poorly Gauged Basin in West Africa Using Atmospheric Modelling and Remote Sensing Information*, 2008, ISBN 978-3-933761-77-4

174 Hrsg.: Braun, Jürgen; Koschitzky, Hans-Peter; Stuhrmann, Matthias; Schrenk, Volker: *VEGAS-Kolloquium 2008 Ressource Fläche III*, Tagungsband zur Veranstaltung am 01. Oktober 2008 an der Universität Stuttgart, Campus Stuttgart-Vaihingen, 2008, ISBN 978-3-933761-78-1

175 Patil, Sachin: *Regionalization of an Event Based Nash Cascade Model for Flood Predictions in Ungauged Basins*, 2008, ISBN 978-3-933761-79-8

176 Assteerawatt, Anongnart: *Flow and Transport Modelling of Fractured Aquifers based on a Geostatistical Approach,* 2008, ISBN 978-3-933761-80-4

177 Karnahl, Joachim Alexander: *2D numerische Modellierung von multifraktionalem Schwebstoff- und Schadstofftransport in Flüssen*, 2008, ISBN 978-3-933761-81-1

178 Hiester, Uwe: *Technologieentwicklung zur In-situ-Sanierung der ungesättigten Bodenzone mit festen Wärmequellen,* 2009, ISBN 978-3-933761-82-8

179 Laux, Patrick: *Statistical Modeling of Precipitation for Agricultural Planning in the Volta Basin of West Africa,* 2009, ISBN 978-3-933761-83-5

180 Ehsan, Saqib: *Evaluation of Life Safety Risks Related to Severe Flooding,* 2009, ISBN 978-3-933761-84-2

181 Prohaska, Sandra: *Development and Application of a 1D Multi-Strip Fine Sediment Transport Model for Regulated Rivers,* 2009, ISBN 978-3-933761-85-9

182 Kopp, Andreas: *Evaluation of CO_2 Injection Processes in Geological Formations for Site Screening,* 2009, ISBN 978-3-933761-86-6

183 Ebigbo, Anozie: *Modelling of biofilm growth and its influence on CO_2 and water (two-phase) flow in porous media,* 2009, ISBN 978-3-933761-87-3

184 Freiboth, Sandra: *A phenomenological model for the numerical simulation of multiphase multicomponent processes considering structural alterations of porous media*, 2009, ISBN 978-3-933761-88-0

185 Zöllner, Frank: *Implementierung und Anwendung netzfreier Methoden im Konstruktiven Wasserbau und in der Hydromechanik*, 2009, ISBN 978-3-933761-89-7

186 Vasin, Milos: *Influence of the soil structure and property contrast on flow and transport in the unsaturated zone*, 2010, ISBN 978-3-933761-90-3

187 Li, Jing: *Application of Copulas as a New Geostatistical Tool*, 2010, ISBN 978-3-933761-91-0

188 AghaKouchak, Amir: *Simulation of Remotely Sensed Rainfall Fields Using Copulas*, 2010, ISBN 978-3-933761-92-7

189 Thapa, Pawan Kumar: *Physically-based spatially distributed rainfall runoff modelling for soil erosion estimation*, 2010, ISBN 978-3-933761-93-4

190 Wurms, Sven: *Numerische Modellierung der Sedimentationsprozesse in Retentionsanlagen zur Steuerung von Stoffströmen bei extremen Hochwasserabflussereignissen*, 2011, ISBN 978-3-933761-94-1

191 Merkel, Uwe: *Unsicherheitsanalyse hydraulischer Einwirkungen auf Hochwasserschutzdeiche und Steigerung der Leistungsfähigkeit durch adaptive Strömungsmodellierung*, 2011, ISBN 978-3-933761-95-8

192 Fritz, Jochen: *A Decoupled Model for Compositional Non-Isothermal Multiphase Flow in Porous Media and Multiphysics Approaches for Two-Phase Flow*, 2010, ISBN 978-3-933761-96-5

193 Weber, Karolin (Hrsg.): *12. Treffen junger WissenschaftlerInnen an Wasserbauinstituten*, 2010, ISBN 978-3-933761-97-2

194 Bliefernicht, Jan-Geert: *Probability Forecasts of Daily Areal Precipitation for Small River Basins,* 2011, ISBN 978-3-933761-98-9

195 Hrsg.: Koschitzky, Hans-Peter; Braun, Jürgen: *VEGAS-Kolloquium 2010 In-situ-Sanierung - Stand und Entwicklung Nano und ISCO -,* Tagungsband zur Veranstaltung am 07. Oktober 2010 an der Universität Stuttgart, Campus Stuttgart-Vaihingen*,* 2010*,* ISBN 978-3-933761-99-6

196 Gafurov, Abror: *Water Balance Modeling Using Remote Sensing Information - Focus on Central Asia,* 2010, ISBN 978-3-942036-00-9

197 Mackenberg, Sylvia: *Die Quellstärke in der Sickerwasserprognose: Möglichkeiten und Grenzen von Labor- und Freilanduntersuchungen,* 2010, ISBN 978-3-942036-01-6

198 Singh, Shailesh Kumar: *Robust Parameter Estimation in Gauged and Ungauged Basins,* 2010, ISBN 978-3-942036-02-3

199 Doğan, Mehmet Onur: *Coupling of porous media flow with pipe flow,* 2011, ISBN 978-3-942036-03-0

200 Liu, Min: *Study of Topographic Effects on Hydrological Patterns and the Implication on Hydrological Modeling and Data Interpolation,* 2011, ISBN 978-3-942036-04-7

201 Geleta, Habtamu Itefa: *Watershed Sediment Yield Modeling for Data Scarce Areas,* 2011, ISBN 978-3-942036-05-4

202 Franke, Jörg: *Einfluss der Überwachung auf die Versagenswahrscheinlichkeit von Staustufen,* 2011, ISBN 978-3-942036-06-1

203 Bakimchandra, Oinam: *Integrated Fuzzy-GIS approach for assessing regional soil erosion risks,* 2011, ISBN 978-3-942036-07-8

204 Alam, Muhammad Mahboob: *Statistical Downscaling of Extremes of Precipitation in Mesoscale Catchments from Different RCMs and Their Effects on Local Hydrology,* 2011, ISBN 978-3-942036-08-5

205 Hrsg.: Koschitzky, Hans-Peter; Braun, Jürgen: *VEGAS-Kolloquium 2011 Flache Geothermie - Perspektiven und Risiken,* Tagungsband zur Veranstaltung am 06. Oktober 2011 an der Universität Stuttgart, Campus Stuttgart-Vaihingen, 2011, ISBN 978-3-933761-09-2

206 Haslauer, Claus: *Analysis of Real-World Spatial Dependence of Subsurface Hydraulic Properties Using Copulas with a Focus on Solute Transport Behaviour,* 2011, ISBN 978-3-942036-10-8

207 Dung, Nguyen Viet: *Multi-objective automatic calibration of hydrodynamic models – development of the concept and an application in the Mekong Delta,* 2011, ISBN 978-3-942036-11-5

208 Hung, Nguyen Nghia: *Sediment dynamics in the floodplain of the Mekong Delta, Vietnam,* 2011, ISBN 978-3-942036-12-2

209 Kuhlmann, Anna: *Influence of soil structure and root water uptake on flow in the unsaturated zone,* 2012, ISBN 978-3-942036-13-9

210 Tuhtan, Jeffrey Andrew: *Including the Second Law Inequality in Aquatic Ecodynamics: A Modeling Approach for Alpine Rivers Impacted by Hydropeaking,* 2012, ISBN 978-3-942036-14-6

211 Tolossa, Habtamu: *Sediment Transport Computation Using a Data-Driven Adaptive Neuro-Fuzzy Modelling Approach,* 2012, ISBN 978-3-942036-15-3

212 Tatomir, Alexandru-Bodgan: *From Discrete to Continuum Concepts of Flow in Fractured Porous Media,* 2012, ISBN 978-3-942036-16-0

213 Erbertseder, Karin: *A Multi-Scale Model for Describing Cancer-Therapeutic Transport in the Human Lung,* 2012, ISBN 978-3-942036-17-7

214 Noack, Markus: *Modelling Approach for Interstitial Sediment Dynamics and Reproduction of Gravel Spawning Fish,* 2012, ISBN 978-3-942036-18-4

215 De Boer, Cjestmir Volkert: *Transport of Nano Sized Zero Valent Iron Colloids during Injection into the Subsurface*, 2012, ISBN 978-3-942036-19-1

216 Pfaff, Thomas: *Processing and Analysis of Weather Radar Data for Use in Hydrology*, 2013, ISBN 978-3-942036-20-7

217 Lebrenz, Hans-Henning: *Addressing the Input Uncertainty for Hydrological Modeling by a New Geostatistical Method*, 2013, ISBN 978-3-942036-21-4

218 Darcis, Melanie Yvonne: *Coupling Models of Different Complexity for the Simulation of CO_2 Storage in Deep Saline Aquifers*, 2013, ISBN 978-3-942036-22-1

219 Beck, Ferdinand: *Generation of Spatially Correlated Synthetic Rainfall Time Series in High Temporal Resolution - A Data Driven Approach*, 2013, ISBN 978-3-942036-23-8

220 Guthke, Philipp: *Non-multi-Gaussian spatial structures: Process-driven natural genesis, manifestation, modeling approaches, and influences on dependent processes*, 2013, ISBN 978-3-942036-24-5

221 Walter, Lena: *Uncertainty studies and risk assessment for CO_2 storage in geological formations*, 2013, ISBN 978-3-942036-25-2

222 Wolff, Markus: *Multi-scale modeling of two-phase flow in porous media including capillary pressure effects,* 2013, ISBN 978-3-942036-26-9

223 Mosthaf, Klaus Roland: *Modeling and analysis of coupled porous-medium and free flow with application to evaporation processes,* 2013, ISBN 978-3-942036-27-6

224 Leube, Philipp Christoph: *Methods for Physically-Based Model Reduction in Time: Analysis, Comparison of Methods and Application,* 2013, ISBN 978-3-942036-28-3

225 Rodríguez Fernández, Jhan Ignacio: *High Order Interactions among environmental variables: Diagnostics and initial steps towards modeling,* 2013, ISBN 978-3-942036-29-0

226 Eder, Maria Magdalena: *Climate Sensitivity of a Large Lake,* 2013, ISBN 978-3-942036-30-6

Die Mitteilungshefte ab der Nr. 134 (Jg. 2005) stehen als pdf-Datei über die Homepage des Instituts: www.iws.uni-stuttgart.de zur Verfügung.